UNIVERSITY OF PARDUBICE
FACULTY OF TRANSPORT ENGINEERING

TRUNCATED CONICAL SHELLS AS ABSORBERS OF IMPACT FORCE

ERDEM ÖZYURT M.Sc.

A THESIS SUBMITTED FOR THE DEGREE OF
DOCTOR OF PHILOSOPHY

2018

Programme of Study:

P3710 Technique and Technology in Transport and Communications

Branch of study:

3708V024 Technology and Management in Transport and Telecommunications

Supervisor:

doc. Ing. Petr Tomek, Ph.D.

Supervisor Specialist:

Prof. Ing. Petr Paščenko, Ph.D.

Doctoral Dissertation Topic:

Truncated Conical Shells as Absorbers of Impact Force

Doctoral dissertation has arisen at the supervising:

Department of Mechanics, Materials and Machines Parts

Author's Declaration

I hereby confirm that:

I have written this dissertation thesis independently. All the reference, literature and information used in this work are quoted in the list of references.

I hereby acknowledge that all the rights and duties resulting from Act No. 121/2000 Coll., the Copyright Act, apply to my written work, especially that the University of Pardubice has the right to make a license agreement of use of this written work as a school work pursuant to § 60 section 1 of the Copyright act. On the condition that the written work shall be used by me or a license shall be provided to another subject for the use hereof, the University of Pardubice shall have the right to require from me a relevant contribution to reimburse the costs incurred for the making of such work including all relevant costs and total overall expenditure and expenses incurred.

I agree with the reference-only disclosure of my thesis in the University Library.

In Pardubice on .... / .... / .....

Erdem ÖZYURT

Acknowledgements

First and foremost, I would like to express my very great appreciation to my supervisor doc. Ing. Petr Tomek, Ph.D. for his patient guidance and useful critiques of this research work. I would also like to thank Prof. Ing. Petr Paščenko, Ph.D., who provided an insight to the inception of my research.

I would like to express my very great appreciation to Anadolu University of Turkey and Council of Higher Education of Turkey for the financial support to my PhD study.

I would also like to extend my thanks to my colleagues in Pardubice for their help and motivation during this research.

Last but not the least, I would like to thank my family: my parents and my beloved wife for supporting me spiritually throughout my PhD study and my life.

Erdem ÖZYURT

Abstract

In this dissertation, energy absorption capabilities of steel-based truncated conical shells with low base angle and end caps are investigated under axial dynamic loading. The numerical models of absorber were placed between two rigid plates to simulate a crush box around the absorber.

In order to investigate the effect of the design parameters on the energy absorption of the conical shells, three different base conical angle (20°, 25° and 30°), four different impact velocity ($5m/s$, $10m/s$, $20m/s$, $30m/s$), four different absorber thickness ($4mm$, $6mm$, $8mm$, $10mm$) and several impact mass values were analyzed. Numerical analyses were performed by FEM software Abaqus.

The simulation results were compared by means of several performance parameters such as peak reaction force F_p, mean reaction force F_m, absorbed energy E_A specific energy absorption (SEA), crash force efficiency (CFE) and dynamic amplification factor (DAF). In this dissertation, also some guidelines on the design of a truncated conical shell with low base conical angle as an energy absorber are presented.

Keywords

finite element method, energy absorption, truncated cone, crashworthiness.

Název Práce

Komolé kuželové skořepiny jako absorbéry rázové síly.

Souhrn

V této dizertační práci jsou zkoumány schopnosti absorpce energie ocelových komolých kuželových skořepin s malým úhlem vzepětí dynamicky zatížených v osovém směru. Numerické modely absorbérů byly umístěny mezi dvě tuhé desky pro simulaci skříně absorbéru. Za účelem zkoumání vlivu konstrukčních parametrů na absorpci energie kuželových skořepin byly analyzovány tři úhly vzepětí (20°, 25° a 30°), čtyři rychlosti nárazu ($5m/s$, $10m/s$, $20m/s$, $30m/s$), čtyři tloušťky absorbéru ($4mm$, $6mm$, $8mm$, $10mm$) a různé nárazové hmotnosti. Numerické analýzy byly provedeny pomocí MKP programu Abaqus.

Výsledky simulací byly porovnány podle několika parametrů: špičkové reakční síly F_p, střední reakční síly F_m, absorbované energie E_A, specifické absorbované energie (SEA), účinnosti deformační síly (CFE) a dynamického faktoru zesílení (DAF). V této dizertační práci je také uveden návrh konstrukce komolé kuželové skořepiny s malým úhlem vzepětí jako absorbéru.

Klíčová Slova

Metoda konečných prvků, absorpce energie, komolý kužel, odolnost vůči nárazu

Table of Contents

List of Figures

List of Tables

Nomenclature

List of Symbols

E	$[MPa]$	Modulus of Elasticity
E_{TAN}	$[MPa]$	Tangent Modulus
F_m	$[N]$	Mean Reaction Force
F_p	$[N]$	Peak Reaction Force
d	$[mm]$	Displacement
d_{max}	$[mm]$	Maximum Deformation Length
V	$[m.s^{-1}]$	Impact Velocity
E_{ABS}	$[J]$	Absorbed Energy
E_{length}	$[J]$	Absorbed Energy per unit Deformation
E_{KE}	$[J]$	Kinetic Energy
E_d	$[J]$	Dynamic Absorbed Energy
E_{qs}	$[J]$	Quasi-Static Absorbed Energy
T	$[s]$	Time
t	$[mm]$	Absorber Thickness
h	$[mm]$	Absorber Height
b	$[mm]$	Edge Ring Width
β	$[deg,^\circ]$	Base Conical Angle
r_1	$[mm]$	Small Diameter of the Cone
r_2	$[mm]$	Large Diameter of the Cone
D	$[m]$	Structural Nodal Displacement
$\dot{D}$	$[m.s^{-1}]$	Structural Nodal Velocity
$\ddot{D}$	$[m.s^{-2}]$	Structural Nodal Acceleration
m	$[kg]$	Mass
σ_Y	$[MPa]$	Yield Strength
ρ	$[kg.m^{-3}]$	Mass Density
υ	$[-]$	Poisson's Ratio
Δt	$[s]$	Time Step

List of Abbreviations

CAD	Computer Aided Design
CAE	Complete Abaqus Environment
CEM	Crash Energy Management
CFD	Computational Fluid Dynamics
CFE	Crash Force Efficiency
CPU	Central Processing Unit
DAF	Dynamic Amplification Factor
ERA	European Railway Agency
EU	European Union
FEA	Finite Element Analysis
FEM	Finite Element Method
GFRP	Glass Fiber Reinforced Plastic
GPU	Graphics Processing Unit
SE	Stroke Efficiency
SEA	Specific Energy Absorption
SHTB	Split Hopkinson Tensile Bar

1 Introduction

1.1 Statement of the Research Problem

Emerging technology in transportation industry comes with a lot of privileges for both passenger and freight transport. Delivering goods and traveling around becomes more fast and intensive. With the development of the transport technology, there is a substantial increase in number of vehicles and passengers. This increase led to a demand for developing more powerful and faster vehicles. On the other hand, same demand also led to an increase in undesirable situations such as fatal accidents and injuries. The authorities have become aware of this safety situation in transportation and have begun to pay attention to the possible causes of the death and injury incidents. Many research and reporting studies have been carried out in the field of statistics and engineering throughout the world over the years.

In comparison with the other modes of transport, railway transportation is one of the safest transport modes in Europe in terms of fatality risks for traveling passengers. The fatality risk for an average passenger is about 0.13 fatalities per billion kilometers. However, a significant amount of accidents and fatalities occur every year. Railway safety performance report of ERA indicates 2068 significant accidents resulting in 1133 fatalities and 1016 serious injuries in the 28 countries across the EU in 2012.[14] Figure 1.1 shows an example of head-on train collision occurred in Vienna/Austria in 2013.

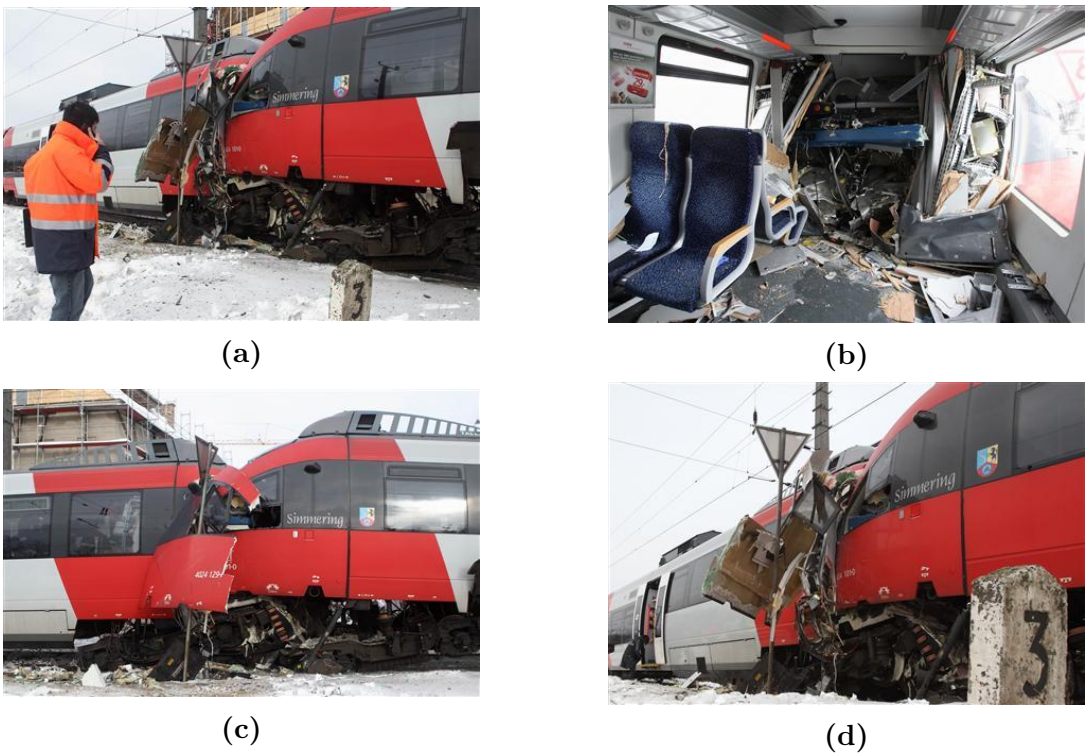

(a) **(b)** **(c)** **(d)**

Figure 1.1: Head-on collision of commuter trains in Vienna/Austria [1]

It is important to be able to prevent any possible accidents or at least to ensure the results of the accidents which are inevitable, with minimal damage or injury. Vehicle safety has also become one of the most important evaluation criteria such as build quality, fuel consumption, and comfort for drivers and transport companies. In order to provide crash-safe vehicles, vehicle manufacturers and researchers have focused on developing safety equipment with different types and different working principles such as seat belts, airbags, collision avoidance systems and energy absorbers. These equipments could be classified as active and passive safety systems which are later described in following relevant sections.

The prevention of collisions may not always be possible despite all collision avoidance systems. So it is of utmost importance to control the possible deformation of the vehicle as a result of the collision. Controlling the deformation basically, means to transfer the impact forces to the appropriate sections selected by the designer. The aim here is to ensure that the collision energy is absorbed by the energy absorbers and to minimize or prevent the possible damage to the structural elements of the vehicle. Thus, the undesired damage to the important sections of the vehicle enclosing occupants can be minimized. In Picture 1.2, various examples of energy absorbers used in different types of vehicles are given.

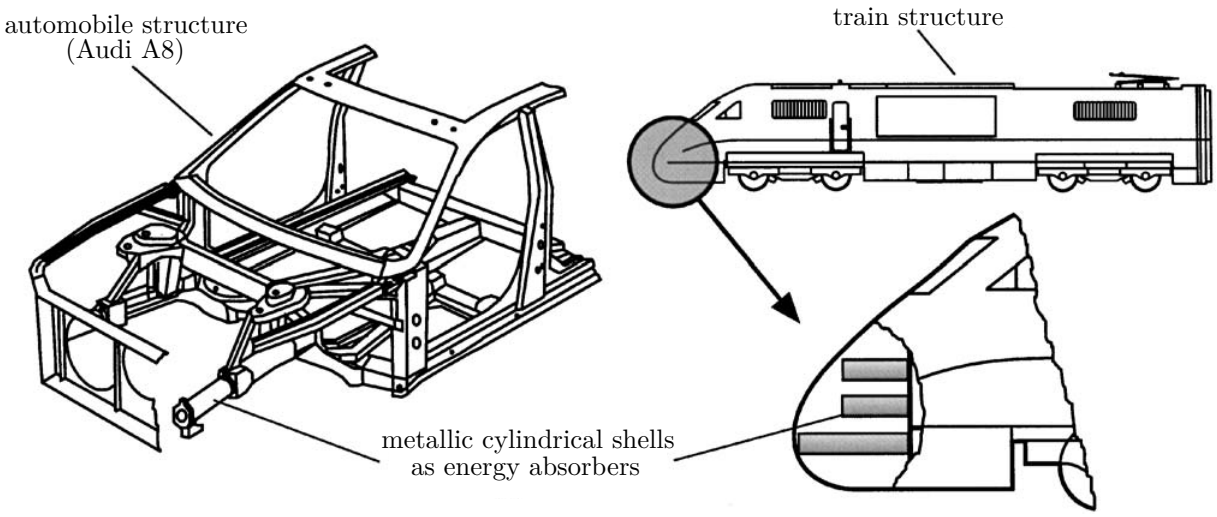

Figure 1.2: Energy absorbers used in automobile/train structures. [2]

Another important step of the safety research is to test the developed energy absorbing structure in order to better understand the crash resistance ability and the response of the structure during the impact. Furthermore, it is also necessary to conduct multiple repetitive tests to obtain trustworthy results and to ensure the accuracy of the tests. However, using numerous real vehicles to conduct full-scale crash tests can be quite expensive. Re-using the same vehicle consecutively is generally not possible due to the destructive characteristics of crash testing. When all the requirements and the limitations are taken into consideration, a virtual testing method using computer simulations become prominent.

The finite element method (FEM) which is extensively used in crash simulations today, was first developed in late 1950's. The FEM had the ability to perform analyses only on linear problems in its first use. However, it gained the ability to solve complex, highly nonlinear problems in many areas with the development of high-performance computers. Over the last decade, FEM has been a very powerful tool in virtual crash simulations. The predictive capabilities of the finite element method provide a great opportunity to the engineers for understanding the crash event in a virtual environment. In other words, engineers can simulate a crash event several times with a precise control of every condition and consider variables. Therefore, a number of real vehicle tests that need to be performed can be limited and thereby save costs and time. Companies developed many software packages and codes such as LS-DYNA, PAM-CRASH, RADIOSS, ANSYS, NASTRAN and ABAQUS which are capable of using FEM for solving numerous types of engineering problems.

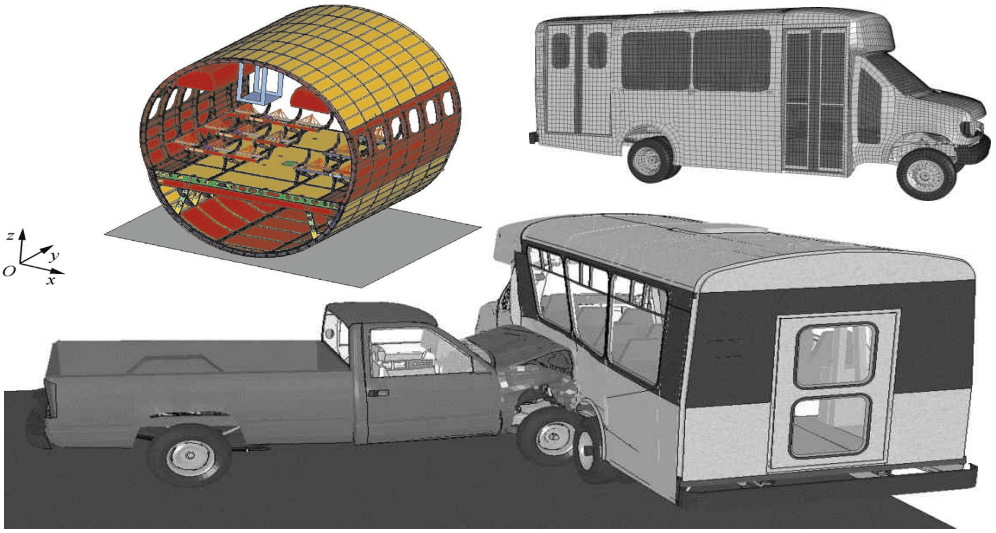

Figure 1.3: Examples of FEM models used for vehicle crash simulations.[3, 4]

Some examples of crash studies by using FEM software are given in Figure 1.3. Detailed information about specific properties of a FEM model and crashworthiness characteristics. In forthcoming sections, a brief review of FEM and crashworthiness requirements of energy absorbers are discussed in detail.

1.2 Aim of the Doctoral Dissertation

Current doctoral dissertation study is built upon the current knowledge about the structures used to dissipate impact energy in case of a collision. Current structures being used as impact energy absorbers use mostly the cylindrical tube and rectangular tube geometries more than conical. Thus, most of the studies in the literature are about these type of geometries. On the other hand, there are also too many studies on conically shaped energy absorbers in the literature but most of them have relatively steep conical geometries close to cylindrical tubes.

In this manner, the main aim of this study is to determine the energy absorbing capacity of capped-end truncated cones with relatively low base cone angles and edge ring. Unlike most of the studies, more shallow structures needed to be examined in detail for using as impact energy absorbers. In this manner it is aimed to investigate conical structures with relatively higher thickness over the thin-walled structures encountered commonly in the literature.

1.3 Layout of Thesis

This thesis consists of 7 chapters. A brief description of each chapter is presented below.

Chapter 1: Introduces the background of the idea including the statement of the research problem. Also, introduces the aims of the current study and explanation of the structure of the thesis.

Chapter 2: Involves detailed information about the crash energy management and energy absorbers. Also, describes general design requirements and performance parameters which must be considered when designing an energy absorbing structure.

Chapter 3: Includes a summarized literature review about energy absorber structures closely related to the field of this study. Also, a general comparison of the current study with the previous studies in the scopes of the study section takes place.

Chapter 4: Describes the numerical method used in the present study with basic procedures. Numerical difficulties of nonlinearity and time integration methods are presented in detail. Also, includes the terminology of the current FEM software which terms are used in the further chapters of the study.

Chapter 5: Provides a detailed description of numerical simulation techniques performed in this study. This chapter also describes the geometrical parameters, material properties and finite element modeling parameters such as loading conditions, boundary conditions and mesh structure of the numerical models.

Chapter 6: Evaluates a detailed investigation of the results obtained from both quasi-static and dynamic simulations in consideration of different performance parameters such as force-displacement curves, absorbed energy, specific energy absorption, and crash force efficiency. The effects of varying loading conditions and model geometry are investigated and presented. Also some basic comparisons of the simulation results to the current literature for the effect of the variables on the performance parameters are given.

Chapter 7: Presents a summary of major conclusions and contributions to the current study. Also includes some design guidelines and a brief description of the further works planned to improve the results of the present study.

2 Background

2.1 Crash Energy Management

Crashworthiness can be defined as the capability of a vehicle to withstand a crash and protect its passengers from the effects of an accident. Main crashworthiness goals are to absorb the kinetic energy of a collision with an acceptable deceleration pulse and maintain a survival space to protect passengers.

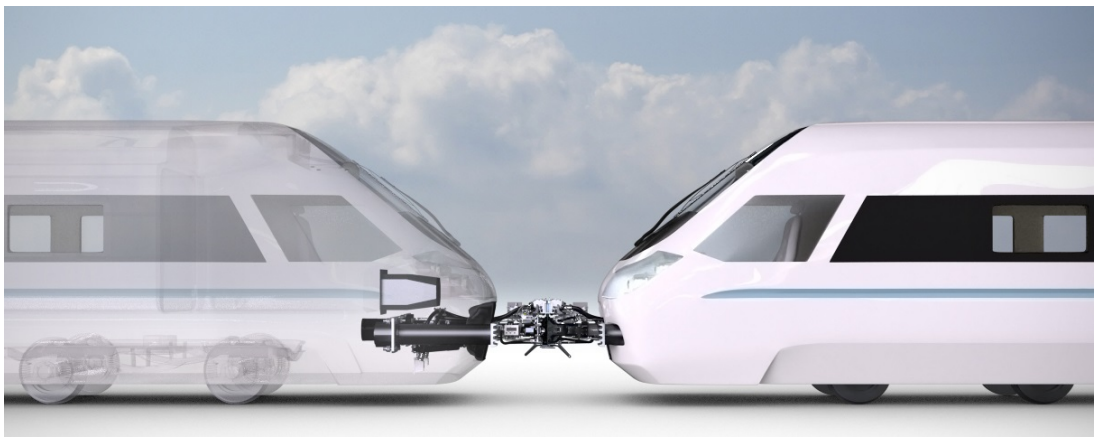

Figure 2.1: CEM system developed by the company DELLNER[5]

Crash Energy Management (CEM) is the sum of the techniques to improve the overall crashworthiness of a vehicle. Possible damages of an accident should be predicted and should be kept under control. With crash energy management systems, damage of a collision is transferred to the parts that designed to absorb the crash energy and protect the main structural elements of the vehicle. A CEM system developed by Dellner company and mounted on a vehicle is illustrated in Figure 2.1. In Figure 2.2, a CEM system developed by the company VOITH with its deformable energy absorption components are shown. The CEM system developed by the company consists of a coupler, an anti-climber unit coupled with 2 lateral energy absorbers.

(a) CEM System **(b)** Pushback Coupler and Lateral Absorber

Figure 2.2: CEM system developed by the company VOITH.[6]

2.2 Energy Absorbers

Energy absorbers absorb energy both in a reversible and irreversible way such as elastic strain energy and plastic deformation energy. Collapsible energy absorbers aim to convert the majority of the kinetic energy of impact into plastic deformation in an irreversible manner.[15] Some energy absorbing structures developed by various companies are shown in Figure 2.3.

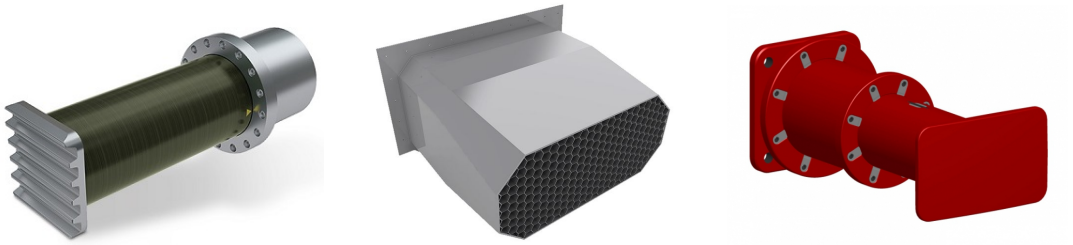

(a) Voith[16] **(b)** Dellner[17] **(c)** Axtone[18]

Figure 2.3: Energy absorbers developed by various companies

2.3 General Design Requirements

In the design phase of an energy absorber, one must consider the specific requirements of the area that absorber is planned to use. Despite the fact that the requirements can change with different applications. In all cases, the main purpose is to scatter crash energy in a foreordained way. In this manner, some essential requirements are listed and described below.[19]

1. Irreversible Energy Conversion
2. Restricted and Constant Reactive Force
3. Long Stroke
4. Stable and Repeatable Deformation Mode
5. Lightweight and High Specific Energy Absorption
6. Low Cost and Easy Installation

2.3.1 Irreversible Energy Conversion

When a load is applied to a structure, the resultant deformation could be in either reversible or irreversible manner. If the applied load is below the yield point of the material hat the structure is made of, then the deformation will be elastic. After the load is dismissed, the structure would regain its initial shape and release the energy stored by elastic strain. This released energy can cause damage to structure and occupants.

Therefore, an energy absorber should dissipate the initial kinetic energy in an irreversible way such as plastic strain energy and friction energy instead of elastic strain energy. Consequently, absorbing the energy by means of deformation is one of the main design requirements of an energy absorbing structure.[19]

2.3.2 Restricted and Constant Reactive Force

In a large deformation process of an energy absorbing structure, peak reaction force and unstable reaction force leads to high rate of deceleration to the occupants and vehicle. Therefore reaction force should be kept constant to avoid damage and injury.[19]

European standard DIN EN 15227:2008 indicates crashworthiness requirements for railway vehicle bodies. According to EN 15227:2008, the mean deceleration rate should be limited as far as is practicable to 5g and shall not be more than 7.5g on the passengers. It will be necessary to accept higher levels of deceleration in driving cab close to the point of impact.[20]

2.3.3 Long Stroke

For an energy absorbing structure, the amount of kinetic energy dissipation is significant. As mentioned above, the reaction force of the absorber should be kept relatively low and this brings out a limitation to the amount of kinetic energy dissipation by means of occupant safety. In this case, displacement or deformation length of the absorber should be sufficiently long to restrict the reaction force and reach the adequate amount of energy to be absorbed. [19]

A basic sketch of a car collision is given in Figure 2.4. According to work-energy principle, the change in the total energy of a particle is equal to the work done on the particle. In a collision, it is expected from an energy absorber to dissipate the initial kinetic energy of the vehicle. Dissipated energy by an absorber can be explained by means of average reaction force and the deformation length as the work done by the absorber.

Based upon the equation 1, deformation length has a great effect on reaction force and therefore the safety of the passengers.

$$\begin{aligned} E_{KE} &= W \\ \frac{1}{2}mV^2 &= Fd \end{aligned} \tag{1}$$

where E_{KE} is the initial kinetic energy of the car, W is the work done by the reaction force, m is the mass of the car, V is the initial speed of the car, F is the constant mean reaction force affected on the car and d is the total deformation of the car.

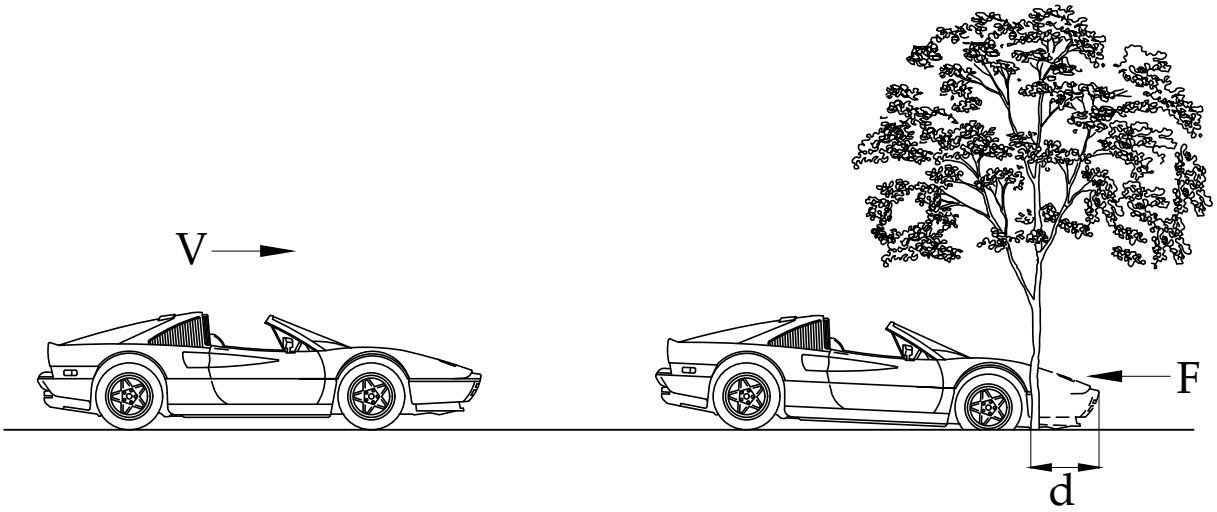

Figure 2.4: Basic sketch of a car crash

2.3.4 Stable and Repeatable Deformation Mode

In real circumstances and working conditions, characteristics of a dynamic load such as impulse loading, loading direction and distribution could be in an extremely wide range. Therefore, an energy absorber should have stable and repeatable deformation modes and should be insusceptible to above-mentioned variability of loading.[19]

2.3.5 Light Weight and High Specific Energy Absorption

As a result of being mounted on the vehicle, an energy absorber should be light to prevent adding too much extra weight to the vehicle. Extra weight comes with additional fuel consumption and pollution. Designers facing a challenge to develop lighter structures without any loss of energy absorbing capacity. In this manner, circular structures become prominent because of having higher specific energy absorption per unit weight of material.[19]

2.3.6 Low Cost and Easy Installation

In comparison to the past, cost reduction is much more necessary for design and production stages due to the competitive market. Energy absorbers are mostly single-use components and needed to be replaced after a deformation or crash. Therefore, manufacturing, installation, and maintenance should be more easy and inexpensive.[19]

2.4 Performance Parameters

Even if the most important parameter of an energy absorber is the amount of dissipated energy, it is not sufficient to estimate the performance of the absorber by considering only the amount of the energy absorbed during the impact. For a reasonable performance estimation, it is needed to define and investigate following parameters:

1. Force-Displacement Curves
2. Energy Absorption
3. Crash Force Efficiency (CFE)
4. Specific Energy Absorption (SEA)
5. Absorbed Energy According to Displacement
6. Dynamic Amplification Factor
7. Stroke Efficiency

2.4.1 Force-Displacement Response

Force-displacement curves are one of the main parameters in analyzing the crush behavior of energy absorbers. Curves show the crushing response of the absorber with respect to deformation and each absorber has its own specific response. It can be achieved by numerical or experimental methods. A typical Force-Displacement curve is given in Figure 2.5.

By using force-displacement curves, one can obtain two main force parameters that are also important for the performance of the absorber, mean crushing force and peak crushing force.

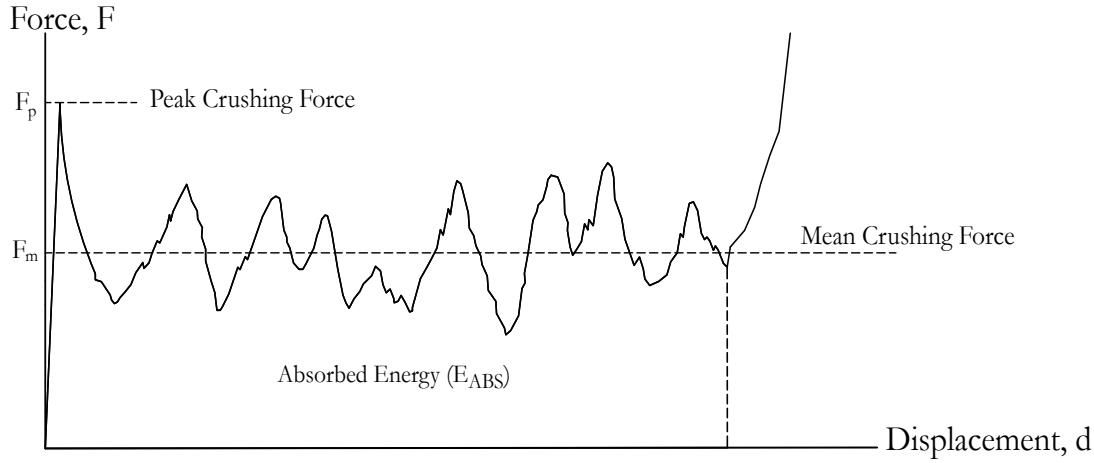

Figure 2.5: Typical Force-Displacement Curve

Mean Crushing Force (F_m) is the force value that absorbing structure deforms stably during the impact. It can be calculated by using force response and total deflection length of the absorber.

$$F_m = \frac{\int_0^{d_{max}} F dx}{d_{max}} \tag{2}$$

where $F_m[kN]$ is the mean crushing force, $F[kN]$ is the crushing force and $d_{max}[mm]$ is maximum crush distance.

Peak Crushing Force (F_p) is the maximum value of the axial force during crush. Peak force occurs when material yields or buckles. Peak crushing force should be kept relatively low or in other words, it should not be far beyond the mean crushing force.

Both mean crushing force and peak crushing force terms are illustrated on the typical force-displacement curve in Figure 2.5.

2.4.2 Energy Absorption

The total absorbed energy of an energy absorber can be defined as the work done by the crushing force at a deformation distance. By using basic mechanics, absorbed energy is simply the area under the force-displacement curve and can be expressed as;

$$E_A = \int_0^{d_{max}} F dx \tag{3}$$

where $E_A[kJ]$ is the amount of the absorbed energy, $d_{max}[mm]$ is maximum crush distance and $F[kN]$ is the crushing force.

2.4.3 Crash Force Efficiency

Crash force efficiency is described as the ratio of mean crushing force to the peak crushing force during the deformation caused by the impact. By describing this ratio, it can be said that if CFE is close to unity, that means there were no rapid changes on deceleration of the system. It is desired to have this ratio close to unity, to approve the absorbing system has a better crash performance. [19]

$$CFE = \frac{F_m}{F_p} \tag{4}$$

Crash force efficiency can be improved by using trigger mechanisms such as notches or holes to make an imperfection and raise the stress at initial loading to ease buckling and reduce the peak force.

2.4.4 Specific Energy Absorption

Specific Energy Absorption (SEA) is an important parameter for an energy absorber and defined as the ratio of total energy absorbed in the system to the mass of the structure. The higher SEA value refers to a more lightweight absorber, which means more energy can be absorbed with a lighter structure.

$$SEA = \frac{E_{ABS}}{m} \tag{5}$$

where $SEA[kJ/kg]$ is specific energy absorption, $E_A[kJ]$ is total absorbed energy and $m[kg]$ is mass of the absorber.

2.4.5 Absorbed Energy per unit Deformation

If the length of the deformation zone is restricted by geometrical conditions, the parameter absorbed energy per deformation becomes prominent. It can be calculated by dividing the total absorbed energy to the maximum amount of deformation;

$$E_{length} = \frac{E_{ABS}}{d_{max}} \tag{6}$$

where $E_{length}[kJ/mm]$ is absorbed energy per deformation, $E_A[kJ]$ is total absorbed energy and $d_{max}[mm]$ is length of deformation.

2.4.6 Dynamic Amplification Factor

Dynamic amplification factor, DAF is another parameter to investigate the effects of the loading conditions of the energy absorbing structure. DAF is simply defined as the ratio of the energy absorbed under dynamic loading to the energy absorbed under quasi-static loading as given in equation 7.

$$DAF = \frac{E_d}{E_{qs}} \tag{7}$$

Despite being an uncommon performance parameter of an energy absorber, it is very useful to investigate the dynamic effects such as inertia and strain rate effects. It has been used by several authors [21, 22, 23, 24] for both investigation and estimation of the dynamic effects on the energy absorbers.

2.4.7 Stroke Efficiency

The effective length of an energy absorbing structure may differ between different designs. It is necessary to determine the amount of length of the absorber deformed to dissipate energy. The stroke efficiency is the parameter to obtain this information and can be expressed as;

$$SE = \frac{d_{max}}{L} \tag{8}$$

where SE is stroke efficiency, $d_{max}[mm]$ is length of deformation and $L[mm]$ is total length of the energy absorber. It is desired to have this ratio close to unity to obtain the maximum length of deformation and improve energy absorption performance of the structure.

3 Literature Review

3.1 Literature About the Current Problem

Commonly used geometrical shapes of energy absorbers in most studies are cylindrical tube [25, 26], square tube [27, 28] and truncated conical tube [29] also known as a frustum. In the current literature, there are various terms used for identifying the conical structures which are conical shells, cones, conical tube, frustum and frusta. It is useful to note that all of these terms have the almost the same meaning before examining the literature review. Although most of the studies are focused on cylindrical and rectangular tubes, crashworthiness of conical structures has been studied by many substantial authors.

This section of the study is divided into two parts in order to examine the literature study more clear. The first part focuses to the studies about the energy absorbing structures and the second part consists of the studies about conical geometry.

3.1.1 Energy Absorbers

Langseth and Hopperstad [30] have studied on the impact behavior of square thin-walled extruded structures subjected to axial loading. Aluminum alloy material AA6060 is used in both static and dynamic tests. Test specimens were clamped at the lower end and free at the top. Projectile mass of 56 kg is used in the dynamic tests while the impact velocity was within the range of 8-20 m/s. Significantly higher dynamic forces than the corresponding static forces for the same axial displacement were obtained, which indicates stronger inertia effects.

Mamalis et al. [31] have investigated the crash behavior and energy absorbing characteristics of axially loaded steel thin-walled tubes of the octagonal cross-section. Numerical simulations were performed by using explicit FEM code LS-DYNA. An isotropic elastic-plastic material, which is characterized by a bilinear elastoplastic behavior with strain hardening was used. Also, a test series of axially compressed octagonal tubes have been carried out under quasi-static load, at a velocity of 10 mm/min. As a result of the study, four deformation modes were obtained. Also, it is found that LS-DYNA has an estimation with a good accuracy at the peak loads of the pre-buckling region and loading variations of the post-buckling region when compared to the corresponding experimental curves.

Tai et al. [32] have analyzed the axial compression behavior and energy absorption of the thin-walled cylinder under impact load by using nonlinear finite element software LS-DYNA. Two different materials as high-strength steel and mild-strength steel were

modeled with equal sectional areas and investigated using a series of analyses. Material characteristic curves were obtained by using Cowper-Symond equation. Analysis outcomes showed that changing the impact mass affected only the impact energy and consequently affected the overall deformation but had no significant effect on energy-absorbing efficiency of the structure. It was also obtained from the analyses that the impact kinetic energy is more sensitive to speed than impact mass which also the fact the determination of the energy absorption.

Tarlochan et al. [33] have studied the design process of a thin-wall structure subjected to both axial and oblique dynamic compression. Six different cross-sectional geometries (circle, rectangle, square, hexagonal, octagonal and ellipse) were investigated with respect to the performance parameters such as absorbed crash energy, crush force efficiency, ease of manufacture and cost. Simulations were made by using A36 steel material under impact velocity of 15.6 m/s (56 km/h) with a lumped mass of 275 kg. Material characterization of A36 steel was done as Johnson-Cook constitutive isotropic hardening model. The hexagonal structure model with a perimeter of 300 mm was chosen as the most efficient model and used to investigate the effects of the thickness, foam filling and using a trigger mechanism on energy absorption as a further study. In conclusion, authors have stated that the hexagonal tube of wall thickness 2 mm with aluminum foam filling and a trigger mechanism has a good potential as an energy absorber.

Abbasi et al. [7] have investigated the axial collapse behavior of several cross-sectional structures (square, hexagonal and octagonal) and a newly introduced 12-edge section. All models can be seen in Figure 3.1. Single-objective and multi-objective optimization processes were applied to all structures with the target of maximizing performance parameters; specific energy absorption (SEA) and crash force efficiency (CFE) as the ratio of mean crushing load and peak crushing load. Numerical simulations were carried out by nonlinear finite element software LS-DYNA in which all structures having the same length of 250 mm.

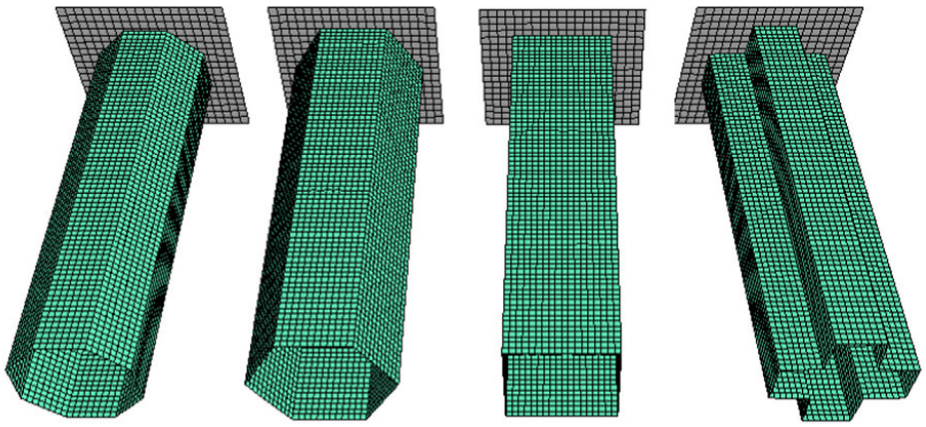

Figure 3.1: Schematic of octagonal, hexagonal, rectangle, and 12-edge columns[7]

An elastic-plastic material model with Von Misses isotropic plasticity algorithm with piecewise linear plastic hardening was used to describe the constitutive material behavior. Four different material models were used as steel with same density and Poisson's ratio and different yield stresses and different ultimate stresses. It was found that the cross-sectional configuration, as well as material type, had significant effects of the SEA, while cross-sectional configuration had the only dominant effect on CFE. It was also found that the 12-edge section made of high-strength steel DP600 was the best choice to reach the maximum SEA value.

3.1.2 Conical Energy Absorbers

Gupta et al. [34] have performed an experimental study on aluminum conical frusta of different semi-apical angles varying over a range from 16.5° to 65° under axial compression. Structures were subjected to quasi-static axial compression between rigid plates at a cross-head speed of $3.33\text{x}10^{-5}$ m.s^{-1}. Authors have also proposed an analytical model for the prediction of load-deformation and energy-compression curves of the metallic conical frusta collapsing due to the initiation of the rolling plastic hinge. It has been seen that at low values of semi-apical angles (up to 30°), frusta collapses in diamond buckling mode. In larger semi-apical cone angles, the collapse was associated with reverse bending at the larger end.

Aljawi and Alghamdi [8] have examined deformation modes of frusta as a collapsible energy absorber with using explicit finite element software Abaqus. Two innovative axial deformation modes (inward inversion and outward flattening) of capped spun aluminum frusta were investigated both numerically and experimentally. Both deformation modes can be seen in Figure 3.2.

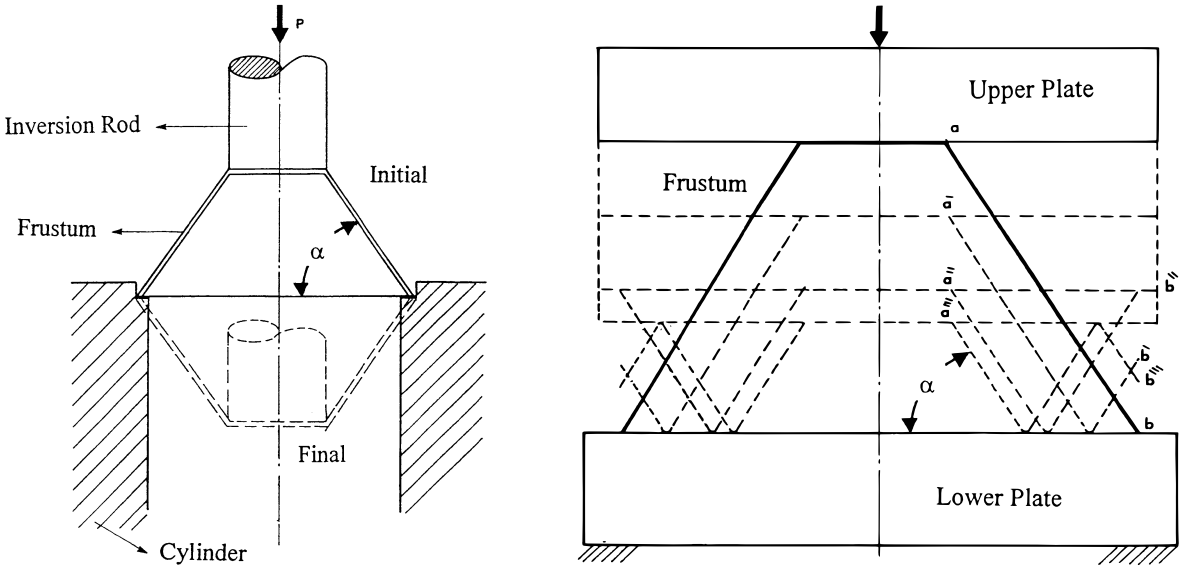

(a) Inward Inversion **(b)** Outward Inversion

Figure 3.2: Inward (direct) inversion and Outward (indirect) flattening of frusta. [8]

Numerical simulations were performed at a velocity of 0.01 m/s which represented the quasi-static case. Twelve different sizes of aluminum frusta (3 different apex angles and 4 different thicknesses) were also crushed by use of a falling weight hammer of 10 m/s striking speed. In conclusion, it has been noted that an absorber in the inversion mode might be re-used by being inverted several times. Also, authors obtained that within the experimental impact speed range of 0-7 m/s, the speed of deformation had no effect on the process of inversion and flattening.

Alghamdi et al. [35] have studied on the classification of the deformation modes of unconstrained capped end frusta under axial loading. Tens of aluminum spun capped end frusta of different semi-apex angles (15-60°) and thicknesses (1-3 mm) were crushed at quasi-static loading conditions. Quasi-static numerical simulations were performed with finite element software ABAQUS at a velocity of 0.17 mm/s. In the experimental part of the study, more than 50 different sizes of frusta made of 3 different materials; aluminum, low carbon steel and nylon plastic were crushed. Five different collapse modes which are combinations of outward inversion of the lower end, inward inversion of the upper end and extensible collapse of the upper end were investigated. It has been found that material type had a large effect on the axial deformation mode followed by semi-apical angle then wall thickness.

Eswara and Gupta [36] have examined a large number of spherical domes and conical frusta of various sizes in order to investigate collapse modes and energy absorption capabilities of structures. Aluminum spherical shells of R/t values between 15.3 and 240.9 and conical frusta of semi-apical angles from 44.5° to 67.1° were tested under both quasi-static and dynamic loading. Quasi-static tests were conducted with a cross-head speed of $3.3\text{x}10^{-5}$ m/s (2 mm/min). Impact tests were performed by using a drop hammer with impact mass between 23.25 and 34.45 kg and impact speed between 2 to 9 m/s. Aluminum sheets of standard thickness i.e. 0.5, 0.7, 1, 1.5, 2, 2.5 and 3 mm were used in the production of test specimens. In conclusion, spherical domes were found a change in collapse modes between quasi-static and dynamic loading. For conical frusta, collapse modes were found to be identical during quasi-static and dynamic tests. Both mean loads and peak loads found to be higher in impact tests when compared to the quasi-static tests for both geometries. Load-deformation curves and collapse modes of conical frusta have shown similar behavior in quasi-static and dynamic tests.

Gupta and Venkatesh [37] have performed experiments on aluminum conical shells of semi-apical angles between 6.84° and 65.35° under axial compression. Experiments were conducted with using a gravity drop hammer set-up and results were compared with numerical simulations which were performed with finite element code FORGE2. Aluminum sheets of thicknesses 1, 1.5, 2 and 2.5 mm were used for manufacturing the

specimens and all of them were annealed by soaking them at 300°C in the furnace for 1h and cooled in the furnace for 24h. Constant mas of 34.75 kg and initial impact velocities ranging between 2.55 to 7.92 m/s were used in the experiments. Impact results were also compared with quasi-static experiments performed at a cross-head movement of 10 mm/min. Energy absorption capacities of structures in impact tests were increased about 8.93-49.6% in comparison with static test values.

Guler et al. [9] have investigated the crash behavior of thin-walled straight and conical shell structures under axial impact loading with respect to the design parameters such as cross-section geometry, wall thickness, and semi-apical angle. Cross-sections of circular, square and hexagon were examined and energy absorption characteristics and crush forces were obtained for each structure. Peak crush force, mean crush force, crush force efficiency and specific energy absorption values were also calculated for a deformation length of 100 mm.

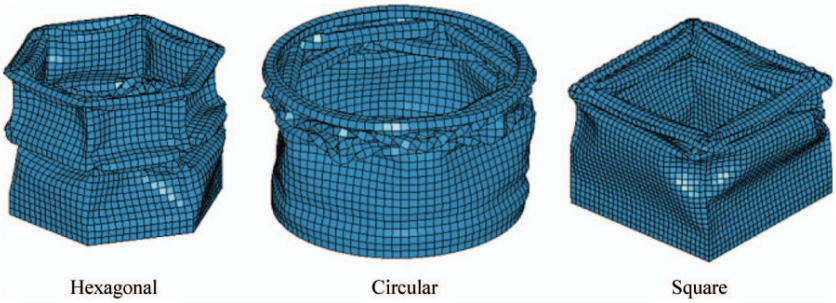

Figure 3.3: Deformation shapes for hexagonal, circular and square models. [9]

In conclusion, it was found that absorbed energy values have increased with increasing the wall thickness of the structure up to a certain value. Additionally, increasing semi-apical angle had a slightly decreasing effect on the absorbed energy but a significantly decreasing effect on the crushing force. It was also seen that the conical energy absorber with a wall thickness of 2 mm and semi-apical angle of 12.5° was the most efficient one among the others. Even though being the most efficient, initial peak force of this structure was still high and modifications such as blanks on the sidewalls and corrugations along the axial direction were made to lower the initial peak force. Modifications have resulted in lower peak forces and also better crash force efficiency values.

Azimi and Asgari [38] have investigated singular and double wall structures to introduce a new structure with better energy absorption and crushing characteristics under both axial and oblique loading conditions. The new developed bi-tubular structure consisted of an inner conical structure with a height of 200 mm and mean diameter of 56 mm and outer circular structure with a height of 230 mm and diameter of 98 mm. An impact mass of 200 kg with a 20 m/s initial impact velocity was used. Aluminum with perfect plasticity and carbon steel with linear hardening were used as the material

behavior of structures. Structures were also investigated with and without foam filler to see the effects of foam filling to the newly developed structure. In comparison, it was found that foam filling the structures may not always result in better performance and may cause higher initial peak load as well as lower specific energy absorption. Also, new developed double wall structure had a lower initial peak load when other crashworthiness parameters remain unaffected. Under oblique impact loading, the new bi-tubular structure was shown better energy absorption characteristics.

3.2 Scope of the Study

With respect to the aims of the dissertation study as mentioned before, the main scope of the present study is to determine the usability of the conical geometries of low base cone angles as an energy absorbing structure. In this manner, models with various geometric parameters such as the base conical angle and the absorber thickness have been modeled. A geometry of conical absorbers reversed and connected together was chosen to make the total length of the absorber more adjustable to compare with other absorbers used in the current literature. All models have been studied numerically with the influence of crashworthiness parameters such as load-deflection curves, crash force efficiencies and specific absorbed energy values.

Based on the aforementioned scope, detailed goals of the study are summarized below.

- To evaluate series of various numerical models for cones of different base angle and thickness values in order to simulate the axial impact of various impact velocities and impact masses by using the Abaqus/Explicit finite element software.
- To perform analysis on the structures modeled as energy absorbers with variable impact velocities, impact masses and geometrical parameters such as the absorber thickness and base conical angle. The numerical simulation results will also be used to develop an understanding of the detailed behavior of structures under impact loading depending on the various parameters.
- To process the data from the numerical results with respect to different result parameters to investigate the effectiveness of structures under impact loading to be used as energy absorbers.
- To generate an opinion on the usability of the structure as an energy absorber by taking into consideration of both commonly used structures.

4 Nonlinear Finite Element Method

4.1 Introduction

Finite Element Method (FEM), also called Finite Element Analysis (FEA) is a numerical method used to seek solutions for engineering problems with an admissible approach. Structure of considered engineering problem is divided into several small pieces, called elements. Nodes are the points that elements are connected together. This procedure is called meshing and constitutes a system of elements with own algebraic equations. By solving all equations for unknowns at nodes, an approximate solution for the whole system will be obtained. In this chapter, the most important parameters and terms about FEM modeling and simulations such as numerical difficulties and software terminology.

4.2 Nonlinearity

In an engineering problem, if the stiffness and/or loading of the system turn into functions of displacement or deformation, then nonlinearity becomes prominent. Thus, stiffness matrix of the structure and the equilibrium equations must be updated in each solution step. Nonlinear equations of a system are difficult to solve because superposition principle cannot be applied like in the linear systems.

Causes of nonlinearities in a system can be grouped into 3 basic categories: *geometry nonlinearity, material nonlinearity, and conditions nonlinearity.*

Geometry Nonlinearity: When the magnitude of displacements is large enough to change the distribution of the direction of the loading. This kind of nonlinear behavior is defined as geometric nonlinearity. The main difficulty of geometric nonlinearity is that all equilibrium equations must be rewritten in each solution step with respect to the deformation of the structure.

Material Nonlinearity: A linear material model assumes that the stress is proportional to strain and linear with a slope of Young's modulus E. For nonlinear materials, actual stress-strain curves are often represented as idealized stress-strain curves for different types of nonlinear behavior.

Conditions Nonlinearity: Conditions nonlinearity occurs if boundary conditions such as supports and contact between parts change during an analysis process. This sudden change in the boundary conditions effects the response of the structure significantly. Therefore, this type of nonlinearities are extremely discontinuous because of the contact and change in the boundary conditions.[11]

4.3 FEM Software and Terminology

The numerical part of this study such as modeling and simulations were performed in commercial finite element software ABAQUS 6.13. The complete Abaqus finite element system covers:

Abaqus/CAE	Pre-processor environment of Abaqus used for modeling, visualization, and process automation.
Abaqus/Standard	Solver program for static and low-speed dynamic problems.
Abaqus/Explicit	Solver program for brief transient dynamic events such as drop testing, crashworthiness, and ballistic impact.
Abaqus/CFD	Solver program for computational fluid dynamics.
Abaqus/Viewer	Part of Abaqus/CAE includes only the visualization of results.

Depending on the subject of the present study, Abaqus/CAE is used for modeling the structures with respect to various design parameters. Abaqus/Explicit solver package have been used to simulate the dynamic loading of the structures. Results obtained from the simulations have been viewed and exported by using the Viewer module of the software.

4.3.1 Element Formulation

In order to simulate a problem numerically, finite elements are used to define the model of the problem. Elements consist of properties such as degrees of freedom, integration method etc. and can be either deformable or rigid. Terminology about the elements used in this study is described below.

R3D4

R3D4 is a rigid, three-dimensional, bi-linear quadrilateral element with four nodes. In the current study, the R3D4 element is used for modeling both striking plates with mass and rigid plate as a wall. The indicators inside the element name are given in Figure 4.1a and node ordering of the element is given in Figure 4.1b.

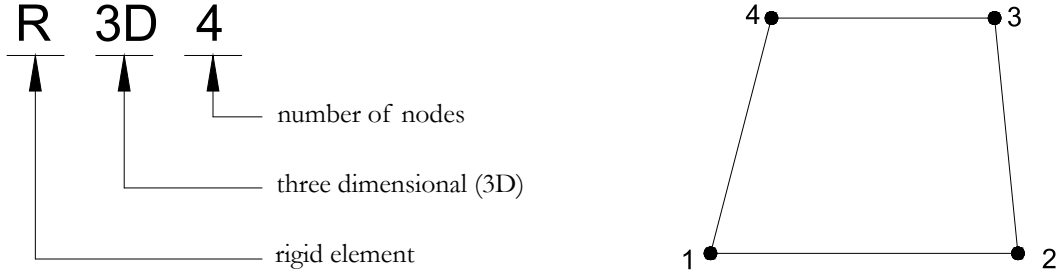

(a) Element Name Indication **(b)** Element Node Ordering

Figure 4.1: Element name indicators and node ordering of the element R3D4 [10]

Rigid elements are not deformable, thus there are no numerical integration points. The only possible output from a rigid element is the motion of the nodes. By using a rigid body reference node, reaction forces and reaction moments can be obtained[11].

C3D8R

C3D8R is a three-dimensional linear continuum (solid) element with 8 nodes, reduced integration and hourglass control. C3D8R elements are used for modeling the absorber structures in the current study. Element name indicators and node ordering of the element is given in Figure 4.2a and Figure 4.2b respectively.

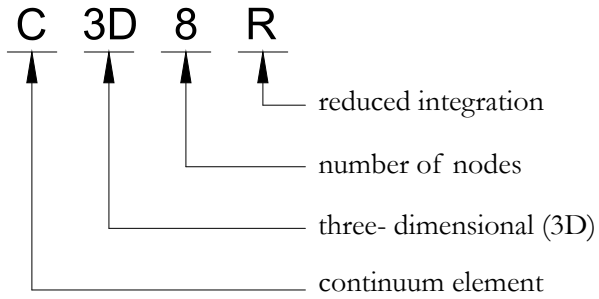

(a) Element Name Indication

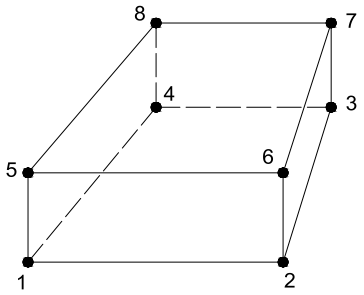

(b) Element Node Ordering

Figure 4.2: Element name indicators and node ordering of the element C3D8R [10]

Full Integration and Reduced Integration

Terms 'Full Integration' and 'Reduced Integration' stand for the integration points required to integrate the stiffness and mass matrices of an element.

In *full integration* scheme, three dimensional solid element C3D8 uses two integration points in each direction(array of 2x2x2)[11]. Integration points of the C3D8 element are shown in Figure 4.3a. Integration points are plotted with a cross (X) sign and nodes with a dot (.) sign.

In *reduced integration* scheme, linear elements use only one integration point in each direction. Integration point of the C3D8R element is located at the centroid of the element as seen in Figure 4.3b.

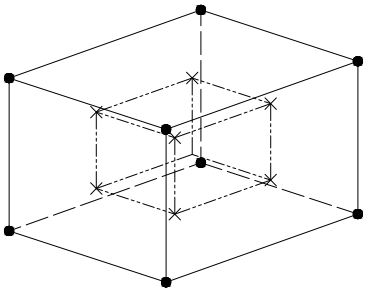

(a) C3D8 element

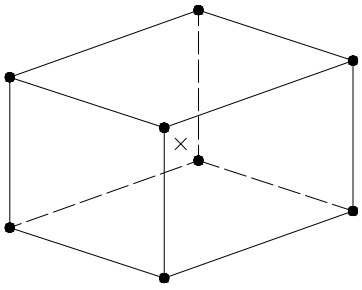

(b) C3D8R element

Figure 4.3: Integration points of (a) full integration (b) reduced integration elements[10].

Reduced integration elements are cheap and effective, thus using this type of elements reduce the computational expense of element calculations. However, these elements are largely dependent on the nature of the problem. Linear reduced integration elements may suffer from their own numerical problem called *'hourglassing'* in stress/displacement analysis[10].

Hourglassing

As a result of having only one integration point for each element, reduced-integration elements can deform in such way that strains at the integration point are zero. Figure 4.4 illustrates the deformation of a C3D8R element subjected to pure bending.

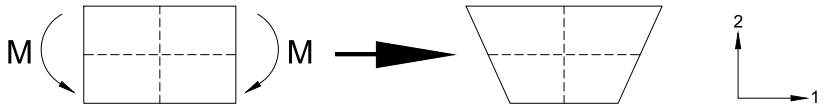

Figure 4.4: Deformation of linear C3D8R element under bending moment [11]

After deformation under bending moment, length, and angle between dotted visualization lines of the integration point remains unchanged. Thus, all stress components on the integration point are zero and no strain energy is generated in this bending mode of deformation. This mode of deformation is called zero-energy mode and the element is not able to resist this type of deformation. This called the hourglass effect and needed to be controlled. Abaqus software adds an artificial 'hourglass stiffness' on the reduced integration elements to limit the hourglassing[10].

4.3.2 Energy Balance

When dealing with an explicit simulation, considering the energy outputs is essential to evaluate a proper response of the system. In Abaqus software, energy balance equation of an explicit numerical analysis is described as below [11].

Unused variables in this study such as external heat energy, fluid cavity energy, etc. are neglected in equations.

$$E_I + E_{VD} + E_{FD} + E_{KE} - E_W = E_{total} = constant \tag{9}$$

where: E_{KE} = Kinetic energy (ALLKE)

E_I = Internal energy (ALLIE)

E_{VD} = Energy absorbed by the viscous dissipation (ALLVD)

E_{FD} = Energy absorbed by frictional dissipation (ALLFD)

E_W = Work of external forces (ALLWK)

E_{total} = Total energy of the system (ETOTAL)

The sum of all energies in the system (E_{total}) should be constant and should not exceed an error of 1% in numerical simulations. Internal energy E_I is also described as;

$$E_I = E_E + E_P + E_A \tag{10}$$

where: E_E = Recoverable elastic strain energy (ALLSE)

E_P = Inelastic dissipation energy such as plasticity (ALLPD)

E_A = Artificial strain energy (ALLAE)

As mentioned below, hourglassing should be prevented and Abaqus software uses artificial strain energy E_A for this purpose. Artificial strain energy includes the energy stored in hourglass resistances and should be kept below a very low percentage of the internal energy. Otherwise, it is needed to make a mesh refinement to use more elements or other structural changes to avoid hourglassing[11].

4.3.3 Constraints

In Abaqus FEM software, constraint definitions can be used to constrain the degrees of freedom between regions of a model. Two of the main constraint definitions used by Abaqus are briefly described below.

Mesh Tie Constraint

A mesh tie constraint is a surface-based connecting method and ties two surfaces during the simulation. It can be used in a large variety of problems such as mechanical, acoustic pressure, coupled temperature displacements, coupled thermal-electrical or heat transfer simulations. This type of constraint can equalize both translational and rotational motion for pair of surfaces.[10]

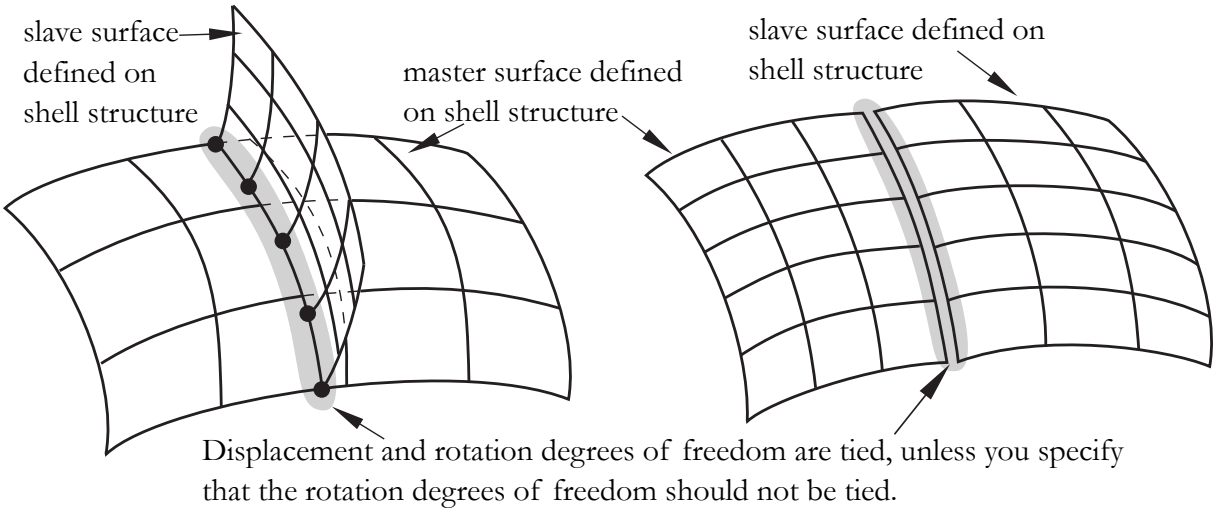

Figure 4.5: Example of two components tied together.[11]

The surface-based tie algorithm used in Abaqus software is illustrated in Figure 4.5. Surface-based tie constraint has two main approaches which are surface-to-surface and node-to-surface. One of the main downside of the surface-based tie constraint is that a rigid surface cannot be defined as a slave surface in a constraint pair.

Coupling Constraint

A surface-based coupling constraint is used to couple the motion of a group of nodes on a surface to the motion of a reference node. Coupling constraints may be used in both geometrically linear and nonlinear analysis as well as with two or three dimensional stress/displacement elements. In the current study, kinematic coupling constraint definitions are used to connect rigid bodies to the deformable structures. The motion in selected degrees of freedom are constrained to the generated rigid body reference node.

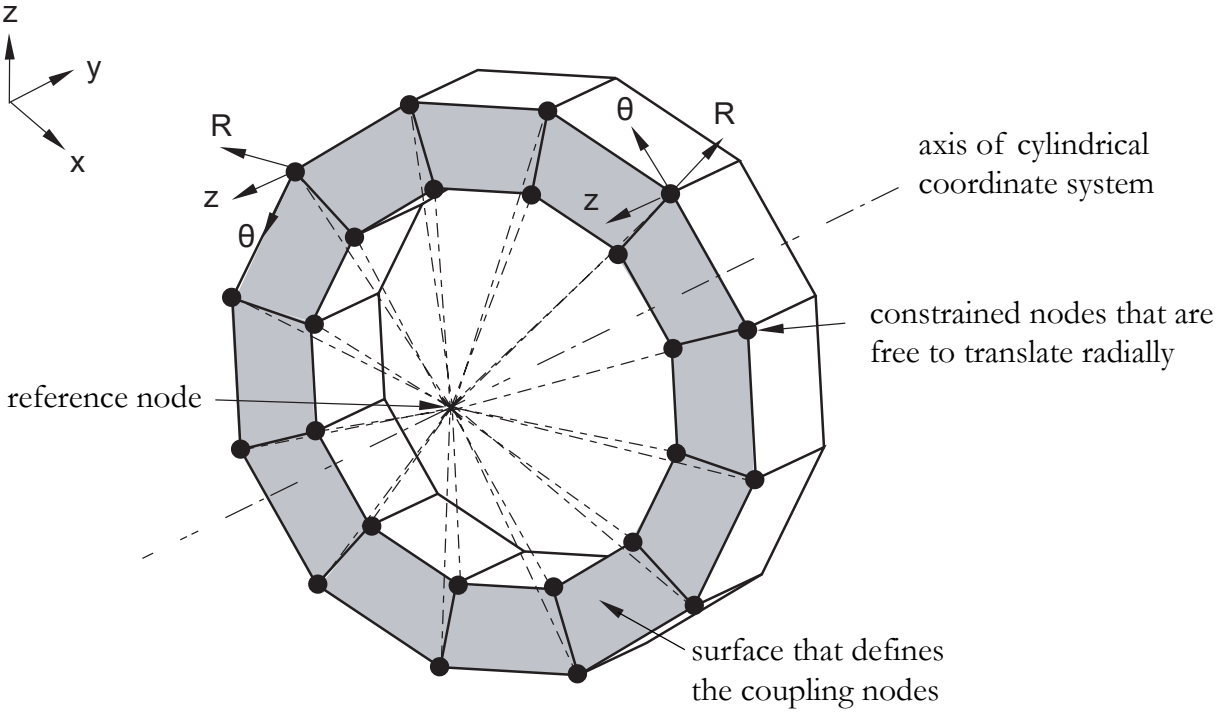

Figure 4.6: Kinematic coupling constraint [11]

The coupling constraint is beneficial to constrain the motion of a group of nodes to the rigid body motion of a single reference node. This type of coupling constraint is called kinematic coupling constraint.

The coupling constraint is mainly used to apply loads and boundary conditions to a model by using surface definitions and a reference node. A kinematic coupling constraint of a model, where a twisting motion is prescribed by using a kinematic coupling constraint in Figure 4.6.

4.3.4 Contact

For a nonlinear finite element simulation, contact is an extremely discontinuous form of nonlinearity and must be defined carefully. In this study, for modeling the interaction between the absorber structure and the rigid plates such as rigid wall and striking plate, some constraints and methods are chosen in Abaqus FEM software. The terminology of these necessary parameters and methods are briefly described below.

Contact Formulation

In the Explicit solution module of Abaqus, a surface-based contact method is used and this method has two main contact algorithms: the general contact algorithm and the contact pair algorithm.

The **general contact algorithm** is an automatic contact algorithm that allows defining contact of a system with automatically generated all-inclusive surface definitions. Despite being an automatic algorithm, one can include/exclude surface pairs if needed. General Contact Algorithm has a very few restrictions on the types of surfaces involved in the contact definition. Thus, it allows very few properties to define the contact in a simulation. This algorithm can be used only in mechanical finite-sliding contact analyses and does not support kinematic constraint enforcement.[11]

The **contact pair algorithm** is a manual contact algorithm used for modeling contact between surface definitions that could potentially be in contact. Contact interactions for contact pair algorithm are defined by specifying surface pairs and self-contact surfaces. In Abaqus, contact pair definition has less restrictions when compared to the general contact. It can be used in a combination with general contact algorithm. It can also be defined to a pair of rigid or deformable surfaces [11]. Figure 4.7 shows a master-slave contact pair defined with contact pair algorithm.

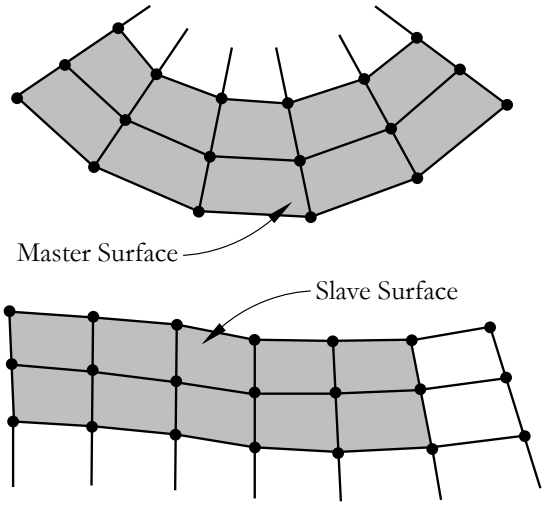

Figure 4.7: A contact pair surface interaction with friction.

Contact Constraint Enforcement

The explicit module of Abaqus FEM software uses two methods for contact constraint enforcement: Kinematic contact formulation and the penalty contact formulation. Both formulations are briefly descried and compared below.

The **kinematic contact formulation** uses a predictor/corrector method to accomplish an accurate agreement within the contact conditions. Software proceeds the first increment under the assumption that contact between surfaces does not exist. If the software detects an over-closure at the end of the increment, it modifies the acceleration to obtain a correct contact constraint enforcement configuration. Because of being a predictor/corrector method, it has no influence on stable time increment of the simulation. The kinematic contact formulation is used as default method for contact pair algorithm in Abaqus/Explicit module but penalty method can also be implemented for individual contact pairs. [11]

The **penalty contact algorithm** cannot enforce the contact formulation but allows for handling more types of contact such as contact between two rigid bodies. Abaqus Explicit module applies a spring stiffness to penetrating nodes to prevent penetration between surfaces. Amount of the spring stiffness applied by the software is chosen automatically and relates the contact force to penetration distance. An opposite contact force with magnitudes equal to the penalty stiffness times the penetration distance is applied to the nodes at which the penetration occurs. Penalty stiffness can be modified for surface-to-surface contact interactions by defining a scale factor to optimize time incrementation and so numerical stability. [10]

Sliding Formulation

The Abaqus/Explicit module, sliding formulation approaches are used to define the relative motion of two surfaces of a contact pair.

Finite-Sliding formulation is the most general approach in Abaqus/Explicit and allows any unpredicted motion of the surfaces such as separation, sliding and rotation. For self-contact or contact involving rigid surfaces can only be modeled by using finite sliding formulation. [10]

Small-Sliding formulation assumes that there will be relatively little sliding of one surface to another, even if two bodies undergo large motions. This formulation has a local tangent plane for each slave node and does not have to monitor slave nodes for any possible contact. By this reason, small sliding is less computationally expensive compared to finite sliding.[10]

Contact Pressure-Overclosure Relationship

The term **"hard contact"** is one of the terms used in Abaqus FEM software to define contact pressure-overclosure relationship. In hard contact property, it is not allowed to transfer any contact pressure between master and slave surfaces when there is no contact. When surfaces are in contact, there is no limitation for the magnitude of the contact pressure. The most useful feature of the "hard contact" property is, this relationship keeps the penetration of the slave surface into the master surface at minimum.[10]

4.4 Johnson-Cook Plasticity Model

The Johnson-Cook plasticity model [39] is a phenomenological model used to describe the plastic and strain-rate dependent hardening of materials. The model introduces three key material responses which are the strain hardening, strain-rate effects and the thermal softening. These three effects are combined in the Johnson-Cook constitutive model in a multiplicative manner.

$$\bar{\sigma} = \left[A + B\,\varepsilon_{pl}^{n}\right]\left[1 + Cln\left(\frac{\dot{\varepsilon}_{pl}}{\dot{\varepsilon_0}}\right)\right]\left(1 - \hat{\theta}^{m}\right) \tag{11}$$

where: $\bar{\sigma}$ = Yield stress at nonzero strain rate [Pa]

ε_{pl} = Effective plastic strain

$\dot{\varepsilon}_0$ = Reference strain rate

A = Initial yield stress at $\dot{\varepsilon}_0$ $[Pa]$

B = Strain hardening coefficient [Pa]

C = Strain-rate hardening coefficient

n = Strain hardening exponent

m = Temperature exponent

The Johnson-Cook constitutive model uses a Mises yield surface with associated flow and it is one of the most used yield criteria in the current literature. The first bracketed term represents the strain hardening of the yield stress of the material. The next term represents the effects of the elevated strain rates on the yield stress. The final part of the model formulates the thermal softening of the yield stress depending on the temperature conditions. The temperature parameter of the model is described below. [11]

$$\hat{\theta} \equiv \begin{cases} 0 & \text{for} \quad \theta < \theta_{transition} \\ (\theta - \theta_{transition})/(\theta_{melt} - \theta_{transition}) & \text{for} \quad \theta_{transition} \leq \theta \leq \theta_{melt} \\ 1 & \text{for} \quad \theta > \theta_{melt} \end{cases} \tag{12}$$

where: $\theta_{transition}$ = Transition Temperature

θ_{melt} = Melting temperature

θ = Current temperature

$\hat{\theta}$ = Homologous temperature

The Johnson-Cook material model is an uncoupled model that can be used with or without each bracketed part of the model. In this study, the model is assumed to be simulated in room temperature, thus the effect of temperature on thermal softening of the yield stress is neglected. The equation of the Johnson-Cook model used in this study is as given below.

$$\bar{\sigma} = \left[A + B\,\varepsilon_{pl}^{n}\right]\left[1 + Cln\left(\frac{\dot{\varepsilon}_{pl}}{\dot{\varepsilon_0}}\right)\right] \tag{13}$$

In the present study, only the necessary values of the Johnson-Cook plasticity model are implemented into the input files of the simulations. In Abaqus software, the values of A, B, n and m are provided as part of the metal plasticity material definition. For the Johnson-Cook rate dependence, the values of C and $\dot{\varepsilon_0}$ are defined. The values of the material definition parameters used in this study are given in further relevant sections.

4.5 Mass Scaling

The explicit central difference method calculations are done by integrating the equations of the problem in time. Thus, the discrete mass matrix of the equilibrium equations is very important for both computational efficiency and simulation accuracy. To simulate a quasi-static problem using the explicit method require a large number of steps because the duration of the event is large. For this reason, increasing the mass of the numerical model artificially (mass scaling) is mostly useful to increase the maximum step size, and so reducing the number of steps and the solution time of the simulation.

Mass scaling can be accomplished by increasing the material density or scaling up the mass of the model. Scaling up the mass by a factor of f^2 increases the time step by a factor of f. [10] This technique has been used for modeling quasi-static crush response of various energy absorber structures under impact loading. [40, 41, 42] In Abaqus/Explicit package, two types of mass scaling can be used; fixed mass scaling and variable mass scaling. Both mass scaling types of the software can be used together or separately to define an overall mass scaling strategy. It can be also applied to the entire model or on a selected element set.When using the mass scaling technique in a quasi-static simulation, the results must be checked to ensure that the inertia and the loading effects are not present. The suitability of the applied mass scaling parameters should be controlled by ensuring the ratio of the kinetic energy to the internal energy is not more than 5%. Also the reaction force should not be affected by the factor of mass scaling.

4.6 Data Processing Method

In this study, resultant data obtained from numerical finite element simulations are processed to eliminate the noise and numerical errors. For this purpose, a data smoothing algorithm is implemented by using a multi-paradigm numerical computing environment MATLAB. The same software is also used to plot the processed data in many different combinations to gain insight about the results of the simulations.

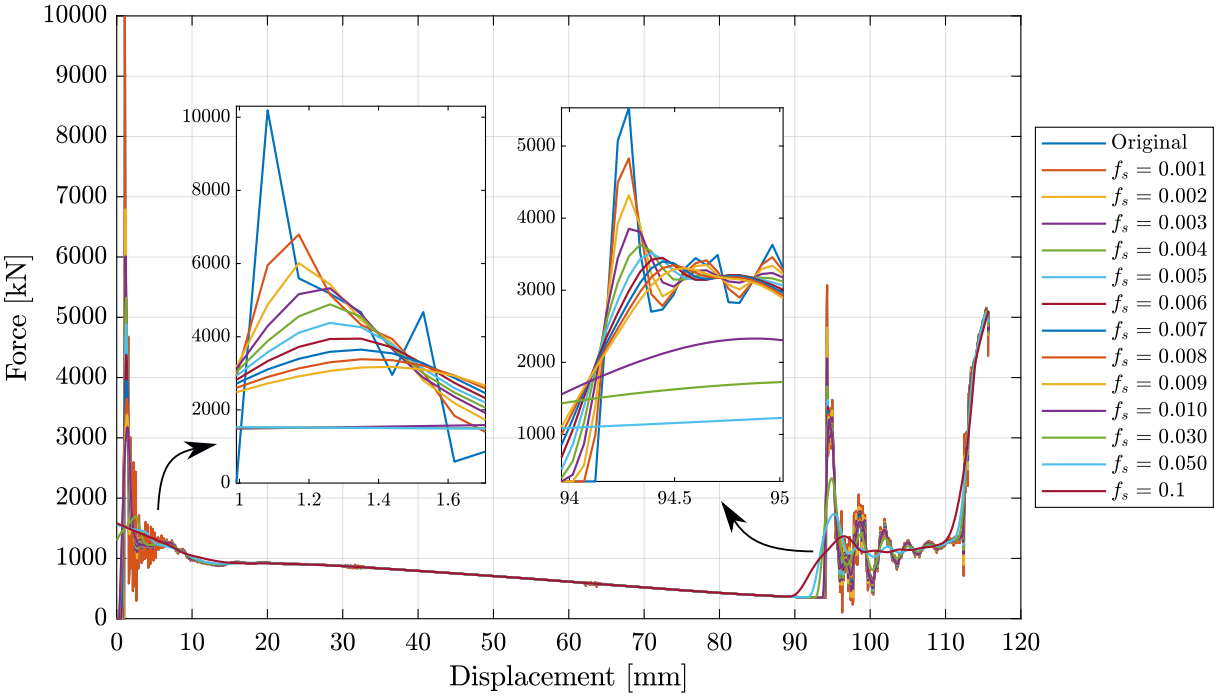

Figure 4.8: Data smoothing results for different span values.

The raw data obtained from the simulations usually have noise and irrelevant numbers due to many possible reasons such as dynamic effects, contact interactions, etc. These meaningless numbers are needed to be extracted from the dataset to obtain a smooth and comprehensible results. In this study, a nonparametric regression method is used to smooth the resultant data recorded from the numerical simulations.

One of the most commonly used regression method 'lowess' is selected to be used for the complete dataset. The word 'Lowess' stands for *'Locally Weighted Scatterplot Smoothing'*, which was introduced by Cleveland in 1979. [43] This method is called local because each smoothed value is calculated by using adjacent data points in the range of selected span. A regression weight function is defined for the data points between the selected span.

The difference of this method to the regression is that 'lowess' uses a linear polynomial. The span used in the method must be selected between 0 and 1. The closer the span to 1, gives a smoother result by using a higher percentage of the total number of data points.[44]

A data smoothing study is performed to the randomly selected datasets to ensure the optimum span to smooth the noisy data. Meanwhile it is important to keep some peak points which may have an important role to figure out the energy absorbing characteristics of the models. Smoothed results for a variety of span (f_s) values are plotted in Figure 4.8 in order to select the most reasonable span.

For all simulation results, a span of 0.006 ($f_s = 0.006$) is selected which is sufficient enough to smooth the noisy data and small enough to keep peak data points of the simulations. Two examples of original raw data and smoothed values for the selected span ($f_s = 0.006$) are plotted in Figure 4.9 for two different impact velocities ($10m/s$ and $30m/s$) and for the model with thickness of $10mm$ and base conical angle of 30°.

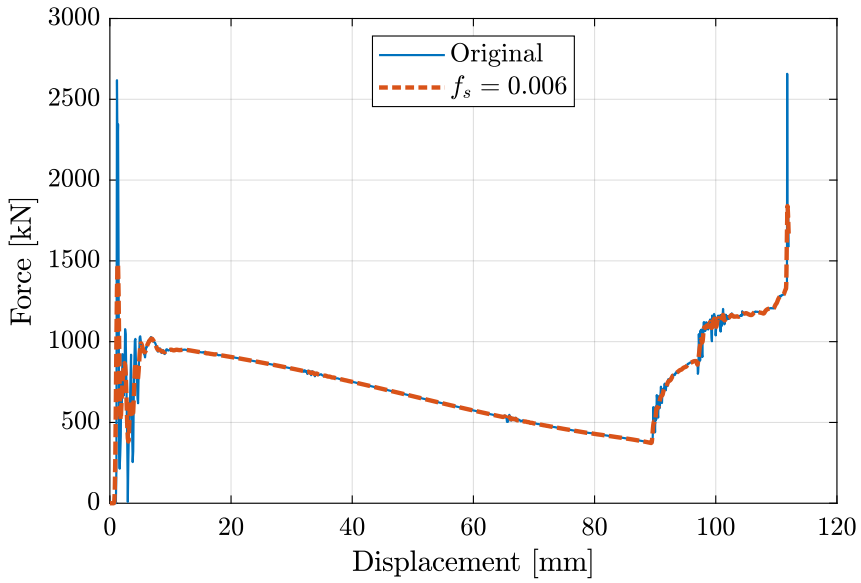

(a) F-d plot for $10m/s$

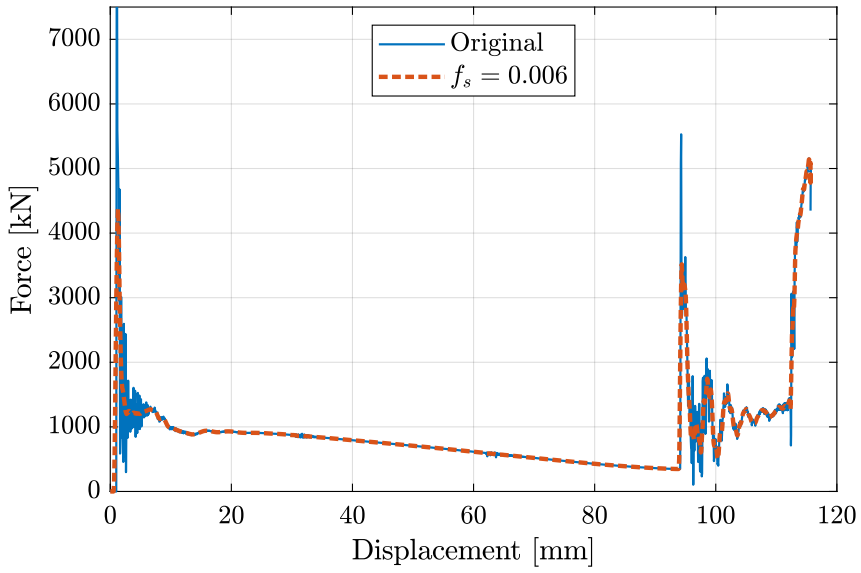

(b) F-d plot for $30m/s$

Figure 4.9: Smoothed force-displacement plots for the velocities $10m/s$ and $30m/s$.

5 Numerical Model and Simulations

The numerical models for the simulations were created using the CAE user interface module of the FEM software Abaqus. [10]

5.1 Model Geometry

In the present study, it is intended to investigate the effect of impact velocity, impact mass, impact energy and the thickness of the absorber. By this reason, almost 150 different input files for the numerical models were created and executed. A basic sketch of the absorber structure is given in Figure 5.1 with dimension parameters.

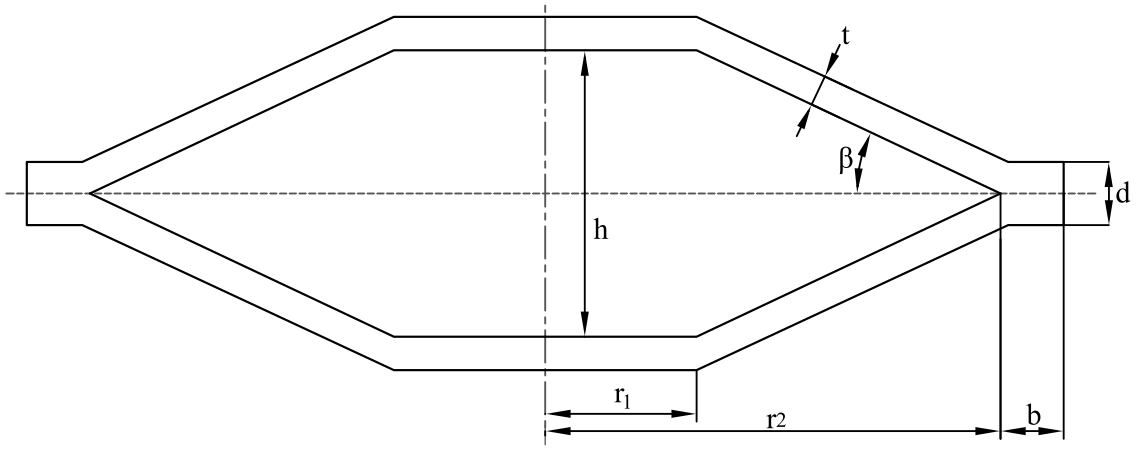

Figure 5.1: Geometry and dimension parameters of the absorber structure.

Dimension parameters used to model the structures are, inner diameter r_1, outer diameter r_2, edge ring width b, edge ring height d, thickness t, cone angle β and deformation length h. The edge ring width b is kept constant in all simulations, hence the effect of this parameter on the energy absorbing capability of the structure is not investigated in the current study. Also the edge ring height d is considered to be two times of the absorber thickness t, which is recalculated for the thickness of each model. Values used for all parameters are given in Table 5.1.

Table 5.1: Dimension values of the absorber structures used in simulations.

β	**h**	**t**	**b**	**d**	$\mathbf{r_1}$	$\mathbf{r_2}$
[deg]	[mm]	[mm]	[mm]	[mm]	[mm]	[mm]
20	72.8	10	20	20	50	150
25	93.3	8		16		
30	115.5	6		12		
		4		8		

The deformation length h is calculated for each model with respect to the cone angle β, inner diameter r_1 and the outer diameter r_2. The varying values of the thickness are modeled as outer offset of the geometry to keep the deformation length constant for all models of the same conical angle. Also the edge ring height d varies depending on the absorber thickness t.

The rigid part instances of the model assembly which are called as the *striker plate*, *top plate* and the *bottom plate* are modeled by using equal dimensions. Since all the simulations were done with quarter model to generate more time-effective simulations, rigid plates were also modeled as quarter circular plates. Numerical model of the rigid plates is illustrated in Figure 5.2 with selected dimensions. Rigid plates were modeled with higher diameter values in order to ensure sufficient contact area after the conical absorber is deformed.

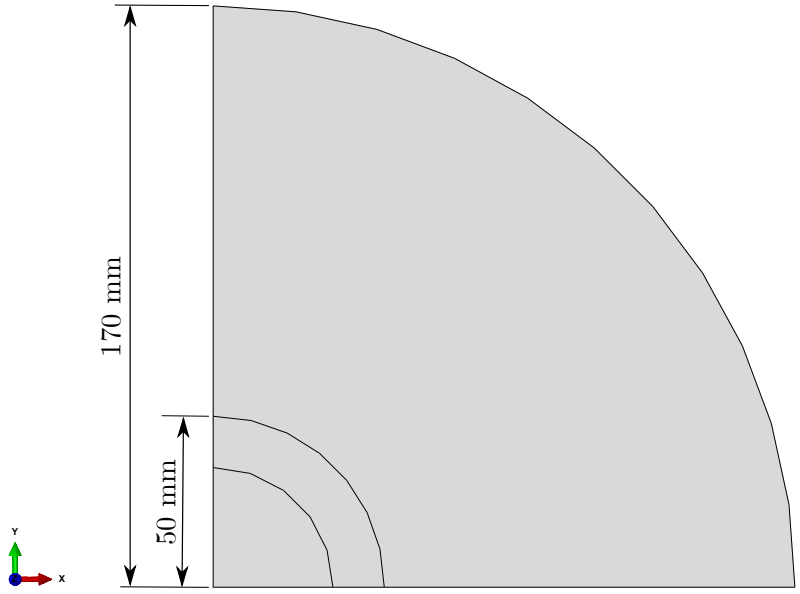

Figure 5.2: Geometry and dimension parameters of the rigid part instances.

In addition to dimension values given in Table 5.1, three different striker mass combinations are also investigated, which required to the analysis to be done again for each mass quantity using the same dimensions. The striker mass combinations are explained in detail in further relevant sections.

5.2 Material Properties

The material used for the simulations were considered to be structural mild steel denominated as S235JR because of its huge implementation in industrial applications and accessibility. Structural steels like S235JR are well known for their applications because they are easy to manufacture, stable and suitable for welding. In numerical analysis, an elastoplastic hardening module was implemented to simulate the material behavior of the structural mild steel S235JR.

Tensile tests were performed to determine the mechanical properties of the selected material S235JR. The tensile test specimens were machined from hot rolled pipe with respect to the geometrical dimension parameters according to the EN ISO 6892-1 standard.[12] The dog-bone geometry of the test specimen is given in Figure 5.3.

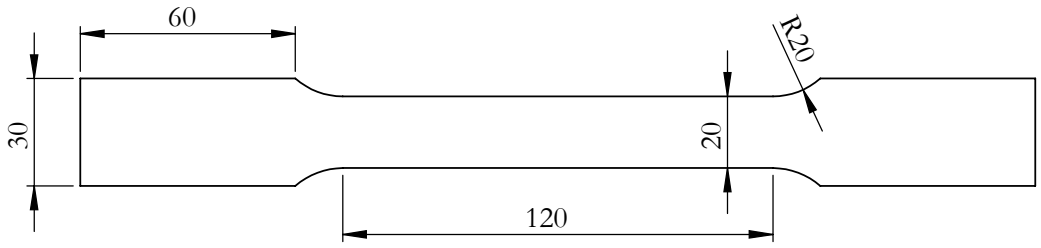

Figure 5.3: Dimensions of the dog-bone specimen. [12]

Tensile tests were performed using a computer controlled testing device manufactured by INSTRON® company. The cross-head velocity was selected to be $5mm/min$ and 3 repetitive tests were made. After placing the specimens to the testing device, a SCHENK® branded mechanical extensometer with a range of $25mm$ from the midpoint were placed on the test specimen. Tensile test setup is given in Figure 5.4.

Table 5.2: Mechanical properties of material S235JR.

Material Property	**Value**	**Unit**
Young's Modulus	200	GPa
Poisson's Ratio	0.29	-
Mass Density	7980	kg/m^3
Yield Strength	296.4	MPa
Ultimate Tensile Strength	381	MPa

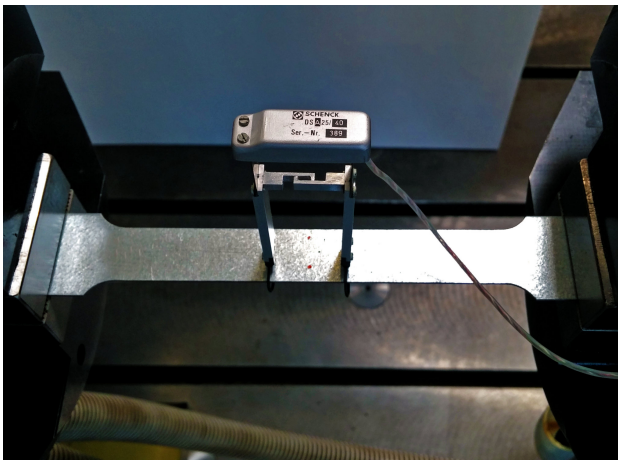

(a) Dog-bone specimen with extensometer.

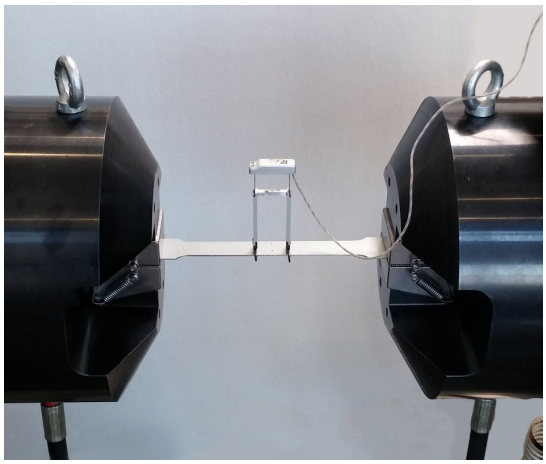

(b) Mounted sample on the test device.

Figure 5.4: Experimental setup for tensile testing.

After completing the tensile tests, Stress-Strain diagrams were generated using the data obtained from the test setup. Mechanical properties of the material are given in Table 5.2. The plastic proportion of the material properties are plotted in Figure 5.5 as engineering and true stress-strain considering the average values of the three repetitive tests. The true stress values were calculated up to the instability point (Necking) using following equations.

$$\sigma_t = (1 + \varepsilon)\sigma \tag{14}$$

$$\varepsilon_t = ln(1 + \varepsilon) \tag{15}$$

where σ_t is true stress, ε_t is true strain, ε is the engineering strain and σ is the engineering stress obtained from tensile tests.

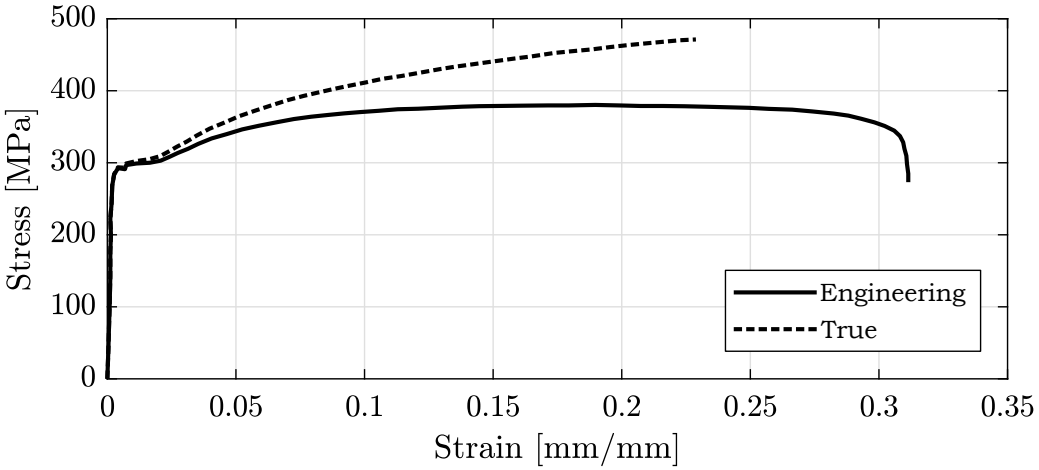

Figure 5.5: Engineering and true stress-strain diagrams of S235JR steel.

Material properties are of great importance at crashworthiness and impact studies. The plastic flow of some materials is sensitive to loading speed, which is known as material strain-rate sensitivity, or viscoplasticity. Strain rate sensitivity varies for different materials, and often change at varying temperature and loading conditions. When the impact occurs or a sudden force is applied, the molecules in the material does not have enough time to reorient themselves and may break immediately and behave like a brittle material. The same material can react differently under different strain rates. Strain rate dependency of the material can be measured in laboratory using special test equipments.

The strain rate sensitivity phenomenon can influence the dynamic response of the energy absorbing structures. Previous studies have indicated that S235 steel displays a significant positive strain rate effect on the yield stress of the material. [13, 45] Verleysen et. al. [13] have investigated the influence of the strain rate on the forming properties of three commercial steel grades including S235JR. They have carried out both static tensile tests and split Hopkinson tensile bar experiments to examine the influence of the strain rate on the stress-strain curves of the materials. The split Hopkinson tensile bar experiment setup is shown in Figure 5.6.

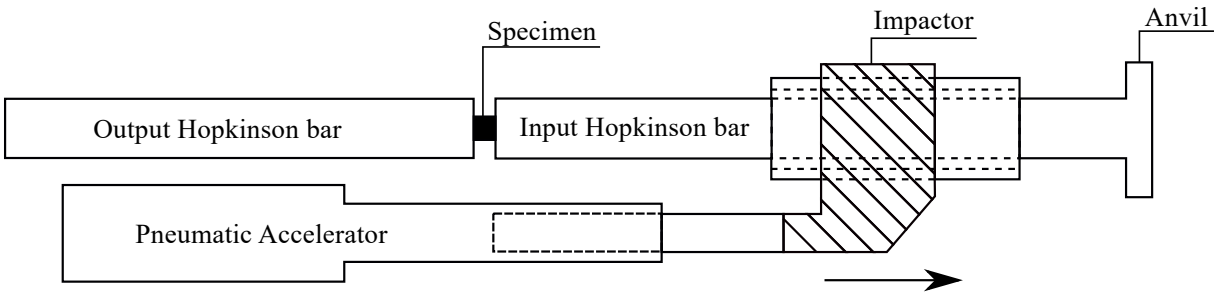

Figure 5.6: Schematic representation of the Split Hopkinson Tensile Bar setup. [13]

The authors then used the obtained tensile test results and the SHTB experiment results to model the behavior of the investigated steel grades. The phenomenological Johnson-Cook model was used in modeling of the constitutive behavior of the steels. Both static and the SHTB experiment results of the S235JR steel are shown in Figure 5.7 as stress-strain curves for different strain rate values.

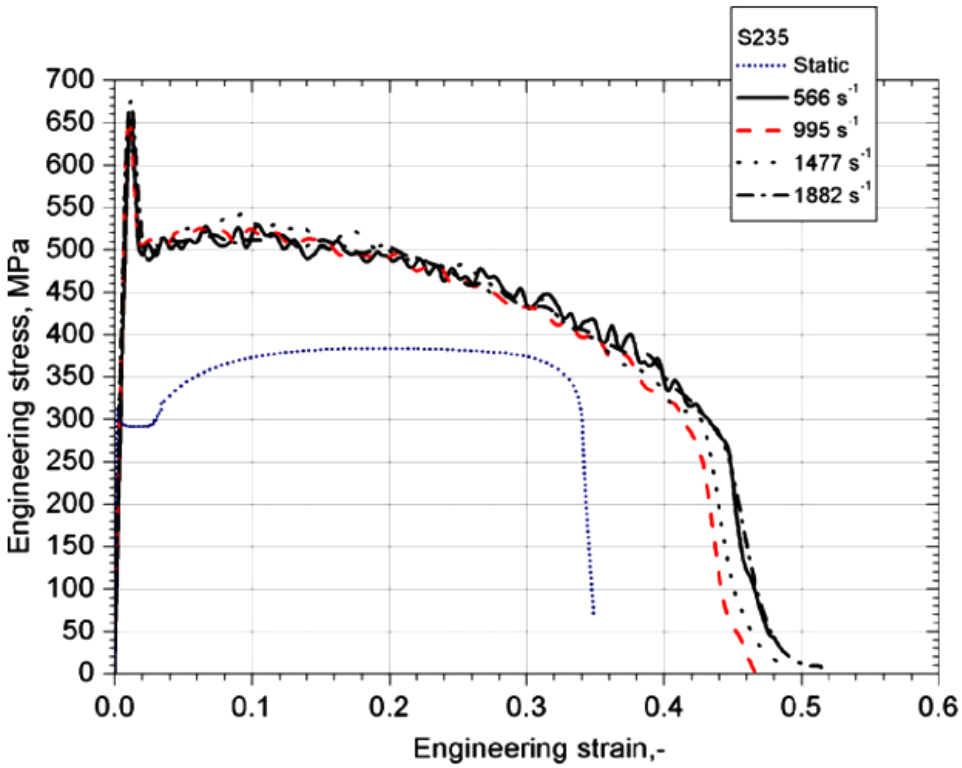

Figure 5.7: Representative static and dynamic engineering stress vs strain curves of the S235JR steel. [13]

The static tensile test results of the present study and the results from the aforementioned article by Verleysen et. al. [13] are compared and they are found to be essentially identical for the S235JR steel. Due to the technical impossibilities and the lack of equipment for SHTB experiments, the Johnson-Cook model of the S235JR steel with strain rate properties are adapted to the numerical models of the present study. Consequently, the Johnson-Cook plasticity model parameters including strain rate used in this study are given in Table 5.3.

Table 5.3: Johnson-Cook plasticity model parameters of S235JR steel. [13]

Parameter	Unit	Value
A	[MPa]	280
B	[MPa]	667
n	[-]	0.72
C	[-]	0.071
$\dot{\varepsilon}_0$	$[s^{-1}]$	5.6x10^{-4}

The variations of the geometry parameters of the model cause the length and weight of the structures to change. The length and the weight of the structures are important parameters when calculating the performance parameters such as SEA and absorbed energy per unit deformation. The weight of the structures for different geometrical parameters are calculated with respect to the material properties and are given in Table 5.4 by means of the conical angle and absorber thickness.

Table 5.4: Mass of the structures by means of base conical angle and absorber thickness.

Conical angle	Absorber thickness			
β	$10mm$	$8mm$	$6mm$	$4mm$
20°	$15.24kg$	$12.16kg$	$9.12kg$	$6.08kg$
25°	$15.68kg$	$12.52kg$	$9.40kg$	$6.28kg$
30°	$16.28kg$	$13.00kg$	$9.76kg$	$6.48kg$

5.3 Model Assembly

Structures were modeled by creating each plate and the absorber as quarter models of real dimensions of structures. The influence of simplification of the geometry as the quarter model definition is investigated and given in Section 5.6.1 in detail. The model assembly includes three equally designed rigid plates and a conical absorber. The conical absorber was positioned between two rigid plates (top and bottom plate) to simulate a crush box and also to control the deformation of the structure. Rigid plates were constrained to the absorber using the constraint definitions explained in further sections. The third plate (striker plate) is used to simulate the striking mass crushing to the conical absorber. A gap of $1mm$ between the top plate and the striking plate was modeled to examine the effect of the first contact more conveniently. Also preventing an initial contact between plate surfaces in the first step of the simulation is decided to be more beneficial for the investigation of the impact. The general assembly of all parts used in models are plotted in Figure 5.8.

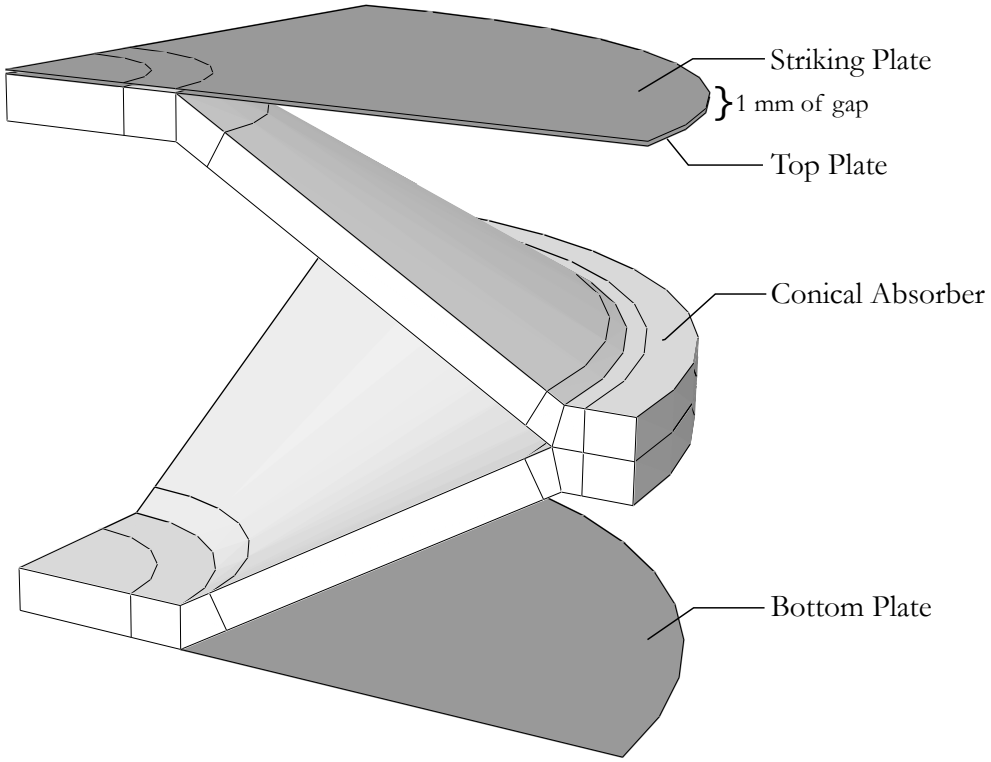

Figure 5.8: Assembly of the quarter model of absorber and the rigid plates.

5.4 Loading Conditions

In the present study, energy absorbing capabilities of the structures were investigated under both quasi-static and dynamic loading conditions. Loading conditions were modeled with different methods which are suitable for each case.

Quasi-Static Loading

In quasi-static numerical simulations, the load is applied very slowly that the deformation of the structure is not affected by the strain rate and inertia forces which are very small and negligible. Therefore, it is possible to investigate the effects of the inertia forces on the deformation characteristics of the structure as a function of impact velocity. For the quasi-static simulations, loading was applied to the rigid striking plate as a predefined velocity over the longitudinal axis of the model assembly. Quasi-static simulation velocity is selected to be $0.01 m/s$ in order to ensure that no inertia effect is present. The existence of the inertia effects were controlled by checking the ratio of the kinetic energy to the internal energy during the simulations.

The motion of the rigid striking plate was defined using the AMPLITUDE option of the FEM software and constrained to translate only in the direction of the predefined velocity. To ensure a smooth motion of the rigid plate, SMOOTH STEP sub-option of Abaqus/Explicit is used. The smooth step sub-option of the software applies the load smoothly by a non-linear interpolation.

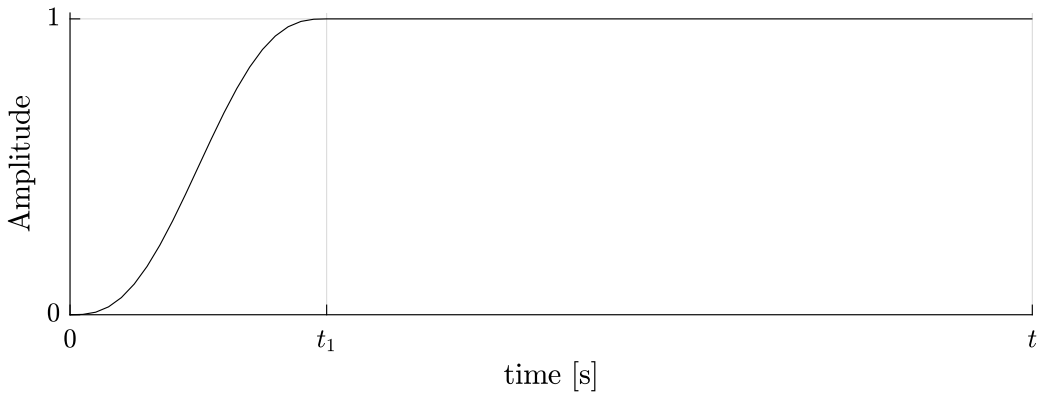

Figure 5.9: Quasi-static loading amplitude of the models with smooth step definition.

The transition time t_1 and the total step time t are defined for each model to ensure the rigid body has a smooth motion rather than a sudden movement which can induce noisy and inaccurate solutions [10]. Figure 5.9 shows the amplitude curve describing the motion of the rigid body, with zero gradient at the start and finish of the selected step time to ensure smooth motion. The transition time t_1 are selected to be $40ms$ which gave reasonable results.

Dynamic Loading

In order to understand the dynamic response of the conical energy absorber, it is planned to apply the load as kinetic energy. The kinetic energy was generated by defining a velocity and a mass to the striking plate. An isotropic mass is specified to each model for the selected combination. Used mass quantities are calculated to obtain $100kJ$ of initial kinetic energy for each model. Moreover, mass values of $1000kg$ and $2000kg$ were defined for each impact speed to investigate the effect of the impact mass. Four different impact velocities ($5m/s$, $10m/s$, $20m/s$ and $30m/s$) were selected and simulated for each impact mass, base conical angle and absorber thickness combination.

All velocity and isotropic mass values were defined to a reference point on the rigid striker plate. Whole motion of and degrees of freedom of the striker plate is controlled by this defined reference point. Impact velocity and impact mass values in previous studies in the current literature and international standard were taken into consideration while selecting the impact mass and velocity for the current study.

5.5 Interactions and Boundary Conditions

5.5.1 Interactions Between Part Instances

Interactions between parts were defined using self-contact and surface to surface contact algorithms. Self-contact was used to define self-contact of absorber structure with penalty contact having a friction coefficient of 0.3 as tangential contact behavior and

hard contact as normal contact behavior. Surface to surface contact is defined between all plates and energy absorber structure as penalty contact with finite sliding in order to make sure that no penetration occurs.

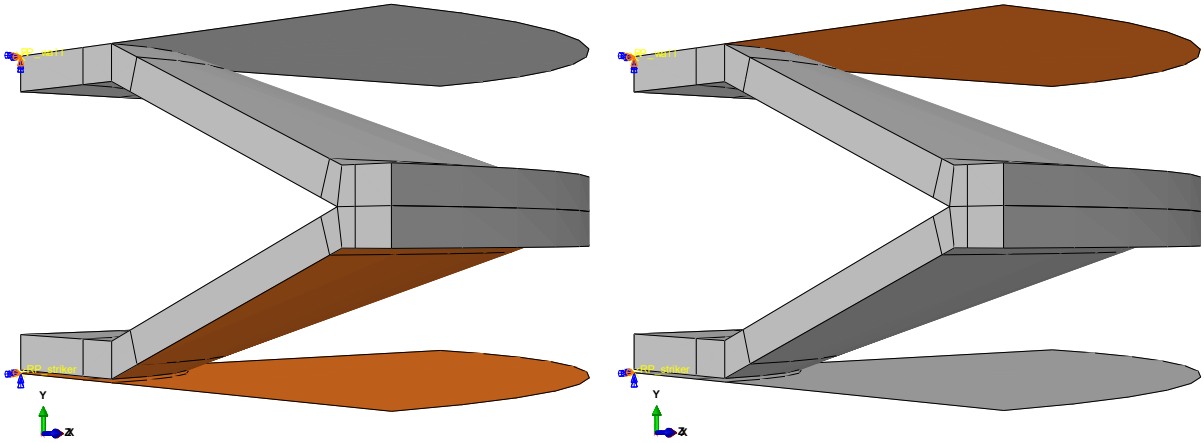

(a) A surface-to-surface contact pair. **(b)** Coupling definition.

Figure 5.10: Visualization of coupling and contact definitions of the model.

To simulate a crush box, the conical energy absorber was coupled to two rigid plates from the top and bottom surfaces. A kinematic coupling definition was used. Top and bottom surfaces of the absorber were coupled to the reference point of the top and bottom rigid plates using a node-to-surface coupling definition. Illustrations of the contact and coupling definitions are illustrated in Figure 5.10.

5.5.2 Boundary Conditions

In order to prevent unrestrained motion of the total assembly, all boundary conditions were defined carefully. Any movement of the bottom plate was restrained using an encastre boundary condition definition. The top plate and striker plate were allowed for translations on the y-axis direction and any other movement of the plates were restrained. All boundary conditions including symmetry and displacement of the plates were plotted in Figure 5.11.

As mentioned before, all simulations were done with quarter models to reduce the time cost of the simulations. For this purpose, symmetry boundary conditions were used for both edges of the absorber. X-symmetry definition for the edge on y-z plate and z-symmetry definition for the edge on x-y plate were made. In order to ensure the accuracy of the results of quarter model simulations depending on the symmetry condition, completely circular models were also generated for selected geometry, mass and velocity combinations. It was clearly seen that the results from the quarter-model and complete model simulations have an exact match on resultant values and deformation modes.

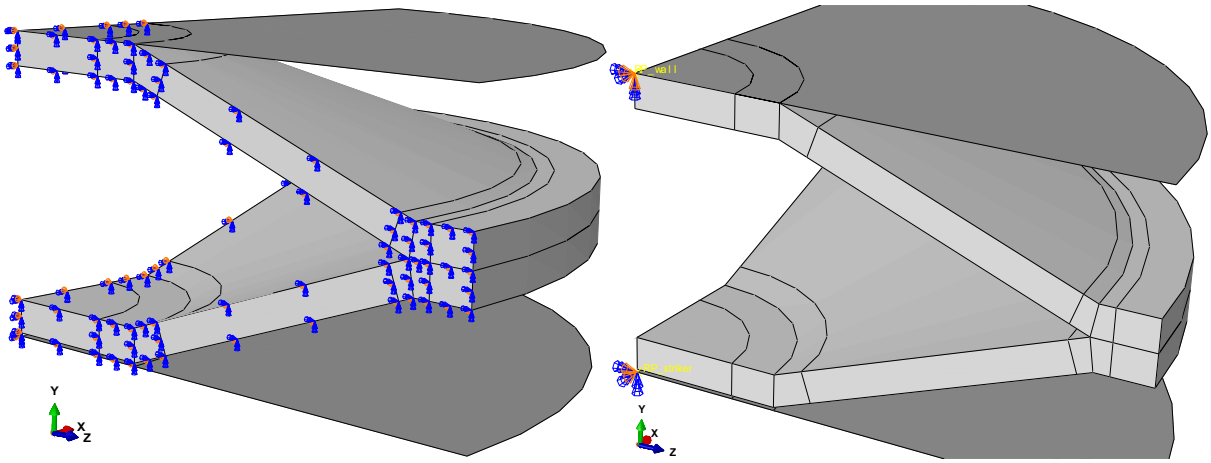

(a) Symmetry boundary conditions of absorber **(b)** Displacement boundary conditions of plates

Figure 5.11: Visualization of boundary conditions of models

5.6 Sensitivity Analysis

The sensitivity of the numerical simulations against the model simplification, mesh size and the mass scaling method were investigated. All of the sensitivity simulations are made on the same computer with hardware specifications given below in Table 5.5 to make a reasonable comparison of the time costs of analyses. Duration values may vary between different hardware configurations as well as number of CPU threads used in parallel.

Table 5.5: Hardware specifications of the computer used for the sensitivity analyses.

Component	Description
Model	HP Z420 Workstation
CPU	Intel® Xeon® E5-1620
Memory	32GB
GPU	NVIDIA® Quadro® 410
Operating System	Microsoft® Windows 7® Professional

5.6.1 Model Simplification

The development of FEA software capabilities and computer hardware power enabled running more complex and advanced analyses such as non-linear, fracture mechanics and explosion. However, such advanced analyses are still dependent on high computing resources and can have extremely long running times. Therefore, some model simplification methods can be used to run the analyses with less time cost and/or computer resources. One of the main simplification method is planar symmetry, in which the model is sliced in half, quarter or even eight equal parts. The main rule for using planar symmetry is, the geometry, loading, material and the boundary conditions must be symmetrical.

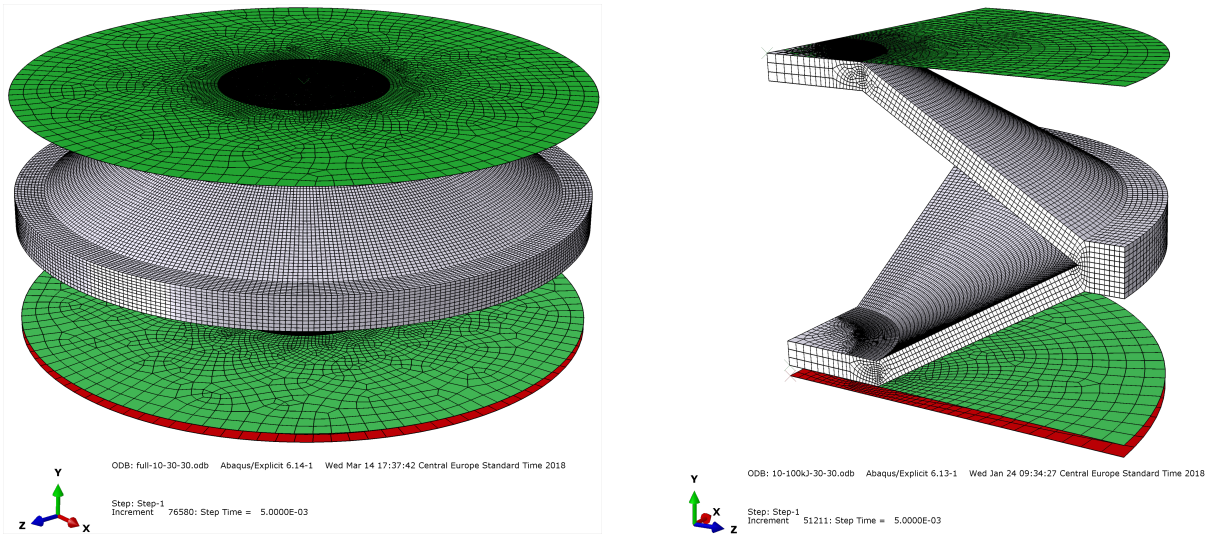

(a) Full model. **(b)** Quarter model.

Figure 5.12: Visualization of the full model and the quarter model.

In the present study, the model, material and the boundary conditions exhibit symmetry. The results of the full model analyses also have symmetric behavior. In this manner, the planar symmetry method is applied to the model and a quarter model is generated. The meshed plots of the full model and the quarter models are shown in Figure 5.12.

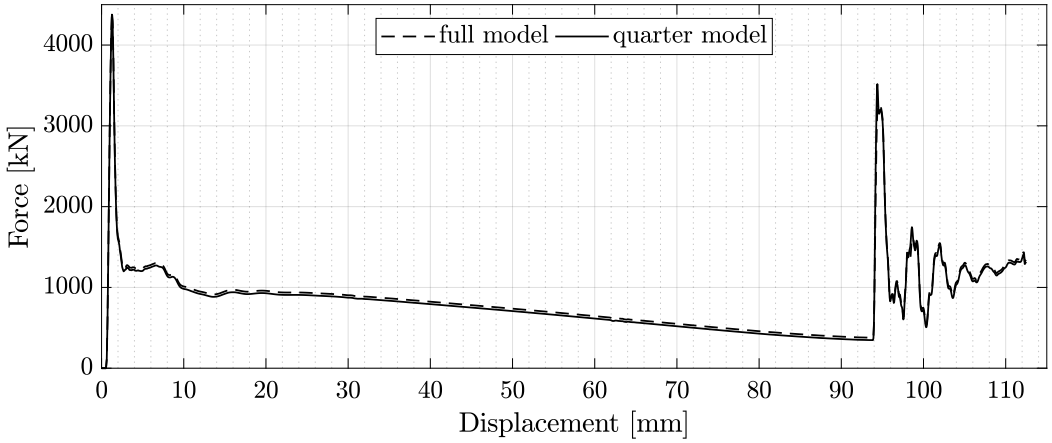

Figure 5.13: Comparison of the force-displacement response of the full model and the quarter model.

Figure 5.13 shows the reaction force history of the full model and the quarter model as a function of displacement. It is clearly seen that there is no significant effect of planar symmetry on the reaction force response of the structure. However, the time cost and the file size of the results decrease significantly while having almost the same output values. Simulations using the full model are approximately seven times slower and requires eight times more drive space to store the output files. The output file size also effects the post-processing stage of the results due to the large amount of data. The comparison of the results for the chosen configuration ($\beta = 30°$, $t = 10mm$ and $V = 30m/s$) taken from both full model and quarter model simulations are given in Table 5.6.

Table 5.6: Comparison of the results of the simulations with full model and quarter model.

Parameter	Unit	Full Model	Quarter Model	Change in %
Number of Elements	$[-]$	836398	143142	-82.9%
Mean Reaction Force	$[kN]$	837.581	830.786	-0.8%
Absorbed Energy	$[kJ]$	86.328	86.012	-0.4%
Analysis Duration	$[min]$	289	33	-86.2%
Output File Size	$[GB]$	20.871	2.504	-88%

The output values of the compared models are almost the same and the change of the values considered to be negligible. Models for the current study were generated as quarter models using planar symmetry method. To ensure the efficiency of the planar symmetry method, symmetry boundary conditions were applied.

5.6.2 Mass Scaling

In explicit solution method, time step is usually very small to obtain a numerically stable simulation. Quasi-static simulations have relatively large solution times due to the small step size and long simulation duration. One of the efficient methods to improve the solution duration of a quasi-static analysis is called 'mass scaling' as mentioned before. Therefore, a sensitivity analysis on the mass scaling factor was performed. Five different mass scaling factors (1, 10, 100, 1000 and 5000) were examined in the sensitivity study. The model with $\beta = 20°$, $t = 10mm$ is used for the mass scaling sensitivity analyses. Two different parameters are decided to be the most important to ensure the accuracy of the solutions when using mass scaling method. The first was that the force-displacement response and the energy absorption response remain unchanged. The second one was that the total kinetic energy of the model is a small proportion of the internal energy.

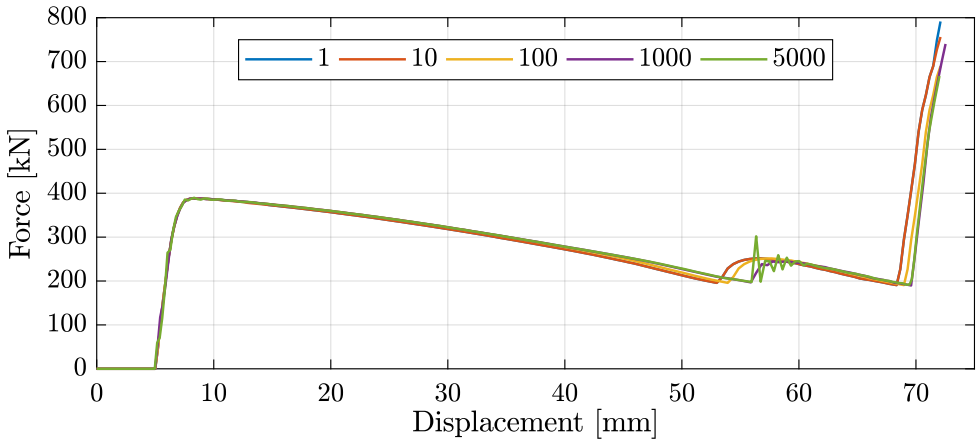

Figure 5.14: Comparison of the force-displacement response of models with different mass scaling factor.

The force-displacement response of the structure with different mass scaling factors are plotted in Figure 5.14. It is seen that scaling the mass by 10 had almost no effect on the solution accuracy. Scaling the mass by a factor of 100 had a small negligible effect on the simulation results. Mass scaling factor of 1000 have small but noticeable effect. However, scaling the mass by a factor of 5000 significantly changes the response of the structure by means of the reaction force and the kinetic energy.

Absorbed energy and the kinetic energy histories of the model with different mass scaling factors are shown in Figures 5.15a and 5.15b respectively. Energy absorption response of the structures were not significantly effected by the mass scaling factor vales. However, the effect on the kinetic of the simulations become noticeable for the mass scaling factor values of 1000 and 5000 which stands for an inaccurate quasi-static simulation.

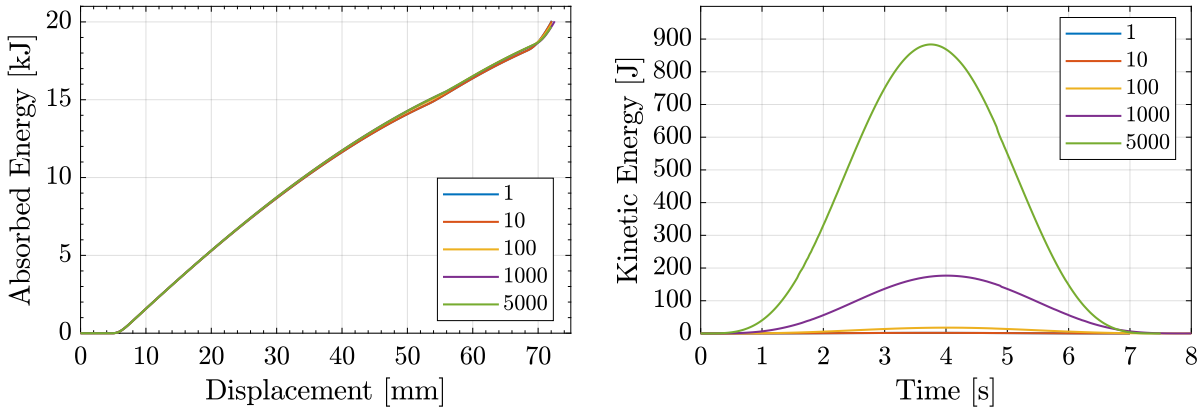

(a) Absorbed energy **(b)** Kinetic energy

Figure 5.15: The absorbed energy and kinetic energy histories of quasi-static models used for mass scaling sensitivity analysis.

The most noticeable effect of the mass scaling factor on the results was the duration of the simulations as seen in Table 5.7. By considering the results and the solution times, a mass scaling factor of 100 is selected for the quasi-static simulations.

Table 5.7: Comparison of results for the selected mass scaling ratios.

Mass Scaling	$\mathbf{F_m}$	$\mathbf{F_p}$	$\mathbf{E_{absorbed}}$	**Duration**	
Factor	[kN]	[kN]	[kJ]	[min]	[hours]
1	307.413	387.916	20.067	81642	1360.70
10	306.993	387.931	20.051	24358	405.97
100	303.609	387.813	20.039	8259	137.65
1000	304.668	388.365	19.889	2556	42.60
5000	293.354	389.664	19.692	863	14.38

5.6.3 Mesh Refinement

A mesh refinement study was performed in order to find the optimum element size and therefore to obtain mesh independent results. Various mesh structures were generated with different element size for chosen configuration ($\beta = 20°$, $t = 10mm$ and $E_{KE} = 100kJ$). Output parameters such as mean reaction force (F_m), peak reaction force (F_p), absorbed energy (E_A), specific energy absorption (SEA) and the time cots of the simulation are compared.

Comparison of the results are plotted in Figure 5.16 and also given on Table 5.8 for different parameters. It is clearly seen in Figure 5.16 that there are no significant changes by means of reaction forces and energy absorption values depending on the mesh size. The model with 5mm of mesh size is the only model with an obviously different force response during the simulation.

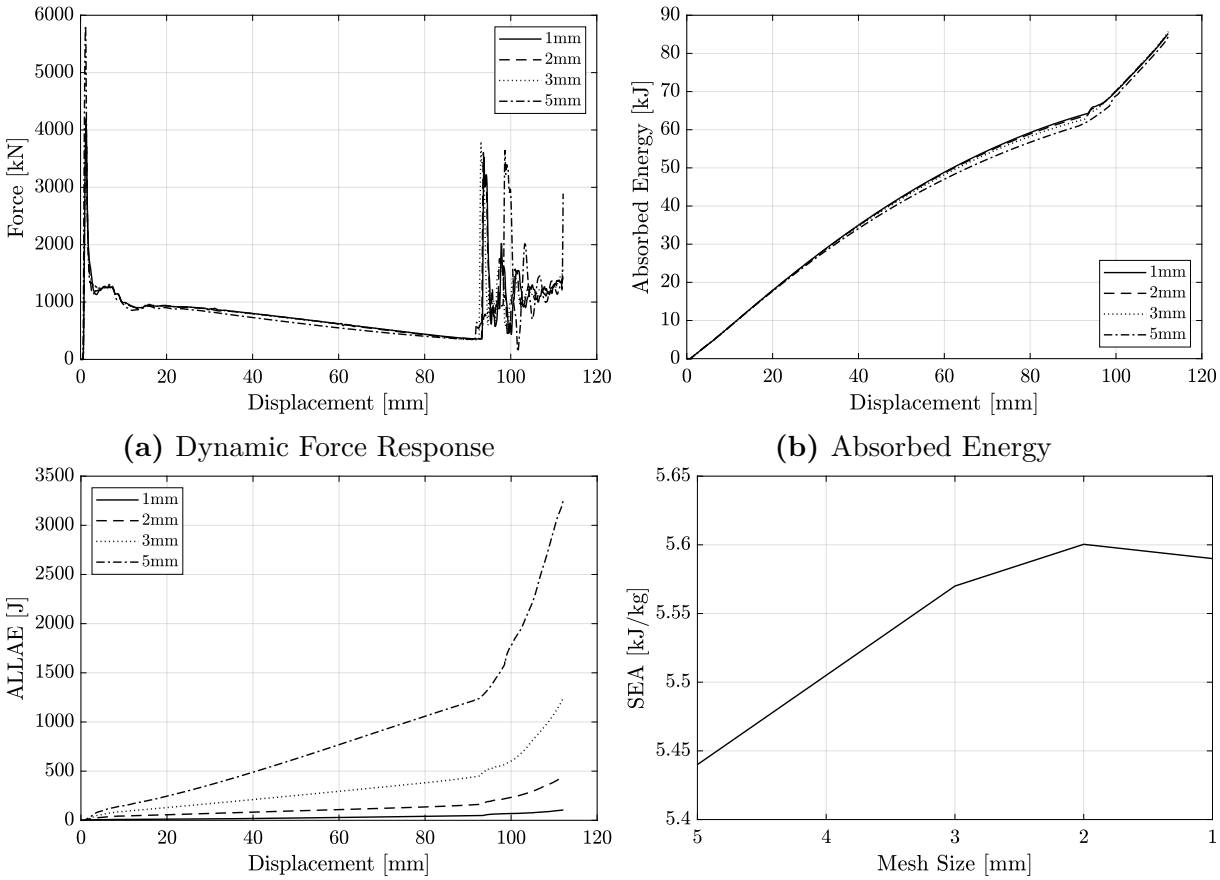

(a) Dynamic Force Response

(b) Absorbed Energy

(c) Artificial Strain Energy (ALLAE)

(d) Specific Energy Absorption

Figure 5.16: Simulation results of models with various mesh sizes.

Besides, for numerical explicit simulations, artificial strain energy (ALLAE) value has a great importance on the accuracy of the simulations. The artificial strain energy (ALLAE) value is recommended to be kept below 5% of the total internal energy (ALLIE) of the structure to obtain a good quality mesh to the model.[11] By considering all parameters together, an element size of 2mm is selected.

The model with element size of 2mm has almost same results by means of reaction forces, specific energy absorption, and deformation mode. The greatest advantage of this model to a finer mesh is the time consumption. By considering that this model is one of the less time consuming model when compared to the other geometrical parameters, the element size of 2mm seem to be the best option for the rest of the simulations. The simulation durations given in Table 5.16 corresponds to the total time of each simulation.

Table 5.8: Comparison of results for the selected element size values.

Mesh Size	Number of Elements	F_p [kJ]	SEA [kJ]	Duration [h:mm:ss]
1 mm	548926	4094.4	5.591	6:22:57
2 mm	74386	4197.3	5.600	0:13:54
3 mm	28106	4141.9	5.572	0:04:33
5 mm	15186	5879.3	5.445	0:01:59

5.7 Mesh Structure

The mesh of all structures are generated by using CAE module of the finite element software Abaqus. Rigid plates are modeled with 4-node 3D bi-linear rigid quadrilateral elements (R3D4). For the deformable absorber structure, element type is selected to be a 8-node hexahedral element with reduced integration. Alongside the standard element features, second order accuracy and hourglass control options are also activated. Although an element size of $2mm$ is chosen from the mesh refinement study, other modifications on the mesh were made. For the sharp edges of the absorber, a $1mm$ of element size was used to obtain better numerical stability and deformation mode. Also the undeformed sections during simulations were detected and mesh size of these sections are increased up to $5mm$ to gain time from the time-cost of the simulations. Example of the mesh modification is plotted in Figure 5.17a.

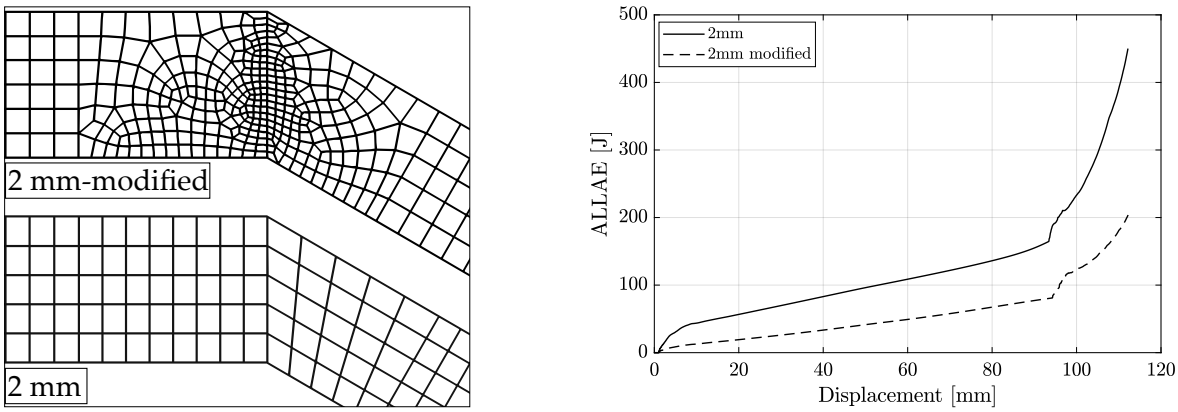

(a) Mesh modification **(b)** Comparison of ALLAE

Figure 5.17: The structure of mesh modification and its effect on artificial strain energy.

The influence of the mesh modification to the reaction force response of the model is shown in Figure 5.18. With this modification, slightly less time-consuming numerical models were obtained. Also even better ALLAE results were achieved. The effect of the mesh modification to the artificial strain energy values of the selected model could be seen in Figure 5.17b.

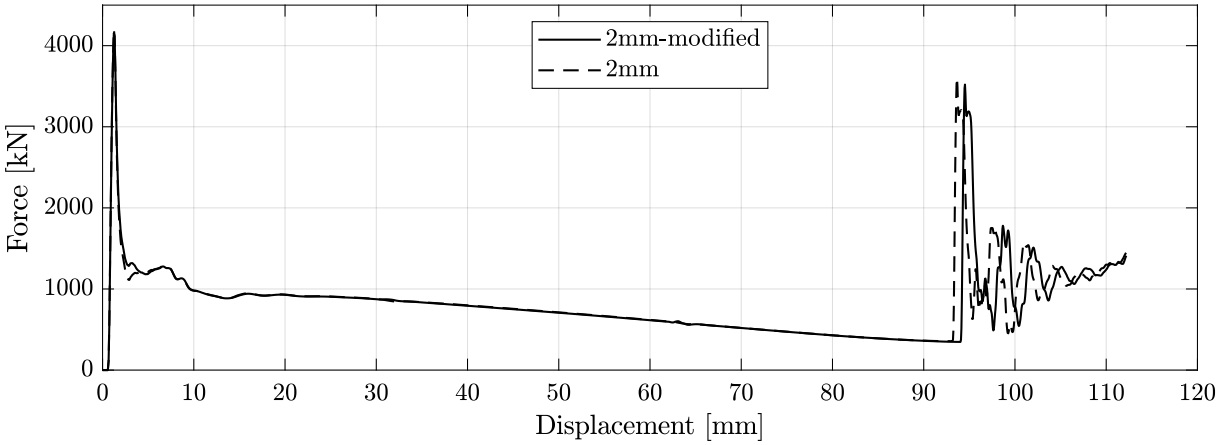

Figure 5.18: Comparison of the force-displacement response after the mesh modification.

For the models with lower thickness values, it is paid attention to have minimum 4 elements across the thickness of the shell regardless of the mesh size. For instance, a $1mm$ of element size is used for the model with $4mm$ of thickness to ensure enough elements through the cross-section, even the element size is chosen to be $2mm$ from the mesh refinement study. Number of elements and element types used in all models and are given in Table 5.9.

Table 5.9: Element types and number of elements for different models used in simulations.

Model	**Element**	**Base Conical angle**		
Thickness	**Type**	20°	25°	30°
Rigid	R3D4	7853	7853	7853
$10mm$	C3D8R	112400	119388	129316
$8mm$	C3D8R	101562	107898	111386
$6mm$	C3D8R	95800	95632	101536
$4mm$	C3D8R	85662	87268	91420

The final mesh structures of the current model chosen for the mesh refinement study are plotted in Figure 5.19. Also the rigid plates are considered in the mesh modification study. The selected critical contact sections of the rigid plates are constituted by using a finer mesh.

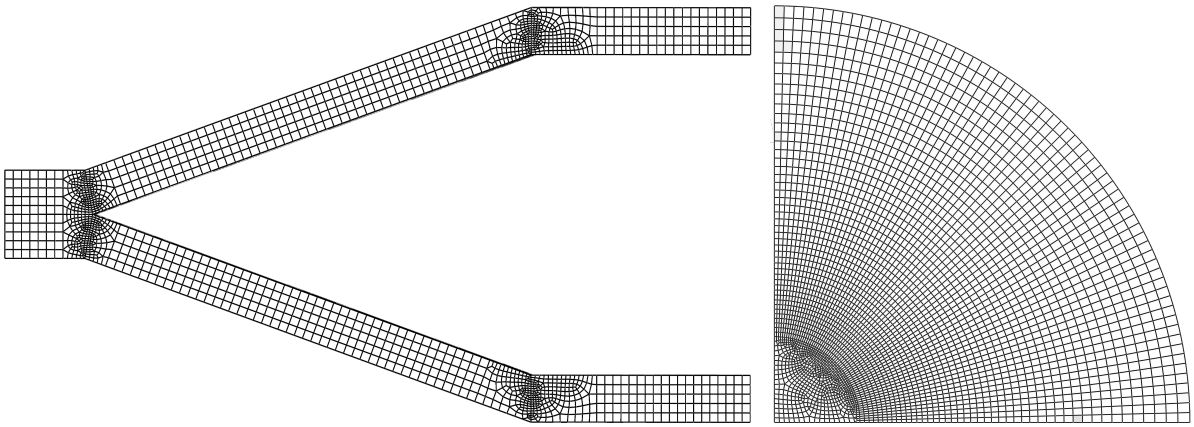

(a) Mesh of the absorber **(b)** Mesh of the plates

Figure 5.19: Mesh structure of the absorber and plates

Mesh Quality

Energy outputs of a numerical simulation is important to ensure the accuracy of the solution of an explicit dynamic analysis. The 'artificial' energy outputs such as the artificial strain energy (ALLAE) should be less than a small fraction of real energies such as the kinetic energy (ALLKE) and the internal energy (ALLIE). Also the total energy during the simulation should be close to a constant value. [11]

Artificial strain energy and internal energy values taken from the FEM software were compared in order to ensure the mesh quality of the model. Artificial strain energy values were in a range of 0.253% - 0.894% of the internal energy of the structures. The maximum percentage of the artificial strain energy to the internal energy are given in Table 5.10. This situation is also taken into consideration by most of the researchers in the current literature. [46, 47, 21] Also the change of the total energy values in the simulations of the current study are very small and can be neglected. The maximum percentage of the artificial energy and almost constant total energy in the simulations indicates a good representative of mesh quality in the models.

Table 5.10: Maximum percentage of artificial strain energy to the internal energy in the numerical simulations.

Conical angle	**Absorber thickness**			
β	$10mm$	$8mm$	$6mm$	$4mm$
20°	0.273%	0.464%	0.497%	0.894%
25°	0.253%	0.422%	0.513%	0.585%
30°	0.262%	0.376%	0.595%	0.609%

6 Results and Discussion

6.1 Introduction

As mentioned before, the current study aims to investigate the quasi-static and the dynamic behavior of a conical absorber under the influence of various parameters such as impact velocity, impact mass, absorber thickness and the base conical angle. For this reason more than 150 different models were created and simulated using the Abaqus/Explicit FEM software. To gain insight about the response of the structure under dynamic loading, resultant data from the simulations must be processed, calculated and compared each other. To compare big amount of data comprehensibly, is not an easy task and should be done in a systematical way.

In this manner, a reference case is selected to begin examining the results by means of the performance parameters introduced in previous sections of the current study. After the results of the reference model are presented, it may be easy to compare the results with respect to the influence of the variables such as impact mass, impact velocity, absorber thickness and the base conical angle. After the results of all variables are presented, conclusions on the results are presented as well as some guidance notes to the design of a conical energy absorber.

6.2 Quasi-Static Response of the Conical Absorber

6.2.1 Reference Case

For the quasi-static loading case, the reference model is chosen with respect to the design parameters and response plots. The thickness (t) and the base cone angle (β) for the reference case are selected to be $10mm$ and 30° respectively. The impact velocity for all quasi-static simulations is selected to be $0.01m/s$ which represents a deformation of $10mm$ per second. The selected design parameters for the quasi-static reference case are given in Table 6.1.

Table 6.1: Design parameters of the quasi-static reference model.

Parameter		Value	Unit
Thickness	t	10	$[mm]$
Absorber length	h	115.5	$[mm]$
Conical angle	β	30	[°]
Impact Velocity	V	0.01	$[m/s]$

The quasi-static numerical simulations have very low loading rates that no dynamic effects exist in the output of the simulations. Therefore, the output data of a quasi-static simulation mostly do not contain any noise or oscillations due to numerical errors. For this reason, the quasi-static results presented below are the raw data obtained from simulations and have not been needed to be smoothed unlike the output data of the dynamic simulations.

In Figure 6.1, the force-displacement response of the reference case is presented. Figure 6.1 also contains the additional gap of $1mm$ of the model assembly. After $1mm$ of displacement, the first contact between the striking plate and the absorber occurs. A stable deformation of the structure was observed after the first peak load throughout the simulation. At the displacement value of approximately $90mm$, the second contact occurs. Each contact between the surfaces in the model assembly causes a peak load in the reaction force response. This situation can be better observed in Figure 6.4.

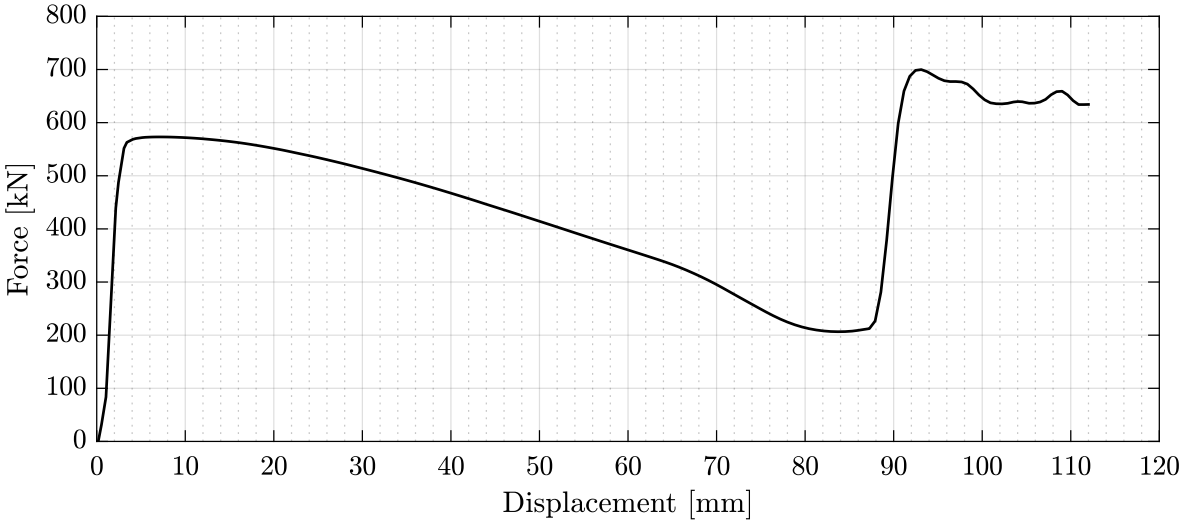

Figure 6.1: Force-Displacement plot of the reference quasi-static model.

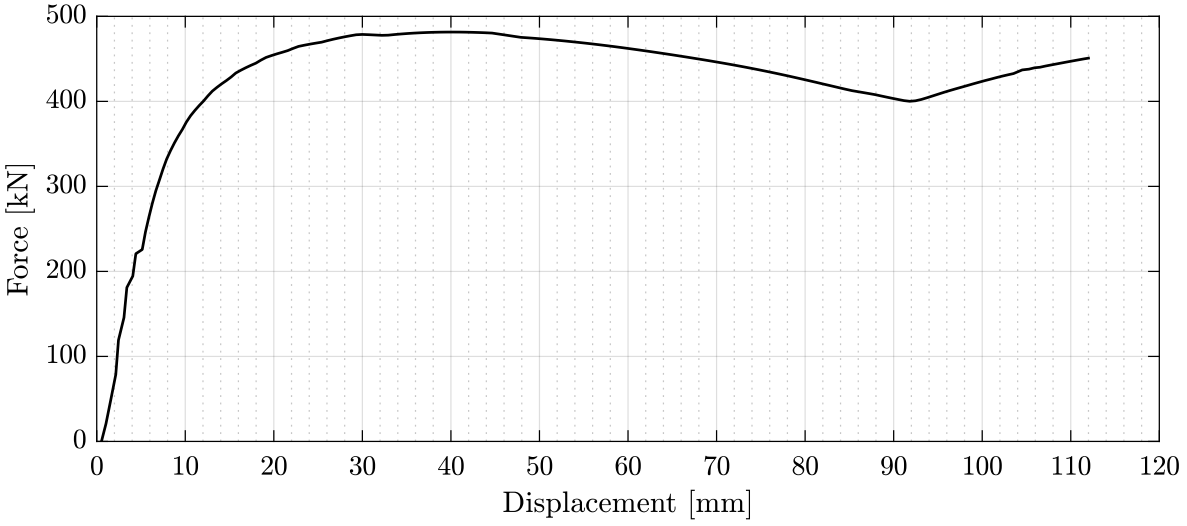

Figure 6.2: Mean Force-Displacement plot for the reference quasi-static model.

The mean force of the reference quasi-static case is shown in Figure 6.2. Mean force data were obtained by dividing the absorbed energy to displacement as explained in previous relevant chapters. As the force-displacement plots are noisy and hard to compare on the same figure, the mean force plots will be used in further sections. Using of the mean dynamic force plots have significant benefits for comparison especially for dynamic simulation results.

Figure 6.3 shows some of the most important energy outputs taken from the software for the quasi-static model. Energy outputs seen in Figure 6.3 are also significant to ensure the numerical accuracy of the model. Artificial strain energy (ALLAE) is observed to be a small fraction of the internal energy (ALLIE), which is a general requirement for an explicit analysis to avoid instability of the simulation due to hourglass effect of the reduced integration elements. [10]

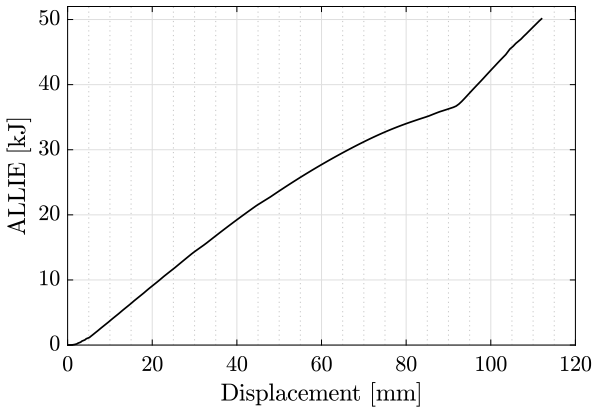

(a) ALLIE, internal energy

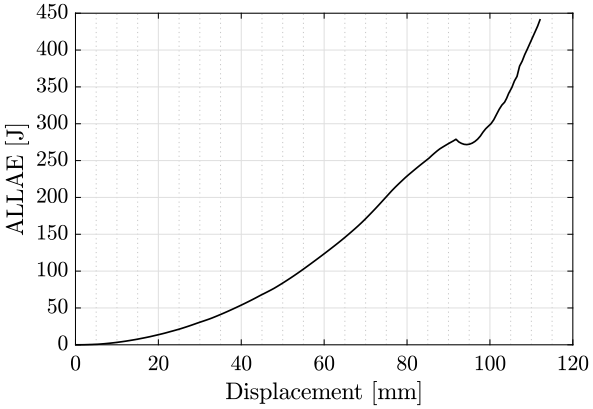

(b) ALLAE, artificial strain energy

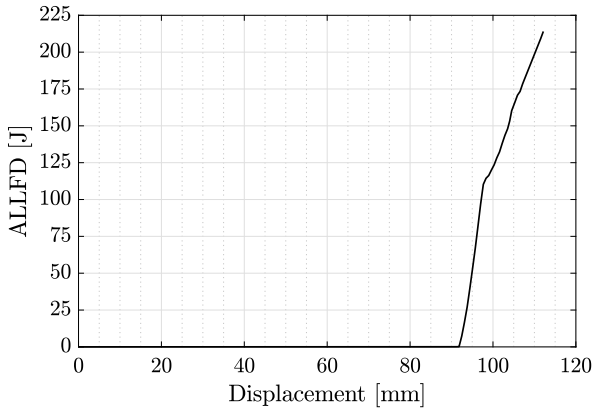

(c) ALLFD, frictional dissipation energy

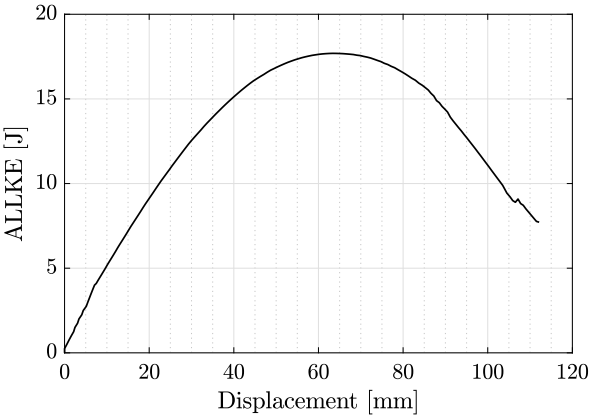

(d) ALLKE, total kinetic energy

Figure 6.3: Magnitudes of different energy types of quasi-static simulation results.

The kinetic energy history (ALLKE) of a quasi-static simulation should also be kept below a small fraction of the internal energy of the model to avoid any dynamic effects caused by the kinetic energy in the simulation. The trend of the kinetic energy history is closely related to the quasi-static loading of the model, which is explained in detail in previous relevant section.

The time history for the internal energy of the model is plotted in Figure 6.3a. It can be clearly seen that the internal energy history share a coherent behavior with the force-displacement response of the simulation. Figure 6.3c shows the energy of the frictional dissipation during the simulation. Frictional energy increases rapidly after the first contact occur at a displacement of approximately $90mm$ and continues this trend due to the friction between the rigid wall and surfaces of the absorber.

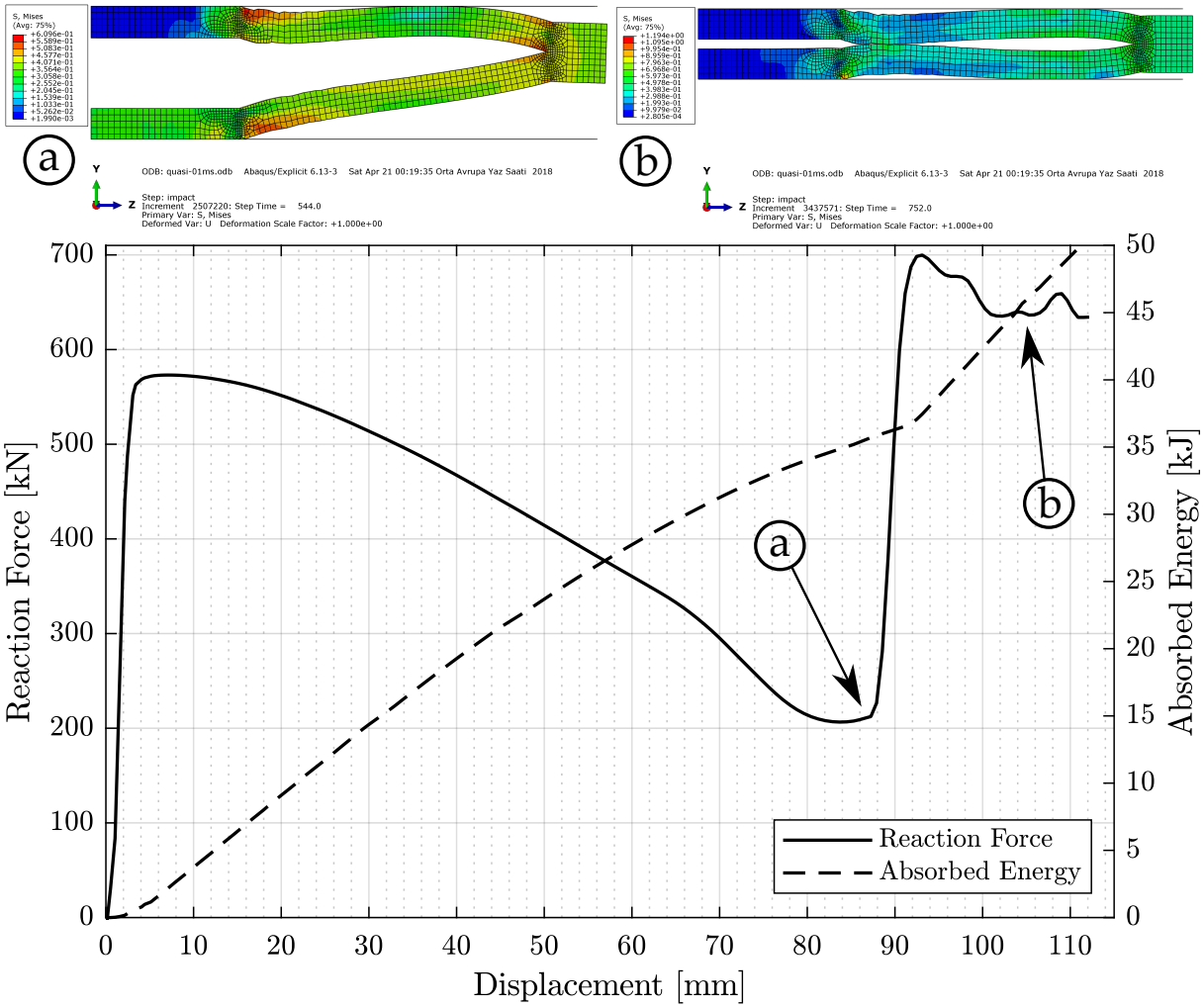

Figure 6.4: Deformation mode for the reference quasi-static case at selected points on reaction force and absorbed energy to displacement plot

Figure 6.4 shows the absorbed energy and the force-displacement response of the quasi-static reference model as a function of displacement. Also the deformed shape of the model is given in Figure 6.4 for selected points to better understand the behavior of the structure under quasi-static axial loading. The selected instants for the simulation of the quasi-static reference model are; a) the contact between the conical surface of the absorber and the rigid wall which causes the second peak on the force-displacement response, b) the last contact during the simulation between the conical surface of the absorber and the striking rigid plate. These two instants are selected because at both instant, a sudden change occurs on the reaction force response of the structure under quasi-static loading.

Performance parameters of the energy absorbers such as the crash force efficiency, specific energy absorption and stroke efficiency are calculated considering the quasi-static results of the reference model. Performance parameters are very useful to understand the behavior of an energy absorber under impact loading. Values of the parameters are also used for the comparison of quasi-static and dynamic response of the conical energy absorber structure in following sections of the current study. The calculated values of the most important output parameters for energy absorbers are given in Table 6.2 for the quasi-static reference model.

Table 6.2: Output values of the reference quasi-static model.

Output Parameter	**Value**	**Unit**
Absorbed Energy E_{ABS}	50.594	$[kJ]$
Mean Force F_m	471.363	$[kN]$
Peak Force F_p	573.084	$[kN]$
Stroke Efficiency SE	0.828	$[-]$
Crash Force Efficiency CFE	0.823	$[-]$
Specific Energy Absorption SEA	3.108	$[kJ/kg]$
Energy per Deformation E_{length}	451.150	$[kJ/m]$

6.2.2 Effect of Base Conical Angle

In this section, the effect of the base conical angle β on the quasi-static response of the structures are investigated. The simulation results of the models within the range of the absorber thickness values under quasi-static loading were used. Each parameter are investigated individually for the influence of the base conical angle of the structure. The mean force and the first peak force values of the models are plotted in Figure 6.5.

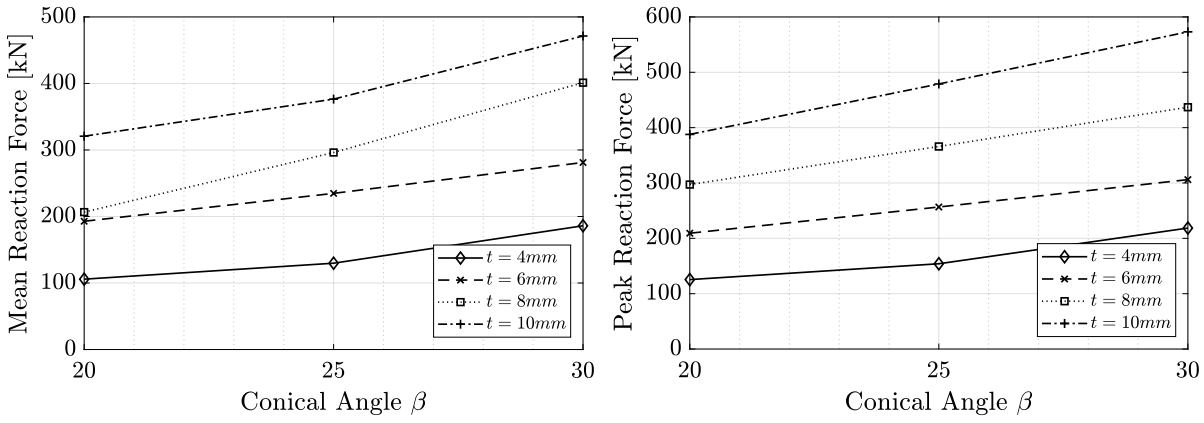

(a) Mean Reaction Force **(b)** Peak Reaction Force

Figure 6.5: Effect of base conical angle on the mean and peak reaction force values of different quasi-static models.

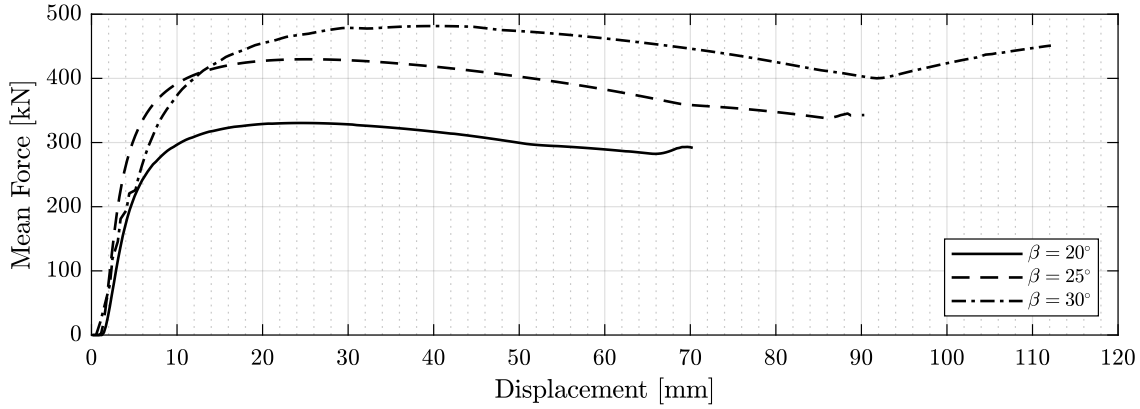

(a) t=10mm

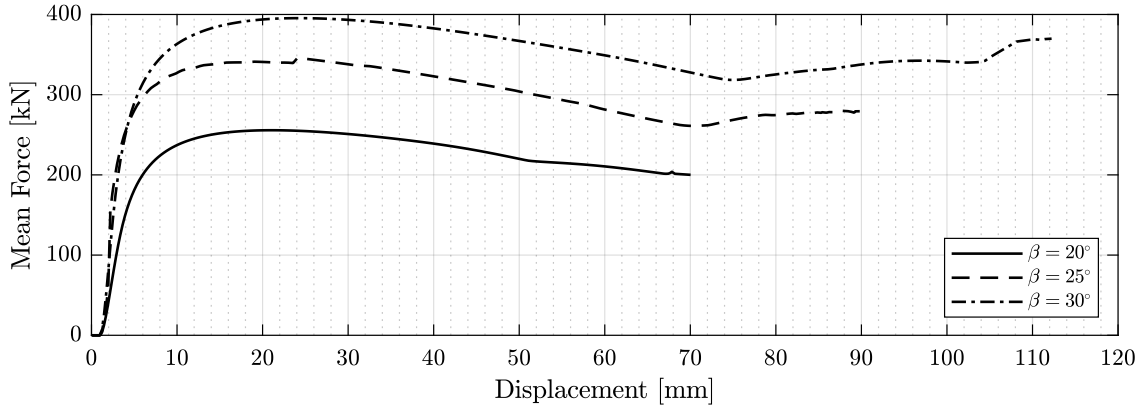

(b) t=8mm

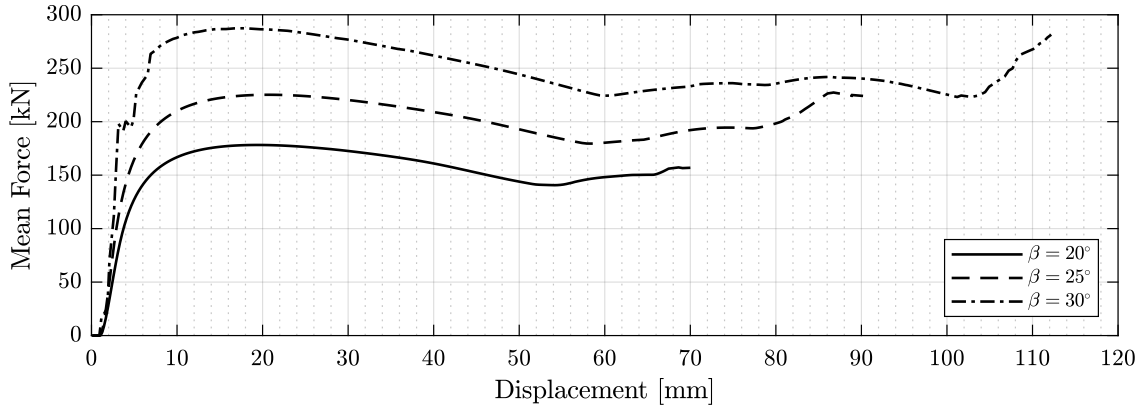

(c) t=6mm

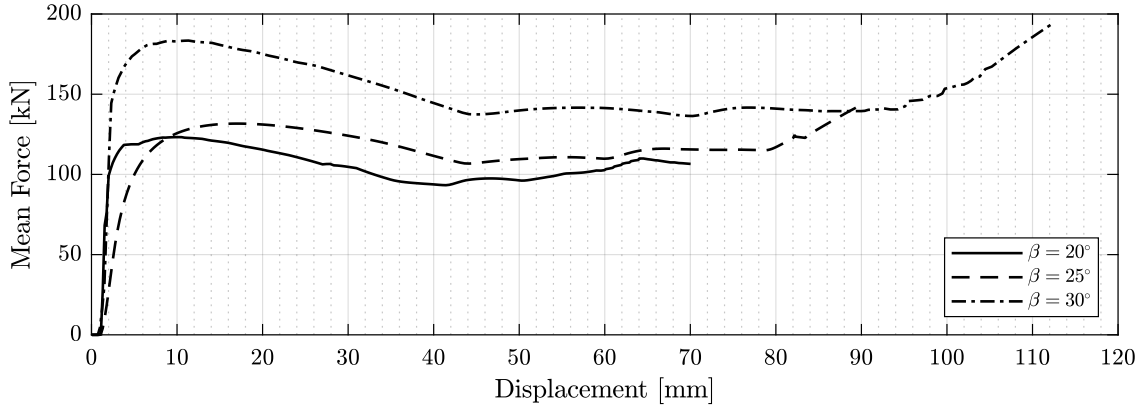

(d) t=4mm

Figure 6.6: Effect of the base conical angle on mean force vs. displacement plots of different quasi-static models.

In Figure 6.5, it is clearly seen that both mean and peak reaction force values have an increasing behavior as the conical angle increases. All models within the selected absorber thickness values have the same increasing trend. In other words, the influence of the base conical angle on the reaction force response are not sensitive to increasing absorber thickness. Force-displacement history of the quasi-static simulations are plotted in Figure 6.6 as a function of displacement. Reaction force responses of the models are affected by the angle as a higher offset of the smaller angle as the base conical angle increases. Structures with higher base conical angle have longer deformation lengths due to the geometry. Because of the longer deformation length, these structures get into contact between surfaces more when compared to the structures with lower deformation lengths. Therefore, they have more sudden load changes during the simulations.

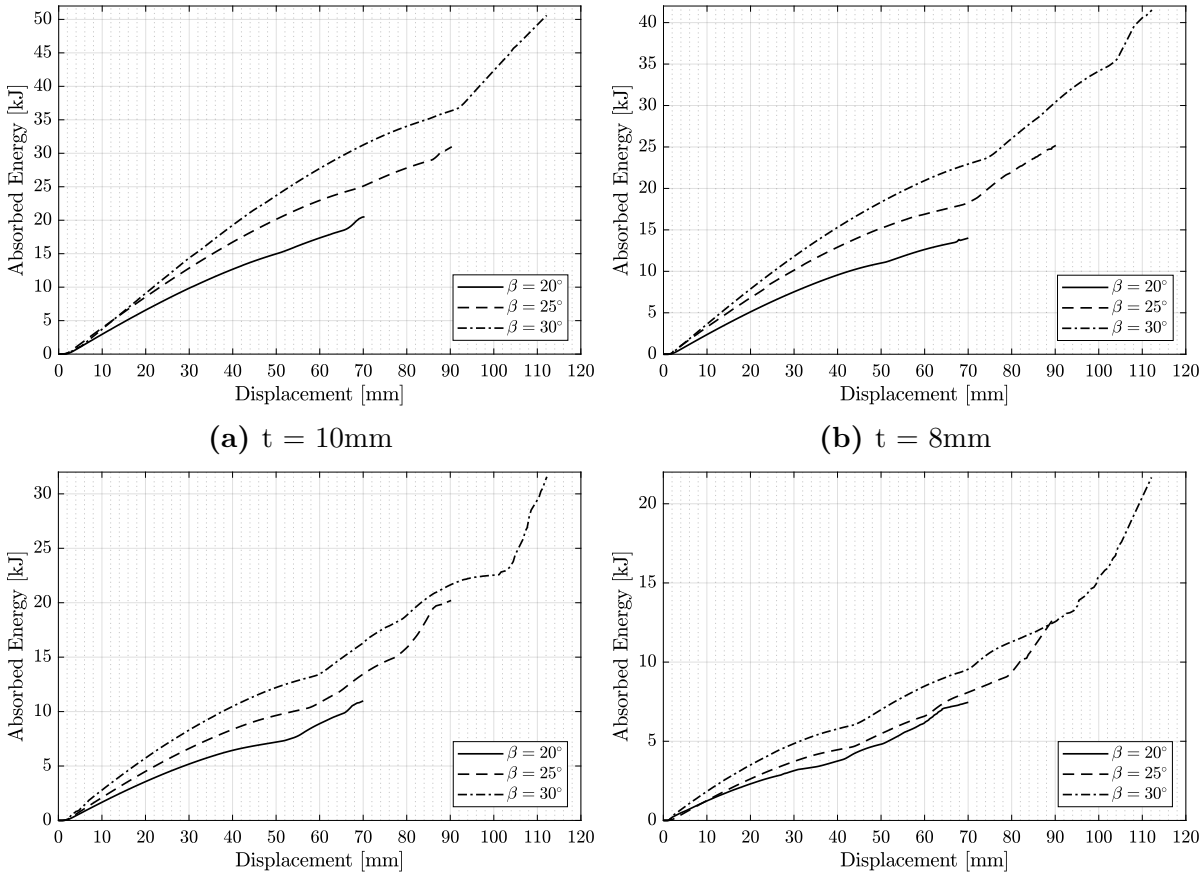

(a) t = 10mm **(b)** t = 8mm

(c) t = 6mm **(d)** t = 4mm

Figure 6.7: Effect of base conical angle on the energy absorption histories of different quasi-static models.

For the structures with lower absorber thickness, the effect of the base conical angle on the difference between the first peak reaction forces are lower. The same behavior is also seen in the energy absorption history of the structures in Figure 6.7. Structures with higher base conical angle require less deformation length to reach the same amount of energy absorption than the structures with lower base conical angle. As the base conical angle decreases, structures become more prone to bending.

Structures with higher β angle are relatively bigger as the length of the structure increases proportionally to the base conical angle. As the structures become longer, the weight of the absorber also increase which directly affects the specific energy absorption values. However, the increase in the absorbed energy values are higher than the increase in the weight of the structures.

The specific energy absorption values are given in Figure 6.8a as a function of base conical angle for different absorber thickness values. The absorbed energy per deformation length values have a similar behavior with the specific energy absorption. Absorbed energy per deformation length values increase as the base conical angle, even though the deformation lengths increase.

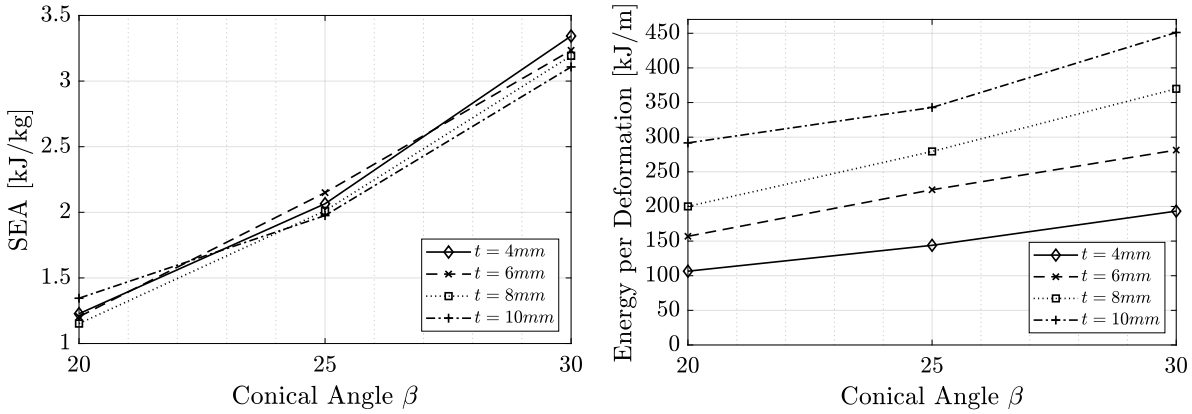

(a) Specific Energy Absorption **(b)** Absorbed Energy per Deformation

Figure 6.8: Effect of base conical angle on the specific energy absorption and absorbed energy per unit deformation length values of different quasi-static models.

6.2.3 Effect of Absorber Thickness

The absorber thickness is another important parameter to estimate the impact behavior of the selected absorber geometry. Figure 6.9 shows the mean reaction force response of the structures within the selected range of base conical angle and absorber thickness values as a function of displacement.

Structures become more prone to bending as the absorber thickness decreases. The peak reaction force values decrease proportionally to the absorber thickness. Also, the structures with lower thickness values have more contact points during the simulations as a result of the number of foldings. Each contact between the surfaces of the structure and the rigid plates cause a sudden increase on the reaction force response. After the sudden increase for each folding, the reaction force starts to decrease gradually.

The effect of the absorber thickness on the CFE values are shown in Figure 6.10. CFE values do not change significantly as the absorber thickness increases. The mean reaction force and the peak reaction force values increase proportionally.

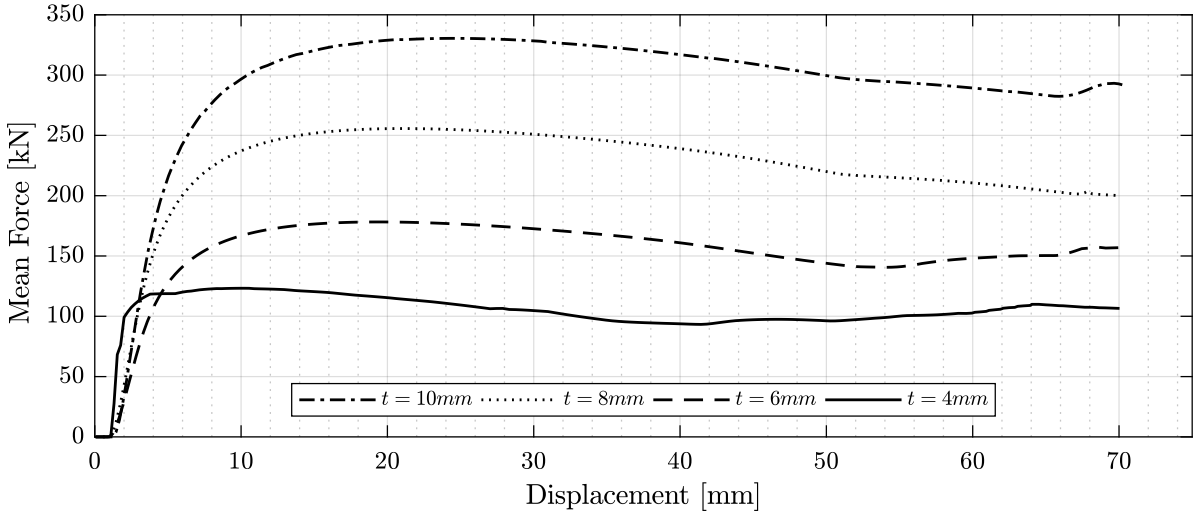

(a) $\beta = 20°$

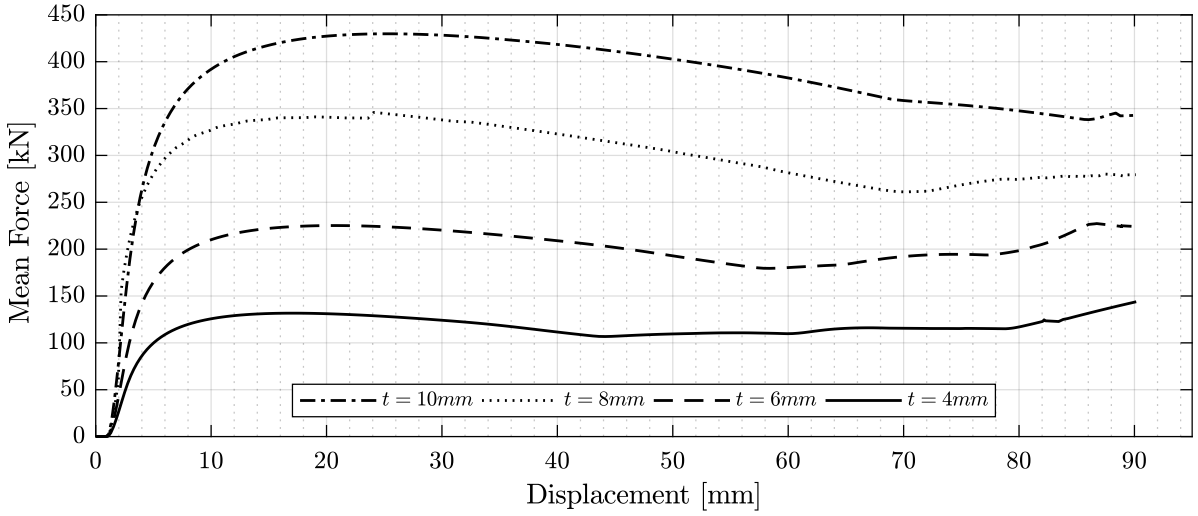

(b) $\beta = 25°$

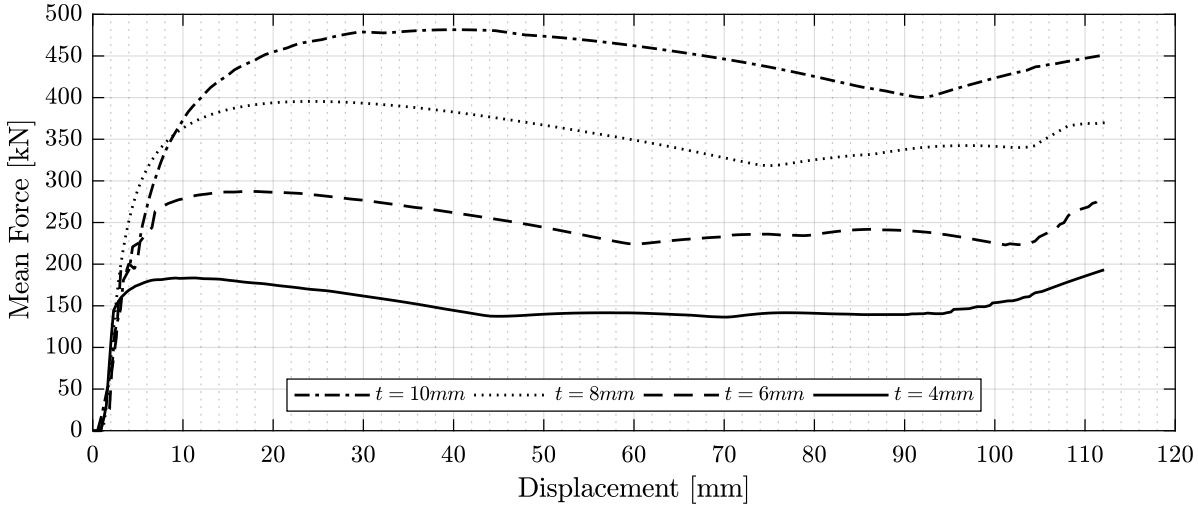

(c) $\beta = 30°$

Figure 6.9: Effect of the absorber thickness on mean force-displacement plots of different quasi-static models.

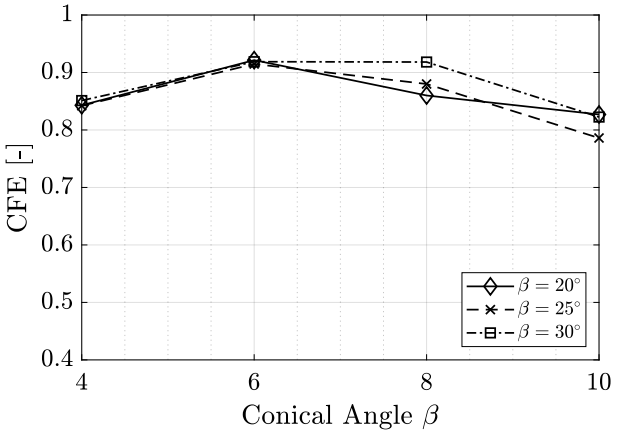

Figure 6.10: Effect of the absorber thickness on the CFE values of the quasi-static models.

Absorbed energy values also increase with increasing absorber thickness as expected. The effect of the absorber thickness on the absorbed energy values is caused by the increasing amount of material available to plastic deformation. The higher thickness values also limit the compression of each fold during the deformation of the structures. The effect of the thickness on the energy absorption trends of the structures are shown in Figure 6.11.

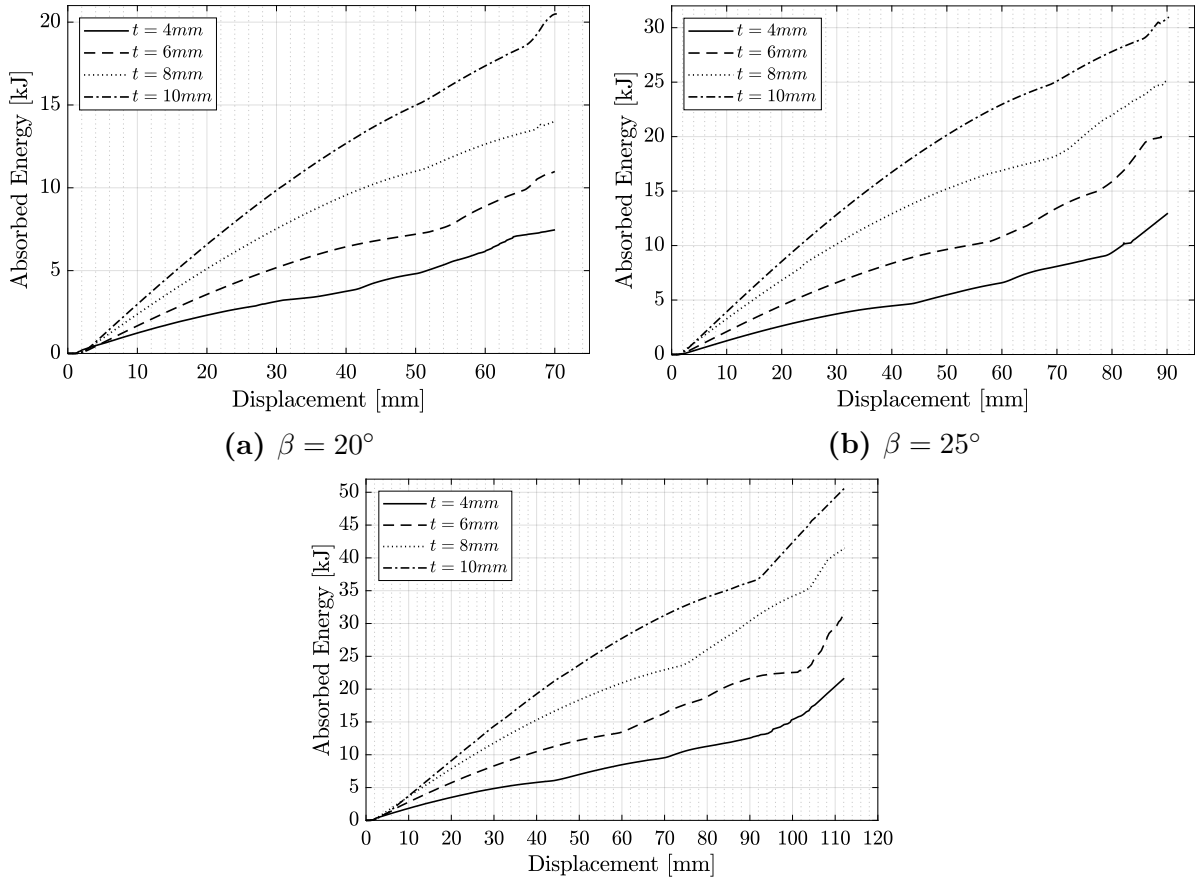

(a) $\beta = 20°$ **(b)** $\beta = 25°$

(c) $\beta = 30°$

Figure 6.11: Effect of the absorber thickness on energy absorption history of different quasi-static models.

The absorber thickness value do not affect the deformation length unlike the base conical angle. Thus, absorbed energy per deformation values increase as the absorber thickness increases due to the increasing absorbed energy values. The absorbed energy per deformation values are shown in Figure 6.12a as a function of absorber thickness for quasi-static models with different base conical angle values.

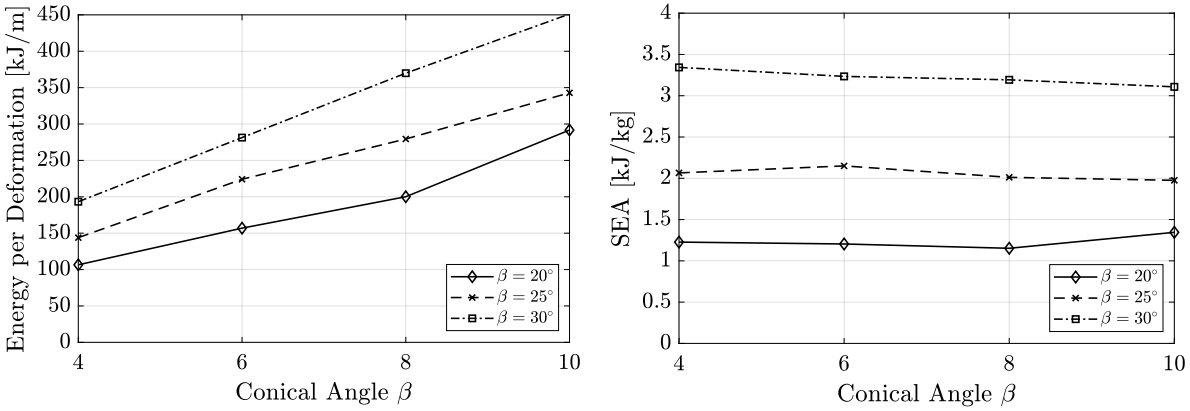

(a) Absorbed Energy per Deformation **(b)** Specific Energy Absorption

Figure 6.12: Effect of the absorber thickness on performance parameters of different quasi-static models.

The effect of the absorber thickness on the specific energy absorption (SEA) values of the of the compared models are shown in Figure 6.12b. Different from the other parameters, absorber thickness does not have a significant effect on SEA values. Although SEA is strictly dependent to the weight of the absorber, which is also changed by the thickness of the absorber. However, the ratio of the absorbed energy and the absorber weight stays almost equal as the thickness changes and SEA values do not change significantly.

6.3 Dynamic Response of the Conical Absorber

6.3.1 Reference Case

In order to gain insight about the general impact response of the conical energy absorber, a reference model is chosen and investigated. The model with a constant impact kinetic energy of 100kJ is chosen for the reference case with respect to the variations of the design parameters and plots of reaction force and absorbed energy. This model is decided to be more suitable for the reference case due to the sufficient impact energy to completely deform the structures. Other two cases included into the present study (impact mass of $1000kg$ and $2000kg$) have not sufficient kinetic energy to completely deform the structures around $5m/s$ of impact velocity. The comparison between three different impact energy cases (constant $100kJ$ impact energy and variable impact energy values for constant impact mass of $1000kg$ and $2000kg$) is given in following relevant chapters in detail. The thickness and the base conical angle are chosen as $10mm$ and 30° respectively. Selected design parameters for the reference model are given in Table 6.3.

Table 6.3: Design parameters of the dynamic reference model.

Parameter		Value	Unit
Thickness	t	10	$[mm]$
Cone angle	β	30	$[°]$
Impact Velocity	V	30	$[m/s]$
Impact Energy	E_{KE}	100	$[kJ]$

The impact response of the selected model is investigated and planned to be a comparison reference. The performance parameters are then calculated and plotted in the following subsections. Understanding the resultant values and response plots is useful to be able to compare the effect of the design parameters. All reaction forces were obtained from finite element analysis results using the predefined reference point coupled to the striking plate. Reaction force data then processed in the commercial software Matlab to smooth the noisy data as previously explained. Smoothed force response for the reference case is plotted in Figure 6.13.

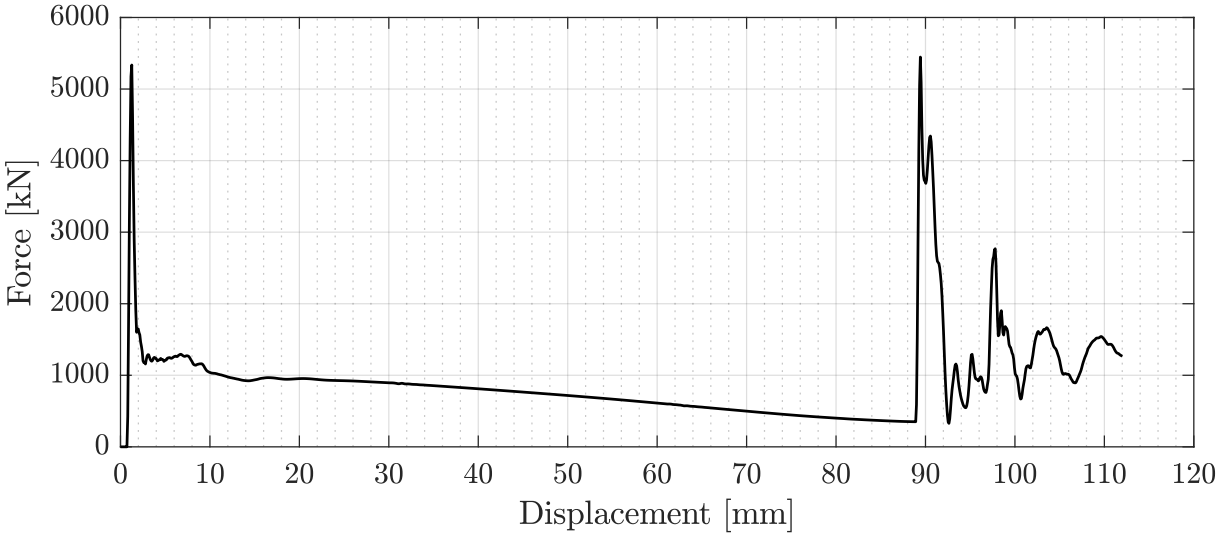

Figure 6.13: Force-Displacement plot of the reference dynamic model.

Displacement values in the Figure 6.13, includes the additional gap of $1mm$ at the interference of striking mass and absorber. At $1mm$ of displacement, the first contact between the striking mass and the absorber structure occurs. As the impact occurs instantaneously, the velocity of the contact surface of the absorber increases immediately. After the first reaction force occurs, the structure exhibits a stable deformation behavior. The reaction force shows a decreasing trend until the next contact between striking plate and the surface of the absorber takes place. This behavior repeats on each contact between surfaces of the absorber and striking plate. The response trend of the reaction force and the absorbed energy can be seen in Figure 6.17 in detail.

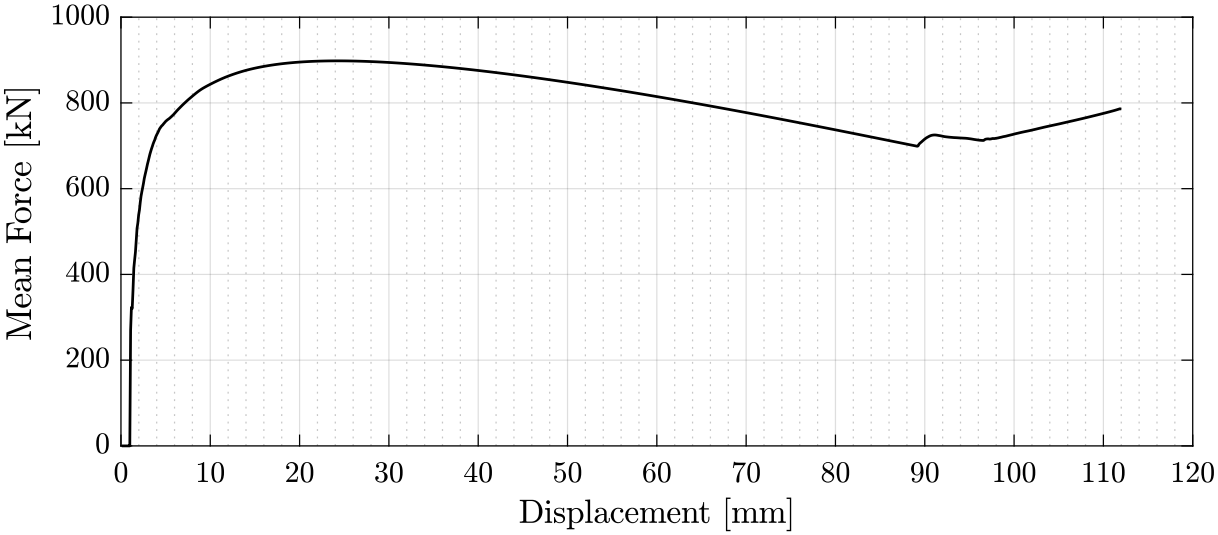

Figure 6.14: Mean dynamic Force-Displacement plot of the reference dynamic model.

The mean dynamic force of the reference dynamic case is shown in Figure 6.14. Mean dynamic force data were obtained by dividing the absorbed energy to displacement as explained in previous relevant chapters. As the force-displacement plots are noisy and hard to compare on the same figure, the mean dynamic force plots may be useful for comparisonof the reaction force responses.

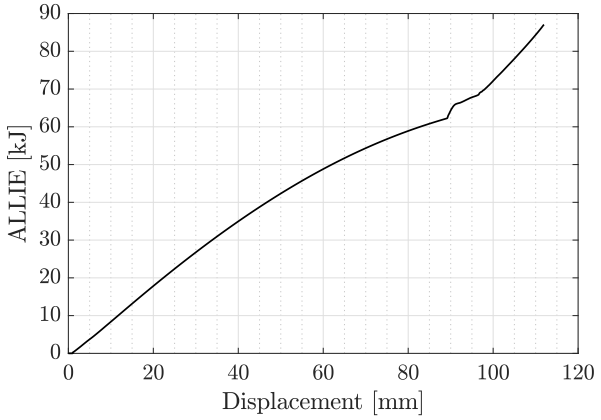

(a) ALLIE, internal energy

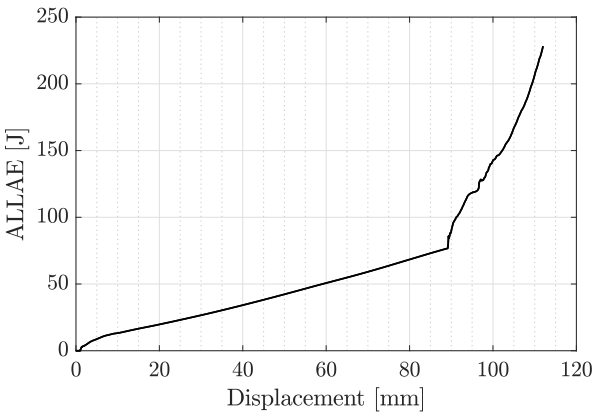

(b) ALLAE, artificial strain energy

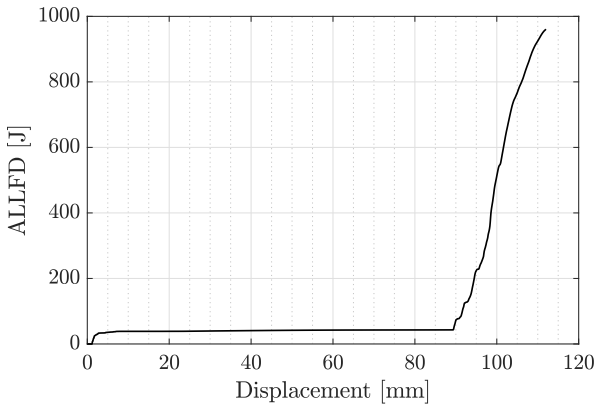

(c) ALLFD, frictional dissipation energy

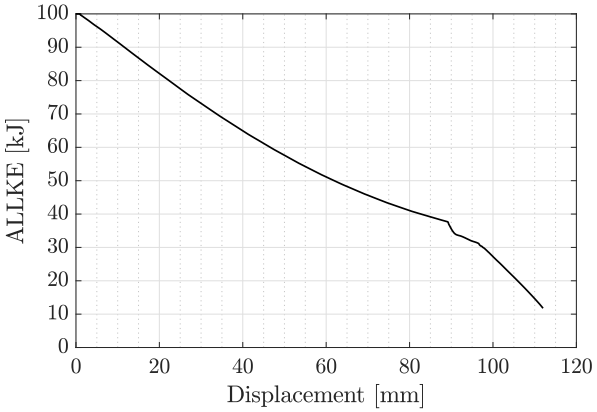

(d) ALLKE, total kinetic energy

Figure 6.15: Magnitudes of different energy types of dynamic simulation results.

The total energy of the model is defined as a composition of different type of energies in the FEM software Abaqus. Basically, it can be said that total energy of the system at the end of the impact is the sum of the absorbed energy and the residual kinetic energy. The absorbed energy is also calculated as the sum of the internal energy (ALLIE), viscous dissipation energy (ALLVD) and frictional dissipation energy (ALLFD) in the finite element software which are mentioned before in previous relevant sections. The magnitudes of the energies used to calculate the energy balance and the numerical accuracy of the model are plotted in Figure 6.15 for the reference model. The ALLFD value as seen in Figure 6.15c shows a sudden increase at the displacement approximately $90mm$ due to the contact between the striker and the surface of the absorber. However, the amount of friction energy is significantly low when compared to the internal energy.

For the reference model, the initial kinetic energy of the striking plate is relatively high due to the higher impact velocity of the model. By this reason, the absorber is totally crushed to its maximum possible crush distance. The initial kinetic energy, absorbed energy, artificial strain energy (ALLAE) and the total energy of the simulations are plotted together in Figure 6.16 to better understand the energy balance of the system during the impact.

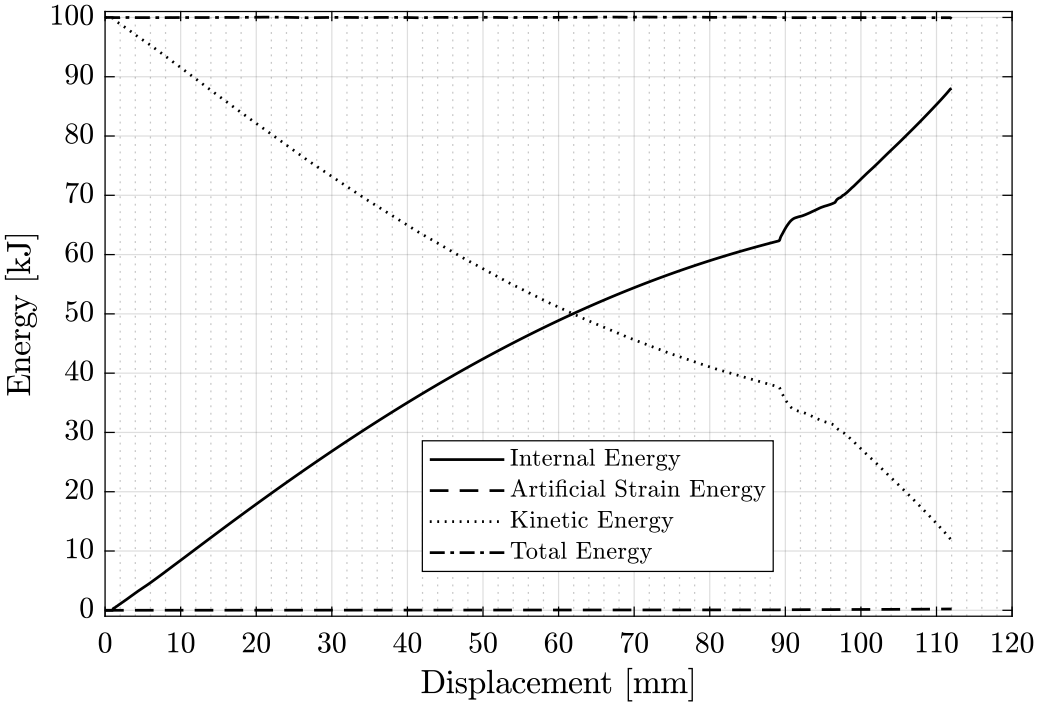

Figure 6.16: Energy balance of the simulation for the reference dynamic model.

Figure 6.16 also shows that the magnitude of the artificial strain energy is kept as a very small proportion of the absorbed energy. The change of the total energy of the system is significantly low. The artificial strain energy is the amount of energy applied by the FEM software to reduce hourglass effect of the elements used in the simulation and the small amount of the ALLAE proves that the model has a good mesh quality.

The total energy of the system is also kept almost constant during the crushing process which indicates that numerical error of the simulation is very low. The percentage of the change in the total energy and the ratio of the ALLAE to the absorbed energy are 0.42% and 0.262% respectively.

The dynamic response of the structure by means of the reaction force and the absorbed energy is plotted in Figure 6.17 together. Also pictures of the deformation mode for selected points are shown together to better understand the behavior of the structure. The selected instants for the reference model are a) the initial contact, and first cone starts bending, b) contact of conical surface to striking plate occurs and second cone starts bending, c) first cone becomes completely flat and contact of the inner surfaces of the cones are achieved.

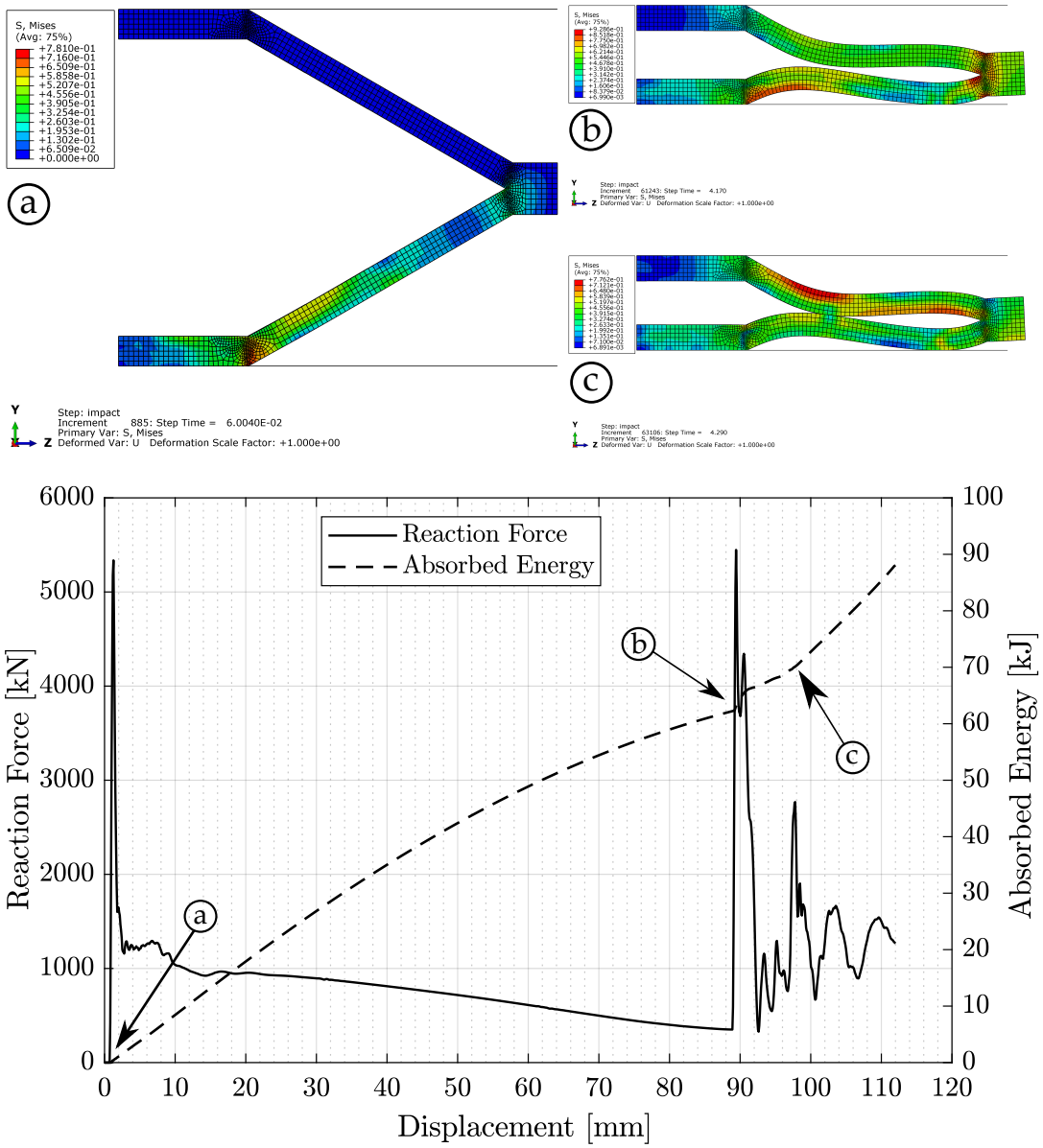

Figure 6.17: Deformation mode for the reference dynamic case at selected points on reaction force and absorbed energy to displacement plot

As mentioned before, the crush force efficiency is the ratio of mean reaction force (F_m) and peak reaction force (F_p). Magnitudes of F_m, F_p and the CFE of the reference model are given in Table 6.4. It is desired to maximize the CFE, since the peak forces during an impact event causes peak deceleration which can lead the structure to fail or injury of the occupants.

Table 6.4: Reaction forces and CFE values of the reference dynamic model.

Mean Force F_m	**Peak Force** F_p	**CFE**
$[kN]$	$[kN]$	$[-]$
931.425	5335.999	0.175

As previously described in Section 2, the weight of the absorber is an important parameter to investigate the performance of the absorber from the crashworthiness perspective. Specific energy absorption values of the structures are calculated with respect to the absorbed energy values obtained from the numerical simulations and mass values of each structure. SEA value of the reference model is calculate as $5.407 kJ/kg$.

Another performance parameter is described to compare the absorbed energy values with respect to the amount of deformation during the crush. This parameter becomes more important when the area of the crush zone is restricted. The absorbed energy per unit deformation for the reference model is calculated to be $793.053 kJ/m$.

Stroke efficiency of the energy absorber is defined as the ratio of the maximum deformable length to the total length of the structure. Models used in this study are conical and have end caps with height equal to the thickness of the absorber, which is a restriction for the absorber to have relatively high stroke efficiency values. For the reference model, the stroke efficiency is calculated as 0.819 which means that the maximum deformable length of the absorber is limited to 82% of the total height of the absorber structure.

6.3.2 Effect of Impact Mass

To better understand the energy absorbing capacity of the structure, one of the important variable of interest is the impact mass. Mass of the striking plate is an important parameter to investigate, since it directly affects the initial kinetic energy of the simulation. The influence of impact mass is compared for models with different variables such as impact velocity, absorber thickness and base conical angle. A $100 kJ$ of impact energy is selected for the reference model. To investigate the influence of the impact mass, constant mass values of $1000 kg$ and $2000 kg$ are also modeled and simulated numerically. The value of the constant impact energy ($100 kJ$) is selected to ensure sufficient kinetic

energy to completely deform the structures for the whole range of impact velocity, absorber thickness and base conical angle values. Impact mass values were calculated for each impact velocity and calculated values were implemented to the numerical solutions. The energy and mass variations used for this comparison is given in Table 6.5 in detail.

Table 6.5: Impact mass and impact energy parameters used to compare he effect of impact mass for three different cases.

Case	Parameter	Unit	Impact Velocity			
			$5m/s$	$10m/s$	$20m/s$	$30m/s$
1000kg	Impact Mass	[kg]	1000	1000	1000	1000
	Impact Energy	[kJ]	12.5	50	200	450
2000kg	Impact Mass	[kg]	2000	2000	2000	2000
	Impact Energy	[kJ]	25	100	400	900
100kJ	Impact Mass	[kg]	8000	2000	500	222.24
	Impact Energy	[kJ]	100	100	100	100

Energy absorption history of the simulations have the same trend for increasing mass values as seen in Figure 6.18. It is clearly seen that the initial kinetic energy has no significant effect on the energy absorption characteristics of the structures.

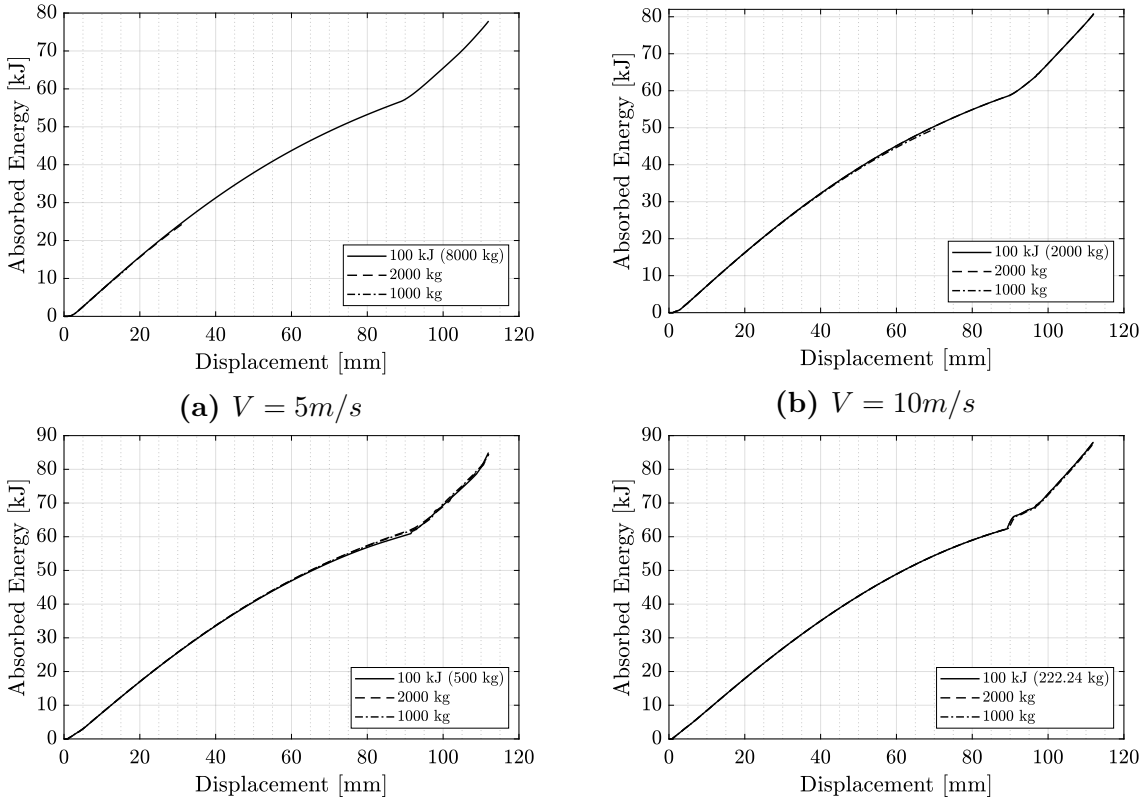

(a) $V = 5m/s$ **(b)** $V = 10m/s$

(c) $V = 20m/s$ **(d)** $V = 30m/s$

Figure 6.18: Effect of impact mass on the absorbed energy values for different models.

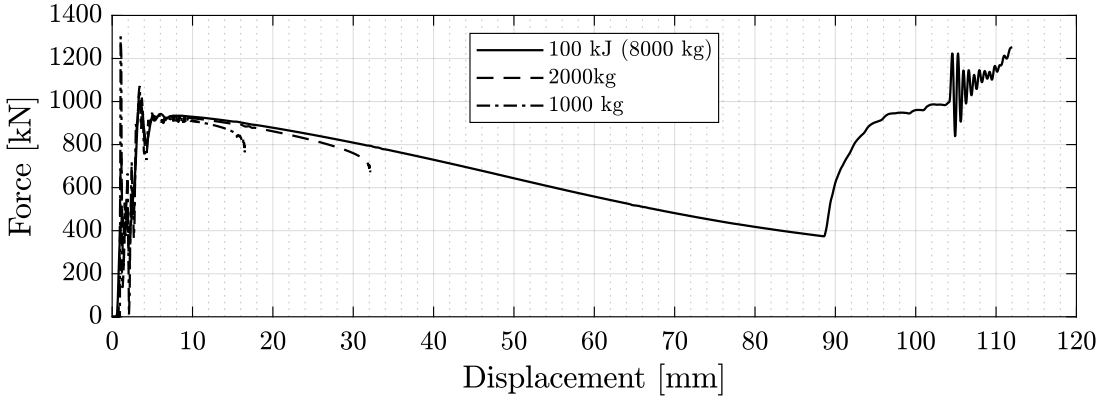

(a) $V = 5m/s$

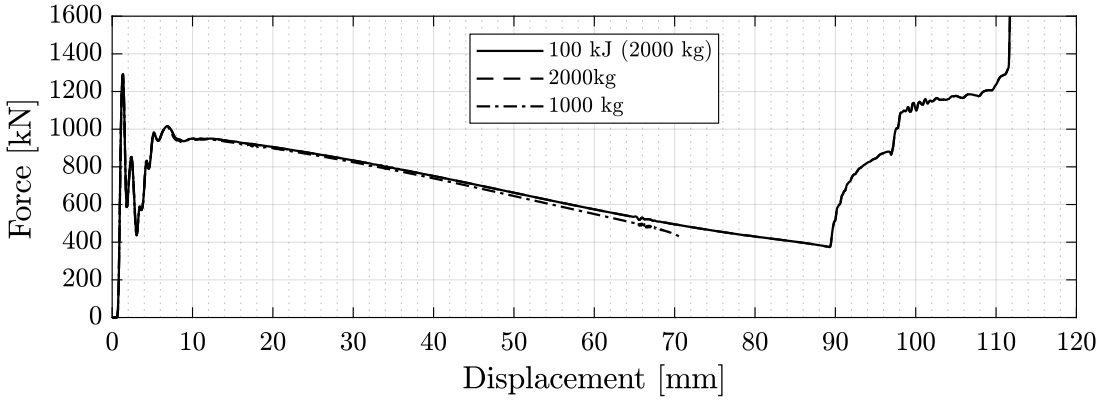

(b) $V = 10m/s$

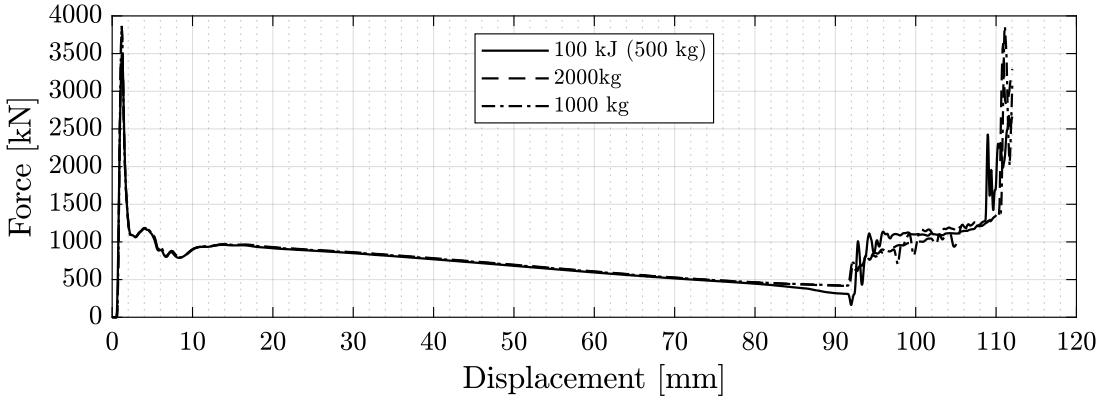

(c) $V = 20m/s$

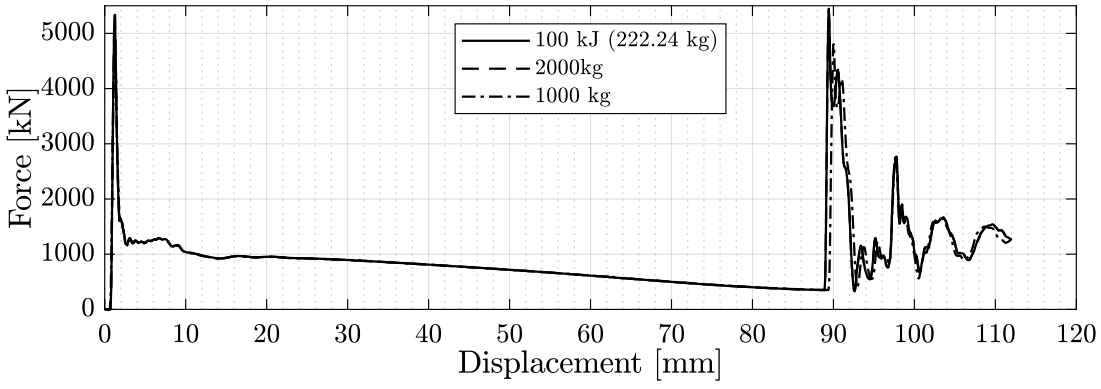

(d) $V = 30m/s$

Figure 6.19: Effect of the impact mass on Force-Displacement plots of different models.

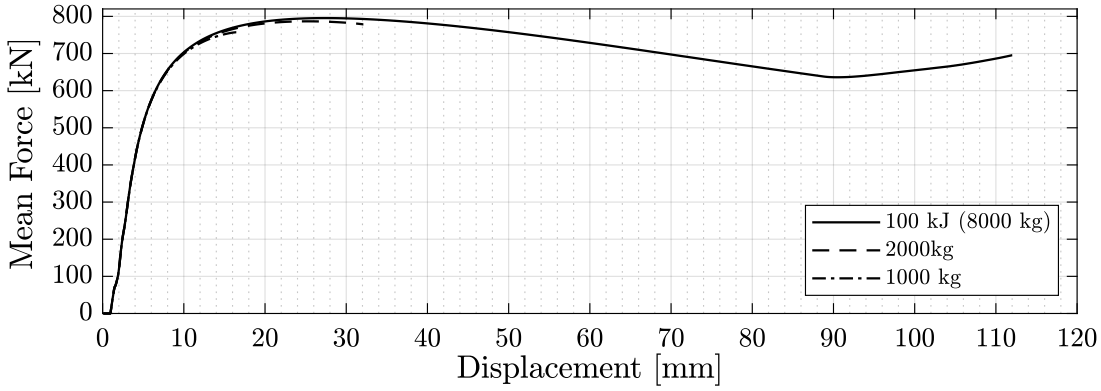

(a) $V = 5m/s$

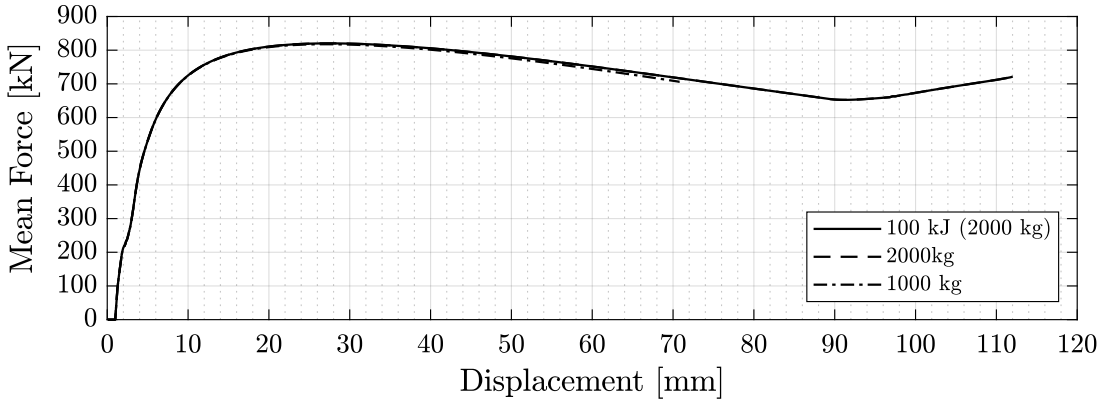

(b) $V = 10m/s$

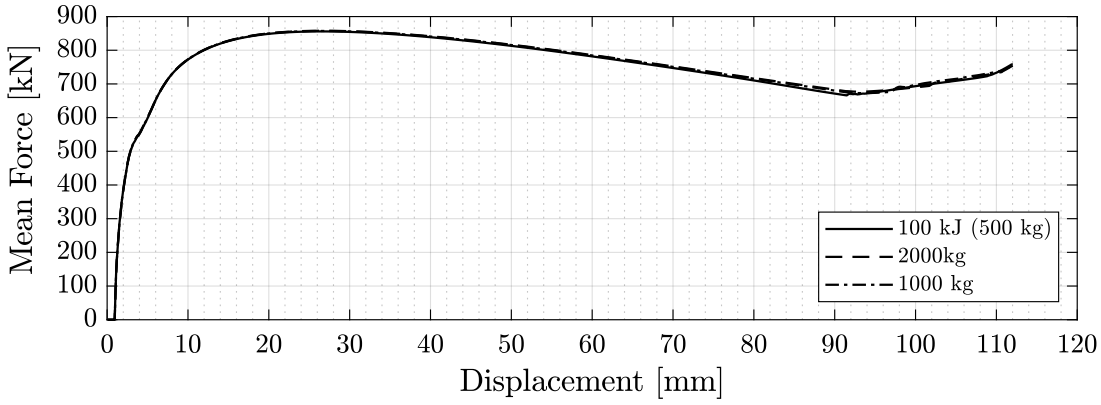

(c) $V = 20m/s$

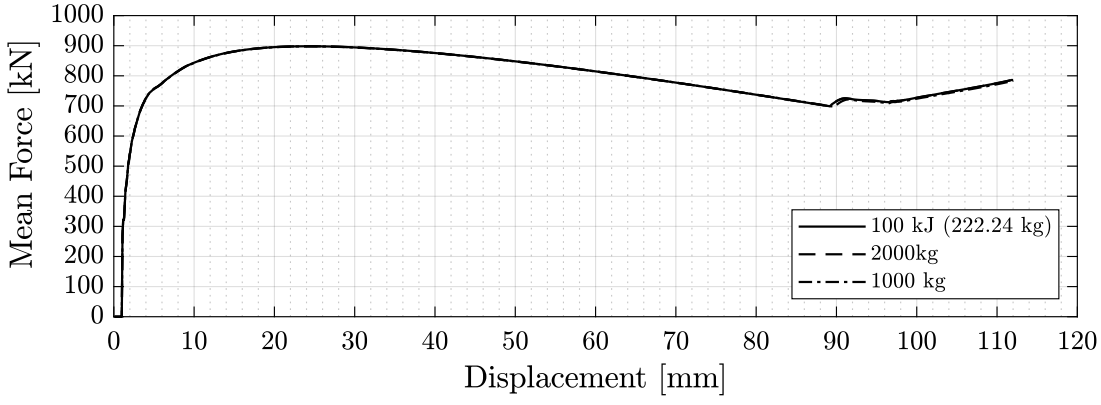

(d) $V = 30m/s$

Figure 6.20: Effect of the impact mass on mean dynamic Force-Displacement plots of different models.

The only change in the force-displacement response can be seen in the Figure 6.19a, where the structure completely deforms only in the $100kJ$ case. For this models, the $100kJ$ impact energy provide sufficient kinetic energy to completely deform the structure at $5m/s$ initial velocity, due to its high impact mass($8000kg$).

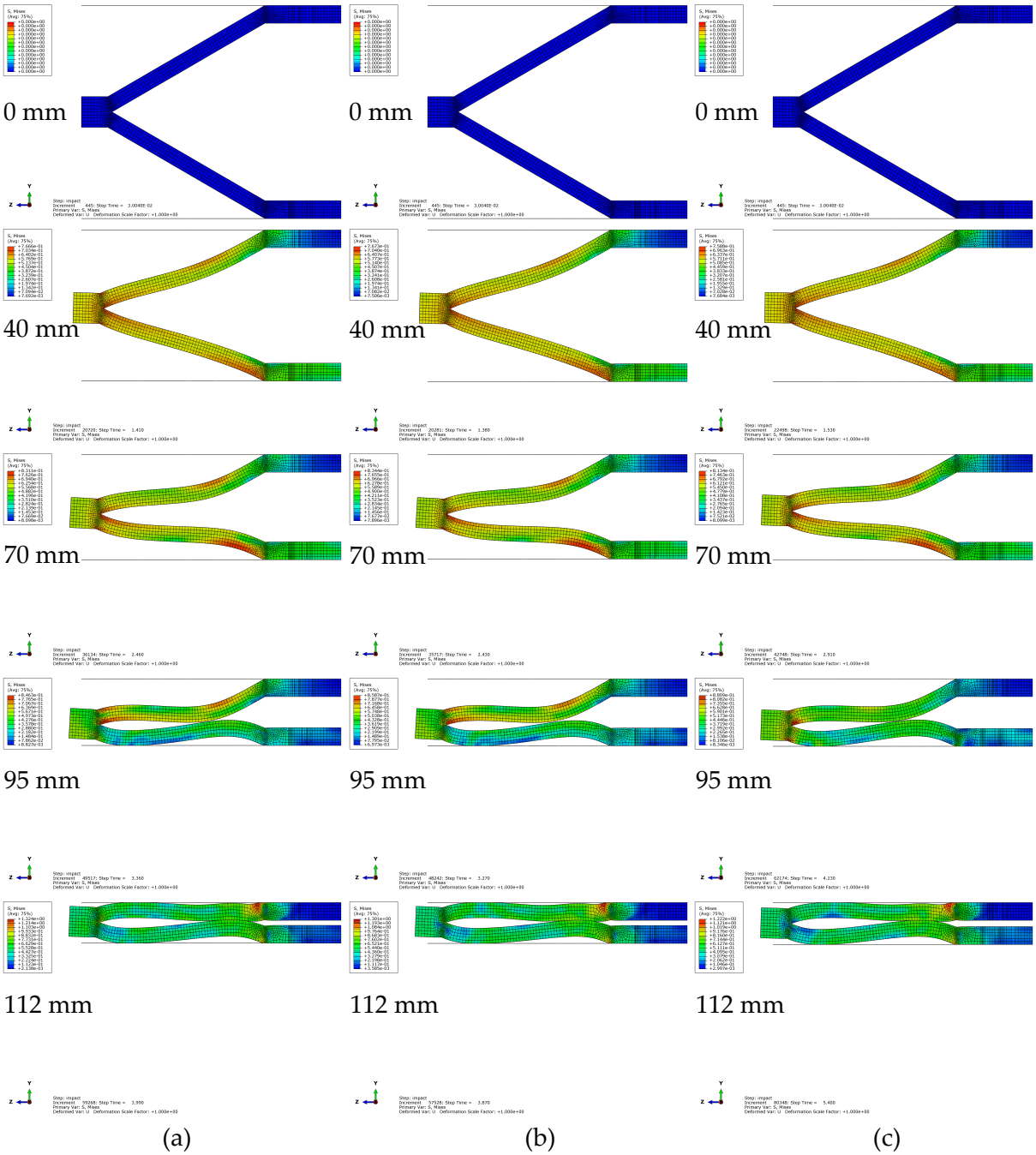

Figure 6.21: Effect of impact mass on the deformation history of the model with parameters of $t = 10mm$, $V = 30m/s$, $\beta = 30°$ for different impact masses; a) $M = 1000kg$, b) $2000kg$, c) $M = 222.24kg(E_{KE} = 100kJ)$

The deformation history of the structures are also compared and shown in Figure 6.21. The deformed shapes of the absorber structures for three different impact masses are almost equal at the same crush distance and the simulation time.

The effect of impact mass on dynamic response of the absorbers are summarized in Figures 6.19 and 6.20 as a function of displacement for the model with $\beta = 30°$ and $t = 10mm$ for varying impact velocities. It can be clearly seen that there is no significant change in the force-displacement response of the conical absorbers even if the impact mass and initial kinetic energy significantly changed. The other performance parameters such as crash force efficiency (CFE), specific energy absorption (SEA) and the absorbed energy per unit deformation are not significantly affected by different impact mass values as they are strictly dependent to force-displacement and energy absorption trends of the structures.

6.3.3 Effect of Impact Velocity

In this section, influence of the impact velocity is compared by using the simulation results. For all of the impact velocity values in the selected range, structures were completely deformed to their maximum deformation lengths.

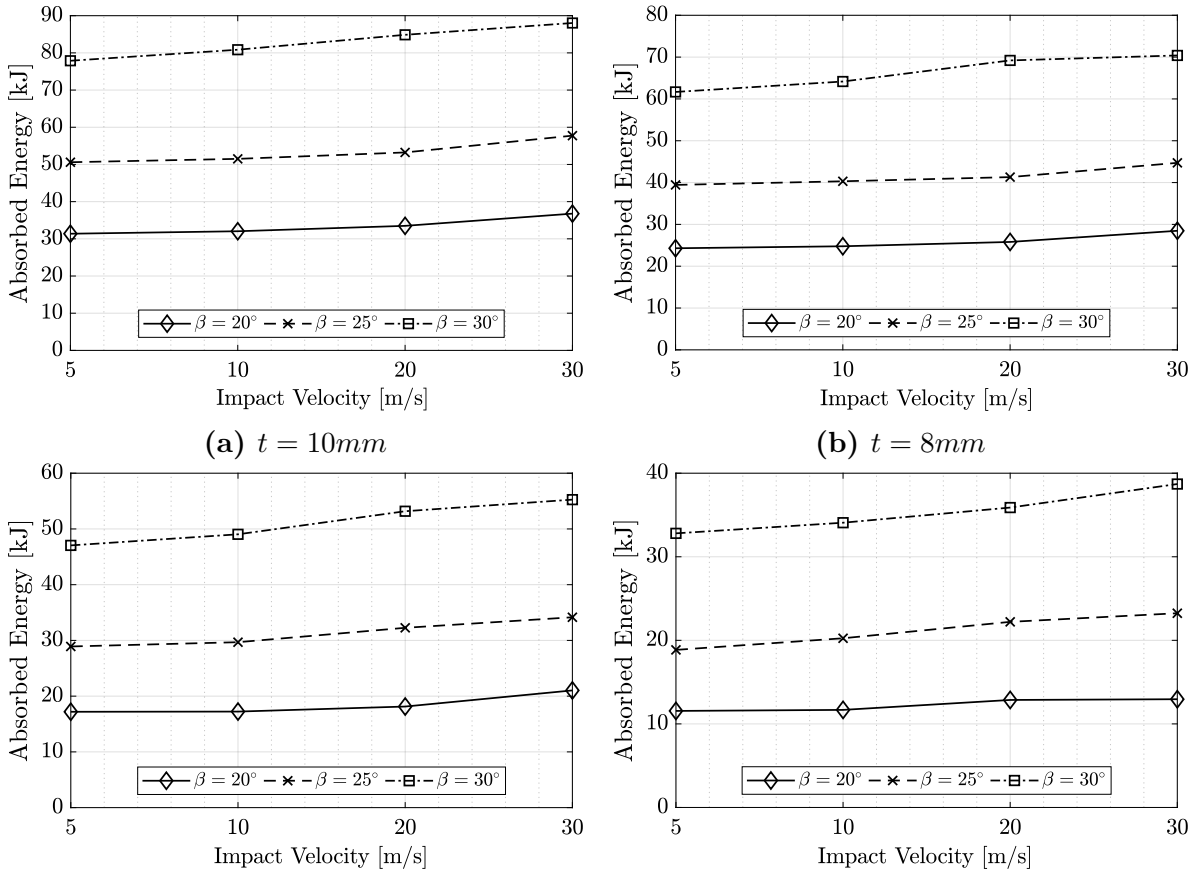

(a) $t = 10mm$ **(b)** $t = 8mm$

(c) $t = 6mm$ **(d)** $t = 4mm$

Figure 6.22: Effect of the impact velocity on absorbed energy values of different models.

Figure 6.22 shows the effect of the impact velocity on the absorbed energy values as a function of impact velocity. It is seen that the initial velocity has a non-negligible effect on the energy absorbing capacity of the structures. The effect of the velocity was observed more prominently on models with higher base conical angle values.

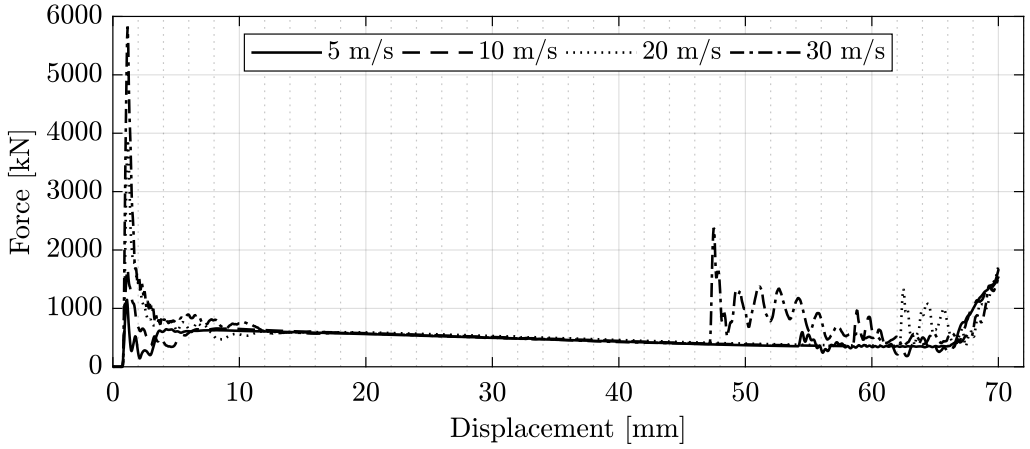

(a) $\beta = 20°$

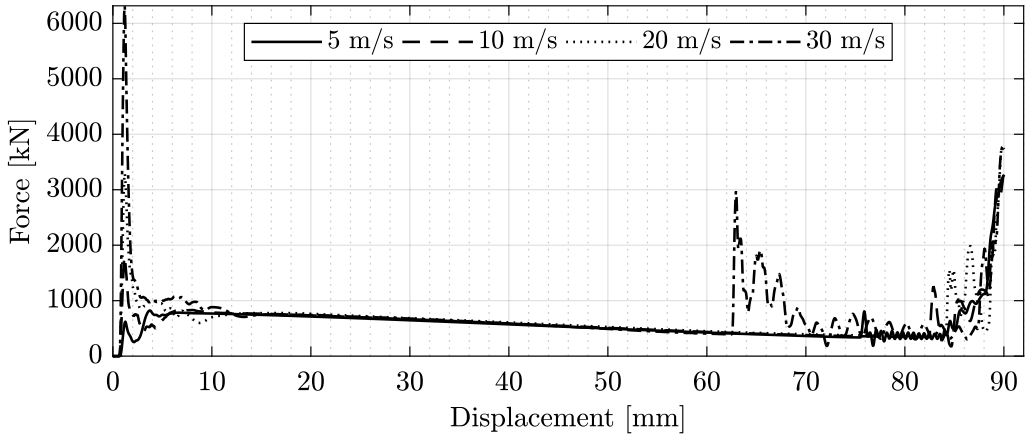

(b) $\beta = 25°$

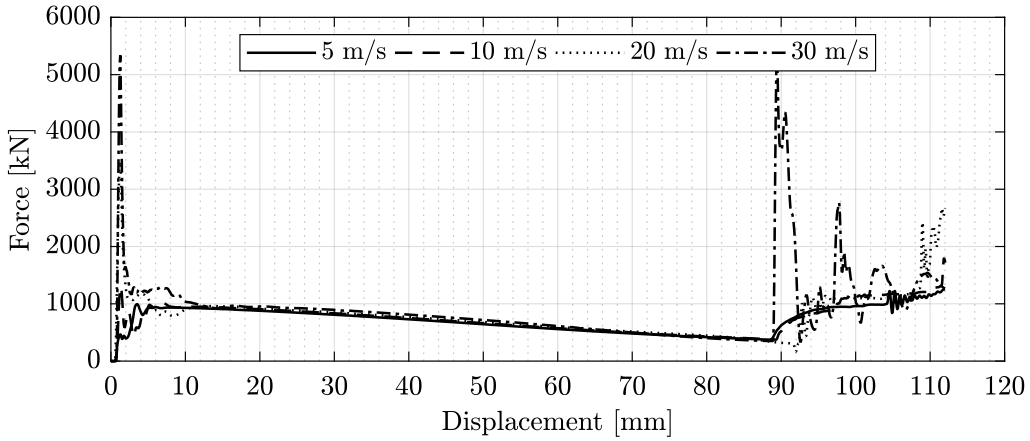

(c) $\beta = 30°$

Figure 6.23: Effect of the impact velocity on Force-Displacement plots of different models.

Figure 6.23 shows the effect of the impact velocity on the force-displacement plots for the models of the reference case. For each model with increasing base conical angle β, increasing impact velocity values causes the first peak reaction force to increase at the first impact of the striking plate and the absorber. After the first contact occurs, the reaction force response of the models have the same decreasing trend regardless of the impact velocity.

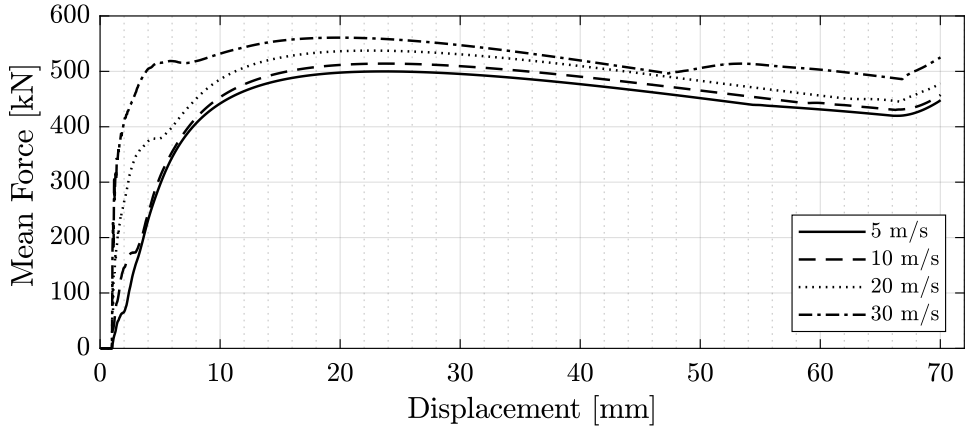

(a) $\beta = 20°$

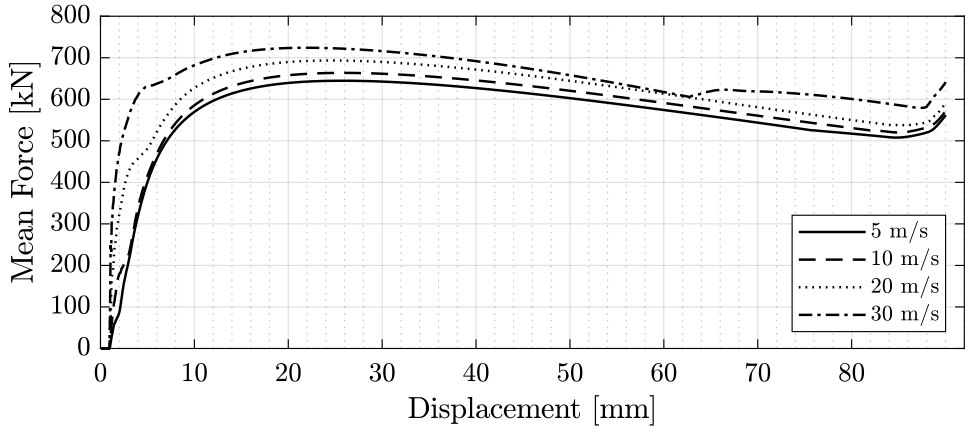

(b) $\beta = 25°$

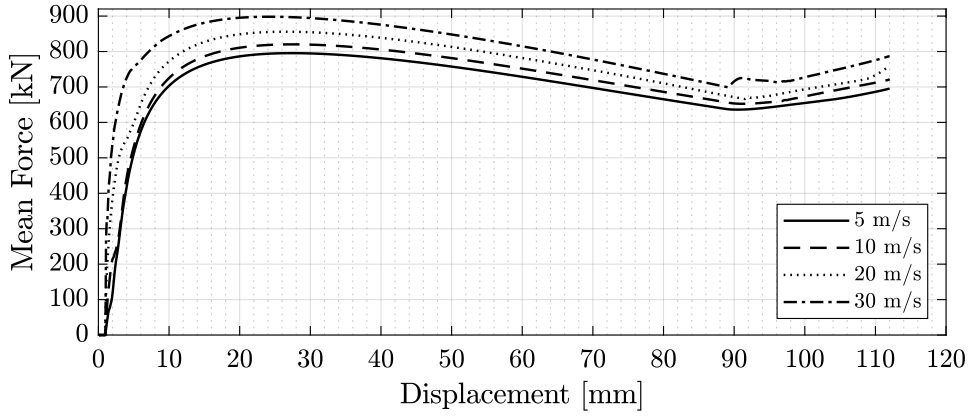

(c) $\beta = 30°$

Figure 6.24: Effect of the impact velocity on Force-Displacement plots of different models.

Increasing the impact velocity affects the mean dynamic load values to increase as seen in Figure 6.24. The mean dynamic force values were calculated by dividing the absorbed energy values to the deflection on the model as mentioned before. From the reaction force-displacement trends of the models, it is observed that both first peak and mean reaction force values have an increasing behavior as the impact velocity increases. It is also seen that, the mean dynamic force plots increase more rapidly for higher impact velocities, which is caused by the increase on the first peak reaction force values.

As seen in Figure 6.23, the second peak loads can be observed more apparently at the impact velocity of $30m/s$. The second and later peaks of the force-displacement curves are caused by the contacts between surfaces of the impactor, absorber and rigid wall and even the self surfaces of the absorber.

The same explicit response of the structure at first and second contact points can also be seen in mean dynamic force responses in Figure 6.24. The change on the response of the structures may be caused by both strain-rate dependent material model and also the inertia effects during the simulations.

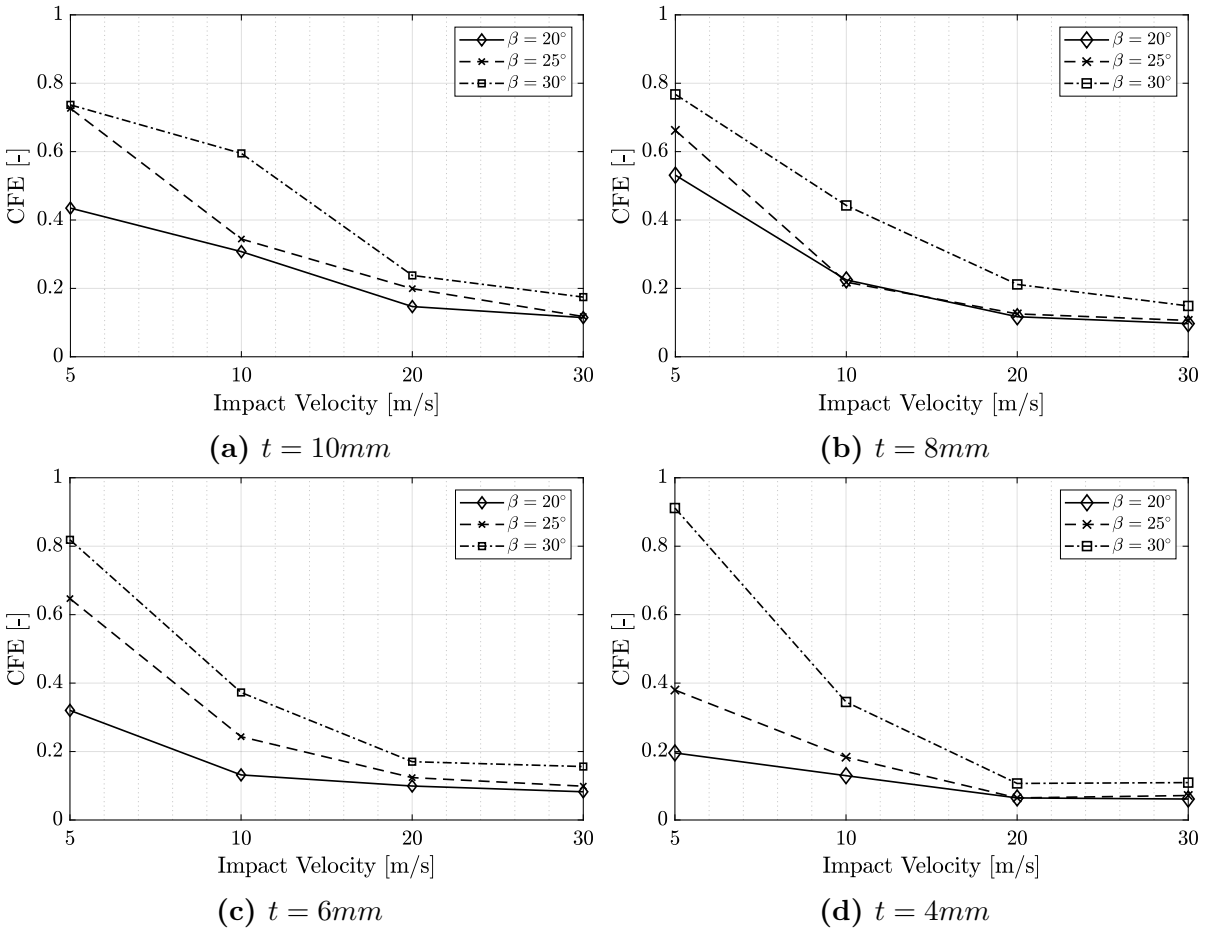

(a) $t = 10mm$ **(b)** $t = 8mm$

(c) $t = 6mm$ **(d)** $t = 4mm$

Figure 6.25: Effect of impact velocity on the crash force efficiency values for different models.

The increase of the first peak reaction force also significantly change the crash force efficiency values of the structures. CFE values are plotted in Figure 6.25 as a function of impact velocity for models with different absorber thickness and base conical angle. The CFE values significantly decrease as the impact velocity increases.

The effect of the impact velocity on the CFE values are more evident on the models with higher base conical angle and lower absorber thickness. For instance, CFE values vary from 0.91 to 0.11 for the model with $\beta = 30°$ and $t = 4mm$ when the impact velocity is increased from $5m/s$ to $30m/s$.

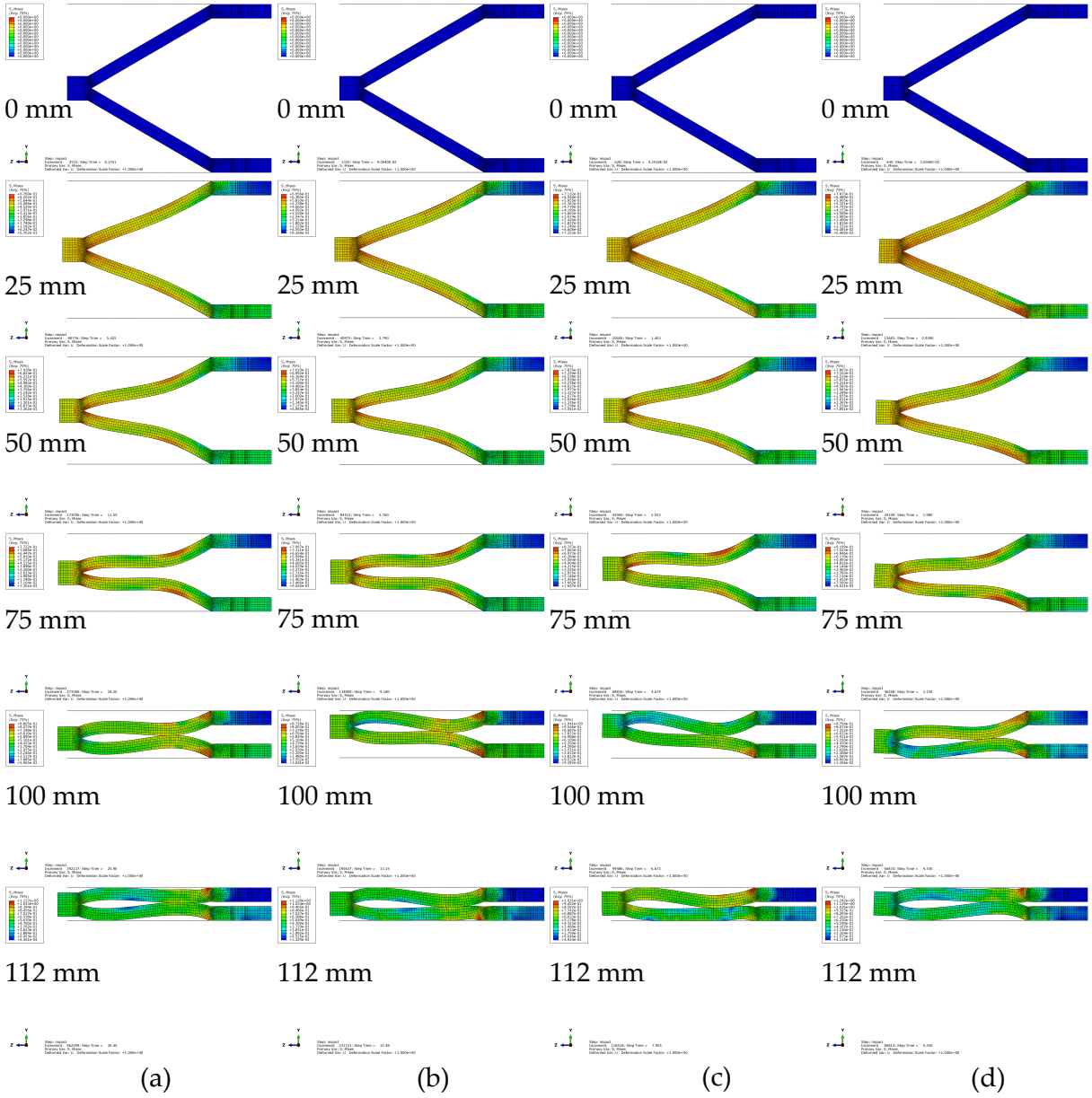

Figure 6.26: Effect of impact velocity on the deformation history of the model with parameters of $t = 10mm$, $\beta = 30°$, $E_{KE} = 100kJ$ for different impact velocities; a) $5m/s$, b) $10m/s$, c) $20m/s$, d) $30m/s$.

The deformation mode of the models are slightly affected by the increasing impact velocity. Deformation history of the models are shown in Figure 6.26 for the model with parameters $t = 10mm$ and $\beta = 30°$. When the impact velocity increases from $20m/s$ to $30m/s$, the change of deformation mode becomes more clear. After some amount of deformation, the deformed shape of the structures change slightly as the impact velocity increases. This situation may be caused by the stress waves as a result of higher velocity impact or strain-rate dependent material model . The inertia effects may become more visible in this particular case. Presence of the inertia effects are investigated in detail in further sections.

The effect of the impact velocity is also compared for the performance parameters such as specific energy absorption and the absorbed energy per unit deformation. The change of the SEA values are shown in Figure 6.27 as a function of impact velocity for the models with initial kinetic energy of $100kJ$. SEA values also have an increasing trend as the impact velocity increases. This is an expected behavior because this parameter is directly related to the mass of the structures and the absorbed energy values. As the mass of the structures are lower for the structures with lower thickness, the increase of the SEA values are more significant. The same situation is also present for the structures with higher base conical angle values which have relatively higher absorbed energy values due to the geometry.

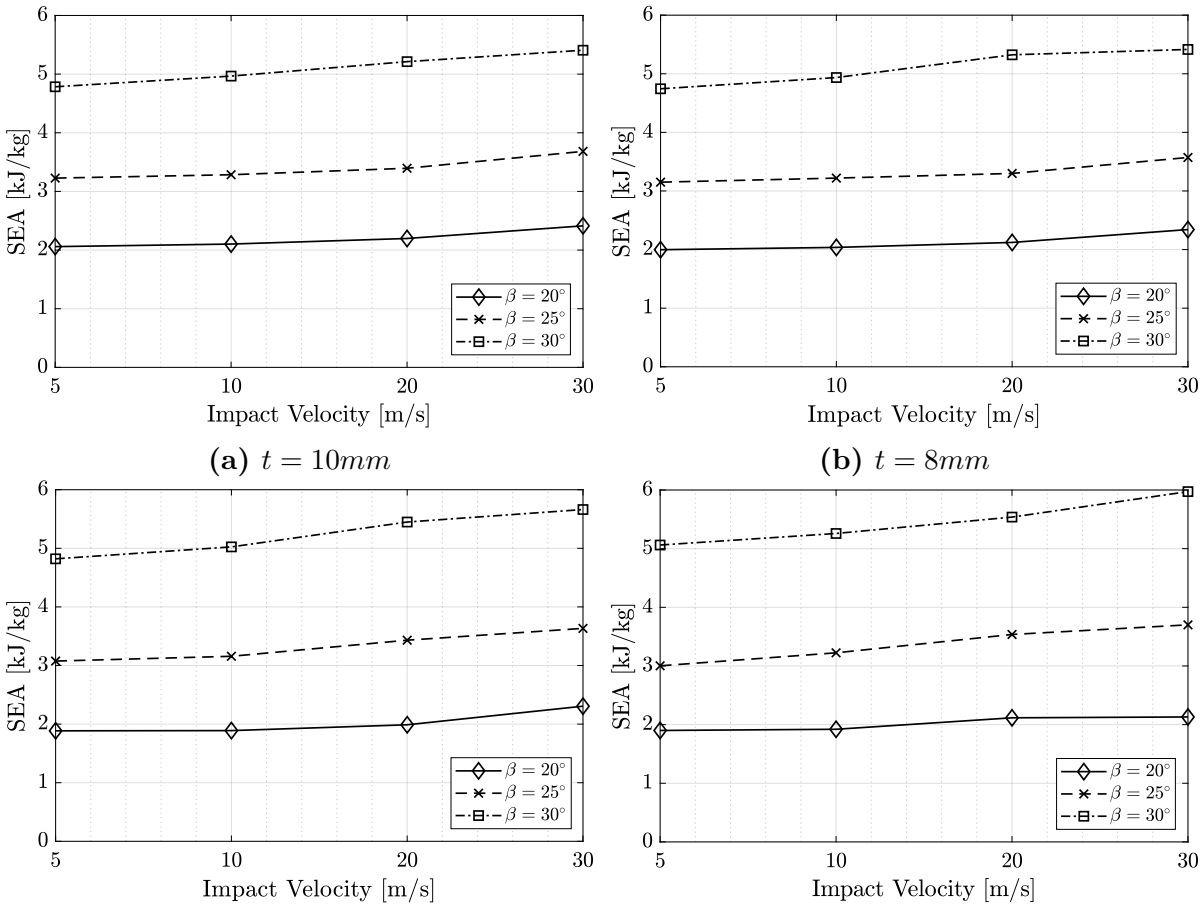

(a) $t = 10mm$ **(b)** $t = 8mm$

(c) $t = 6mm$ **(d)** $t = 4mm$

Figure 6.27: Effect of impact velocity on the SEA values for different models.

Figure 6.28 shows the influence of the impact velocity on the absorbed energy values per unit deformation. Both three models with different conical angles have their own constant maximum deformation lengths due to the geometry and all models are completely deformed. Therefore, the absorbed energy values per unit deformation have an increasing behavior as the absorbed energy values increase with increasing impact velocity. For the structures with lower base conical angle, the influence of the velocity is more significant at higher impact velocity values due to the lower deformation length caused by the geometry.

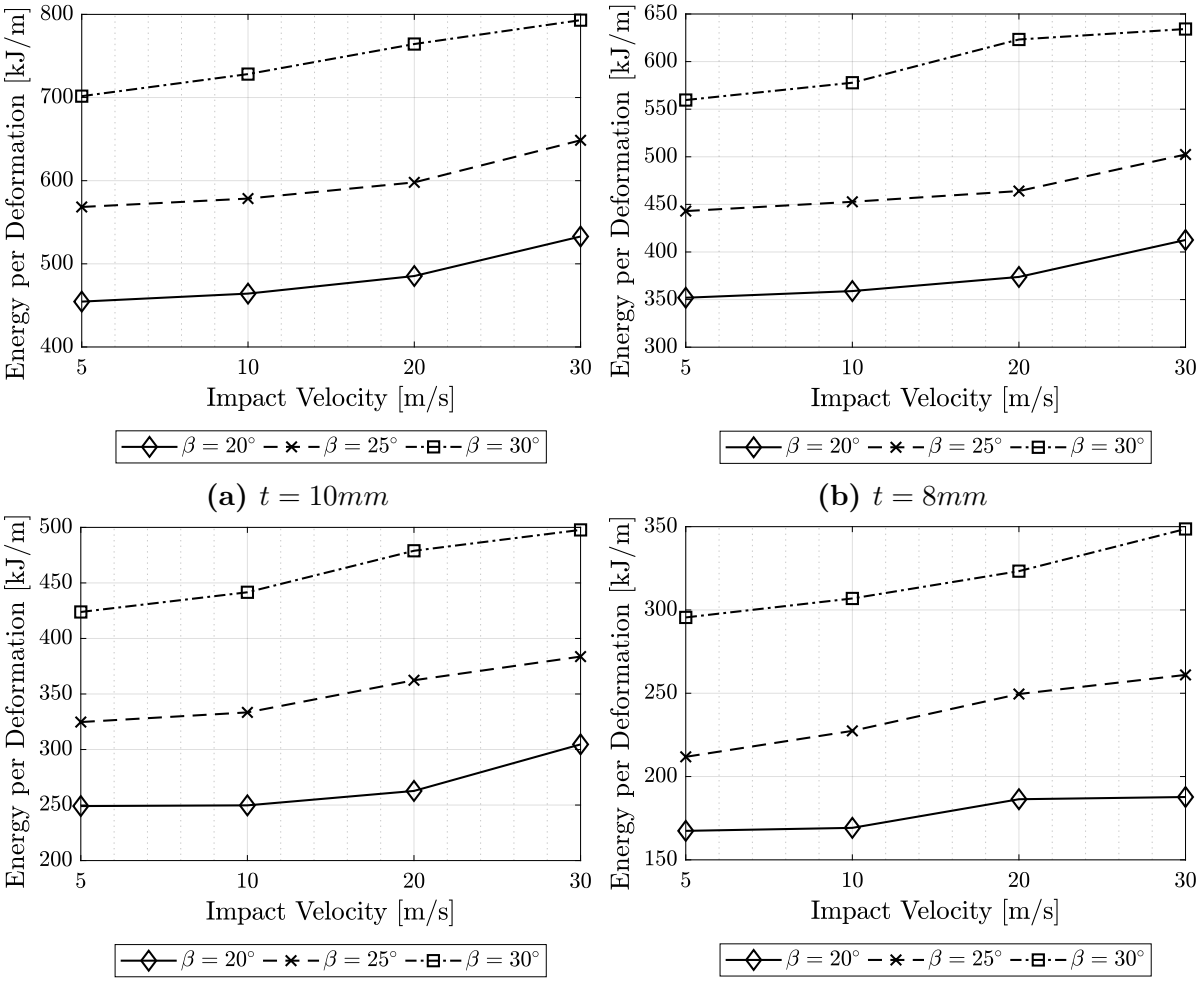

(a) $t = 10mm$ **(b)** $t = 8mm$

(c) $t = 6mm$ **(d)** $t = 4mm$

Figure 6.28: Effect of impact velocity on the absorbed energy values per unit deformation for different models.

6.3.4 Effect of Base Conical Angle

The base conical angle is also an important parameter because it significantly changes the geometry and impact behavior of the structure.Three different angle values ($\beta = 20°$, $\beta = 25°$ and $\beta = 30°$) are selected and compared. The range of the conical angle is selected by considering the absorber to have a shallow geometry as it is one of the aims of the present study. The comparison of the effect of the selected conical angles on the dynamic and mean dynamic reaction force values is presented in this chapter, by using the model with absorber thickness of $10mm$, and the impact energy of $100kJ$. Dynamic force response of the models are shown in Figure 6.29 as a function of displacement for four different impact velocities to easily compare for each case. It is clearly seen that, the initial peak load for each impact velocity, have an increasing behavior as the base conical angle increases. This is caused by the effects of the angle on the geometry and so on the bending stiffness of the structure. With increasing angle, the maximum force to start the bending of the structure increases. However, the base conical angle does not have a significant effect on the characteristic of the force-displacement curves.

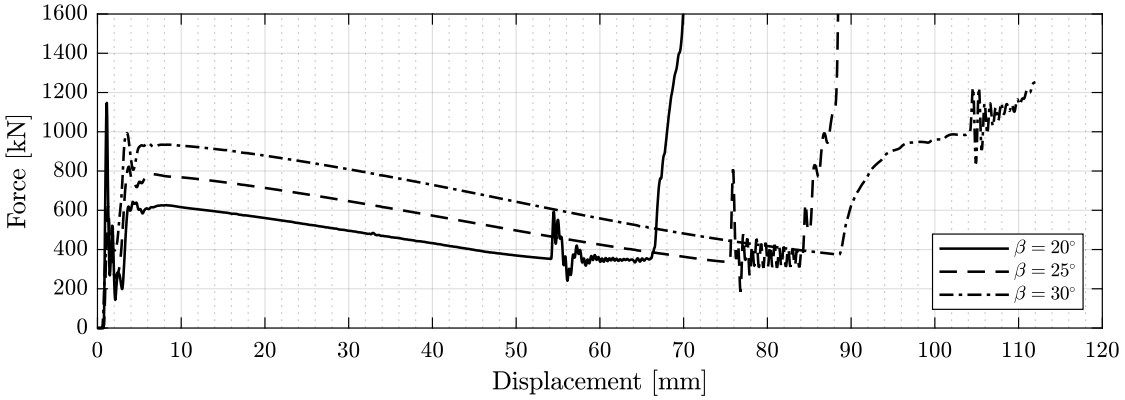

(a) $V = 5m/s$

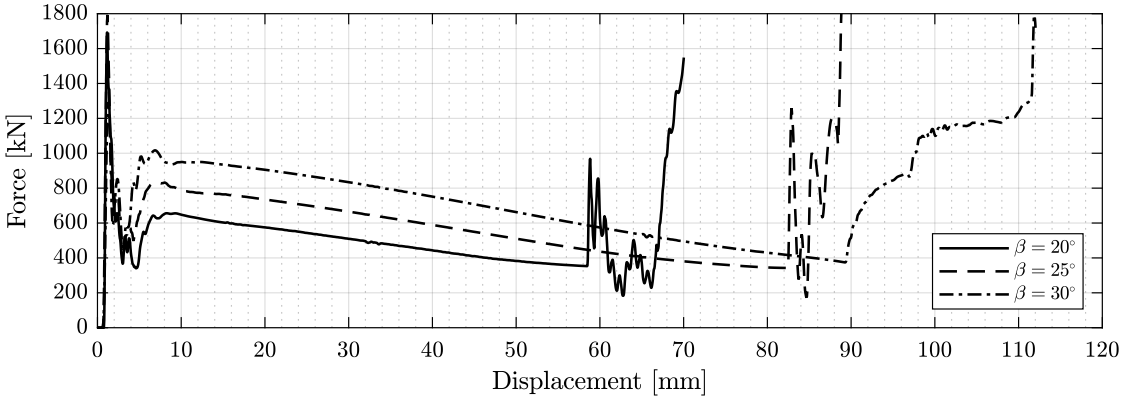

(b) $V = 10m/s$

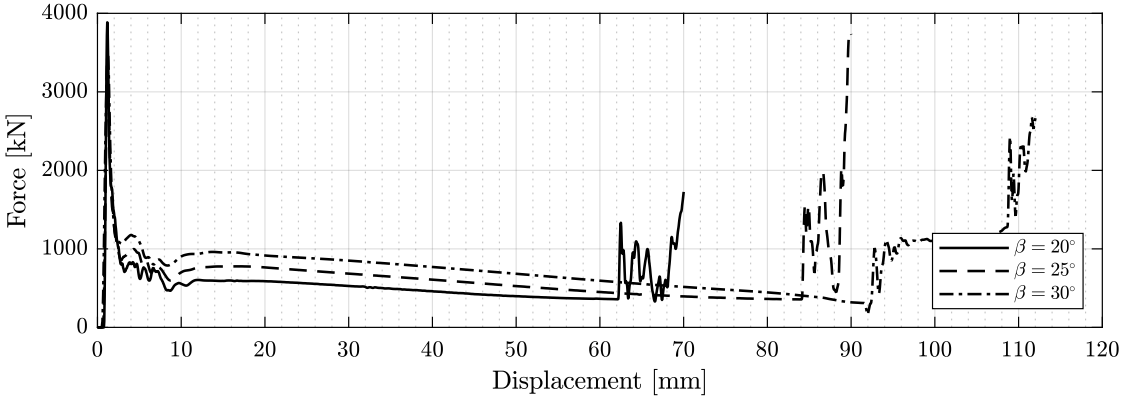

(c) $V = 20m/s$

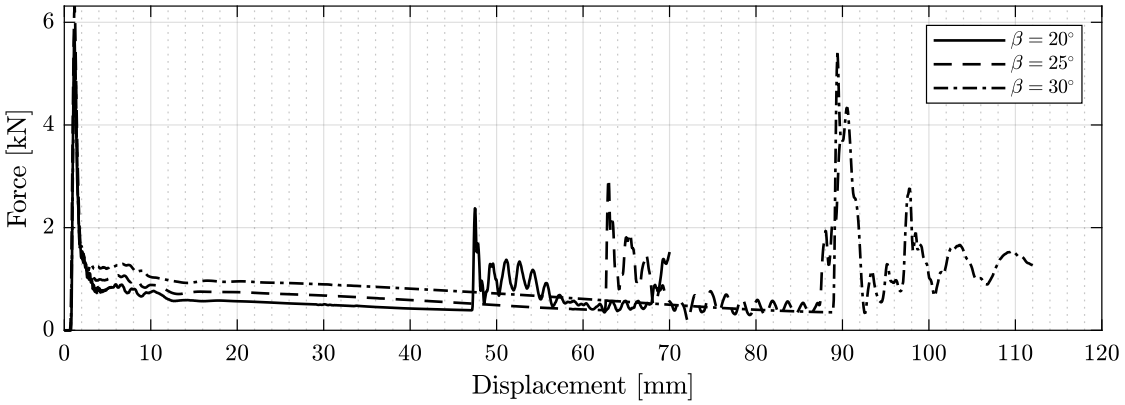

(d) $V = 30m/s$

Figure 6.29: Effect of the base conical angle on Force-Displacement plots of different models.

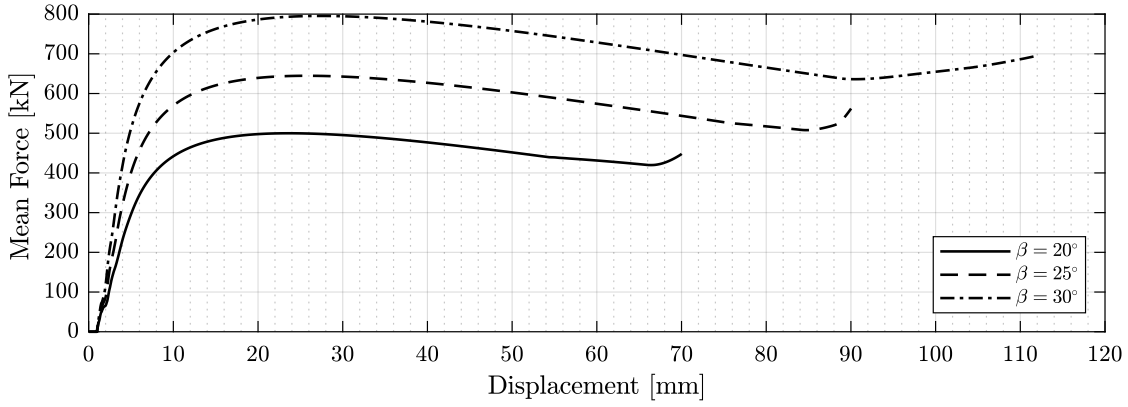

(a) $V = 5m/s$

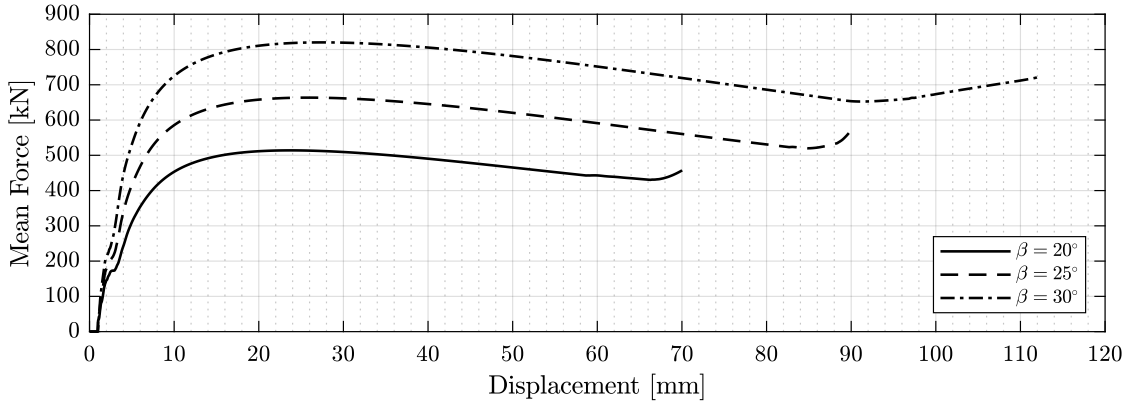

(b) $V = 10m/s$

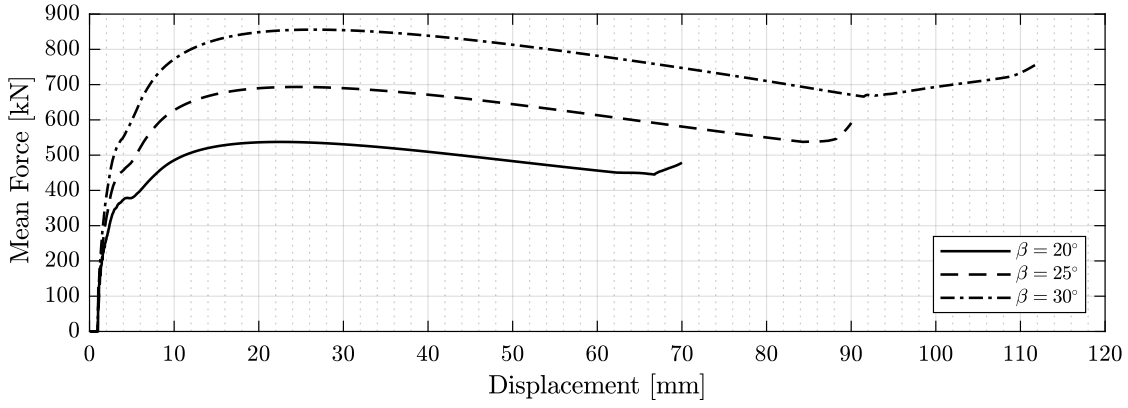

(c) $V = 20m/s$

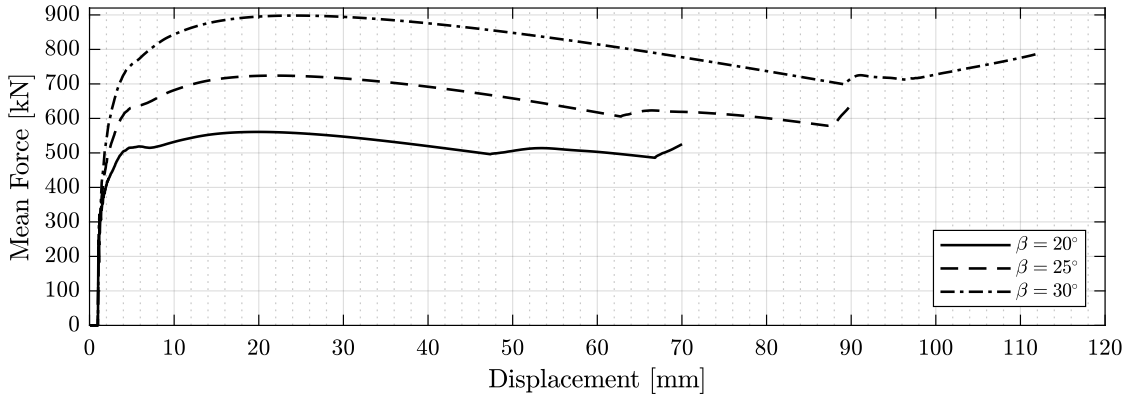

(d) $V = 30m/s$

Figure 6.30: Effect of the base conical angle on mean dynamic force response of different models.

The absorved energy values of the structures under the influence of the base conical angle, are shown in Figure 6.31. The energy absorption curves also show a similar behavior as the reaction force curves. For the same amount of absorbed energy, the structure with higher conical angle reaches to the amount in less deformation. In other words, structures with higher conical angle, absorbs more energy at the same crushing distance. Structures with lower base conical angle are more prone to bending due to their shallow geometry. This situation is also the result of the force-displacement characteristics of the investigated absorber structures.

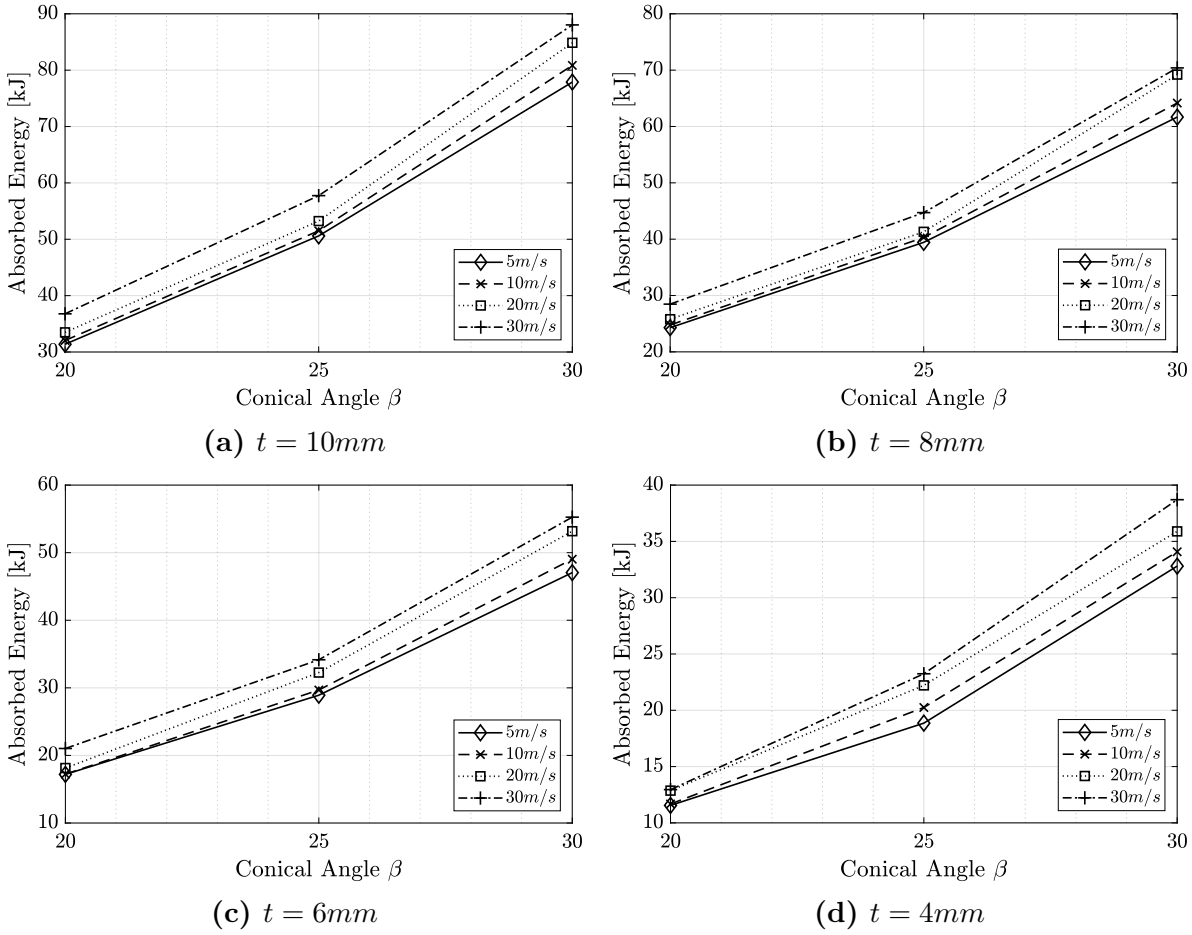

(a) $t = 10mm$ **(b)** $t = 8mm$

(c) $t = 6mm$ **(d)** $t = 4mm$

Figure 6.31: Effect of the base conical angle on the absorbed energy values of different models.

On the other hand, the base conical angle of the structure has no significant effect on the deformation modes of simulations up to a certain deformation. The deformation history of the models with three different conical angle are shown in Figure 6.32. The structures with higher conical angle have longer deformation length as expected.

All models have similar bending shapes but at different deformation length. Figure 6.32 contains the deformation history of the model with a thickness of $10mm$, impact energy of $100kJ$ and at the impact velocity of $30m/s$. Other combinations of variables also have similar behavior with the current model.

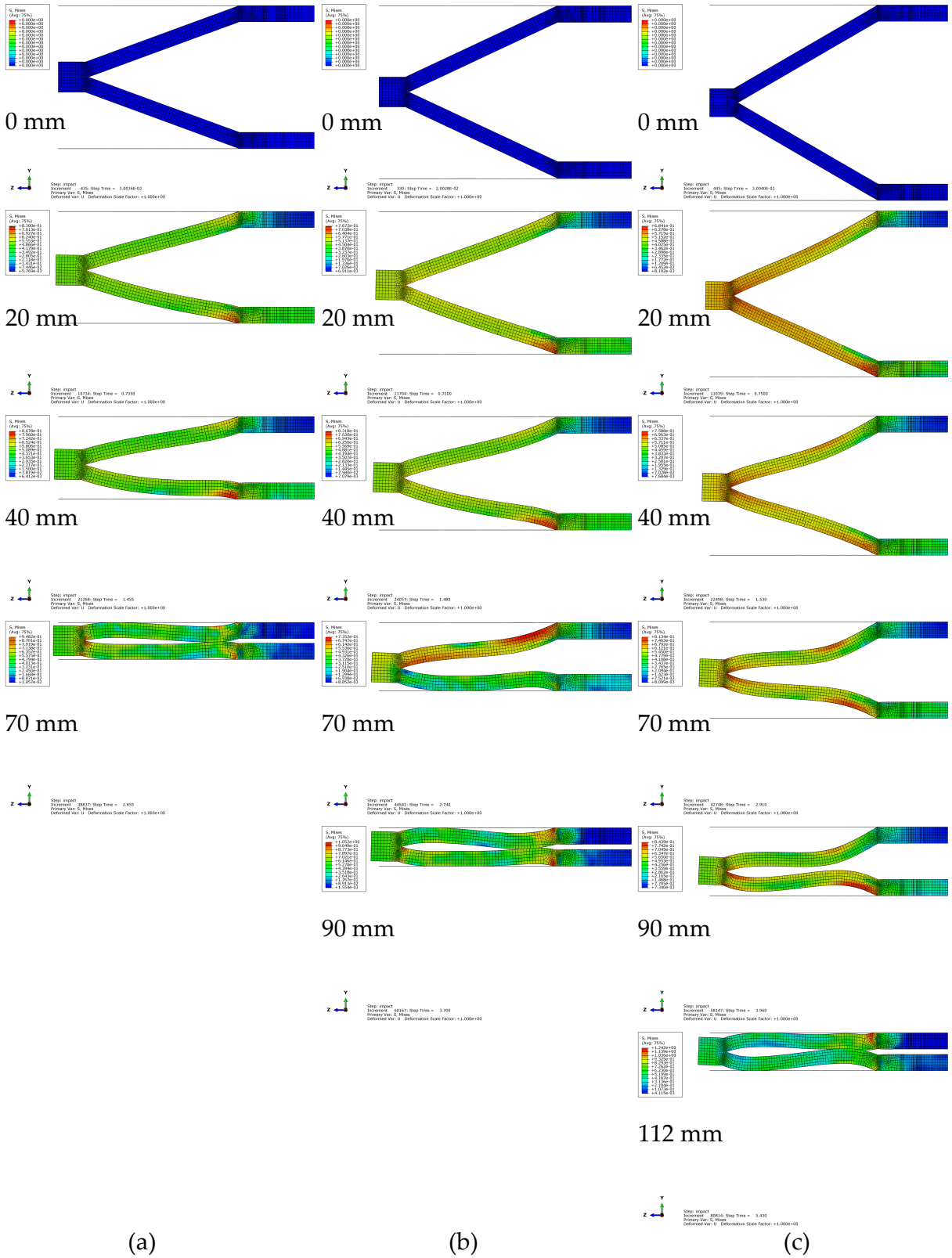

Figure 6.32: Effect of the base conical angle on the deformation history of the model with parameters of $t = 10mm$, $V = 30m/s$, $E_{KE} = 100kJ$ for different conical angles; a) $\beta = 20°$, b) $\beta = 25°$, c) $\beta = 30°$

The peak reaction force values also increase as the conical angle (β) increases. Structures become more resistant to bending with increasing β values. Therefore, structures have higher peak and mean reaction force values as the impact occurs. This behavior can also be seen in Figure 6.29 as complete reaction force history of the models.

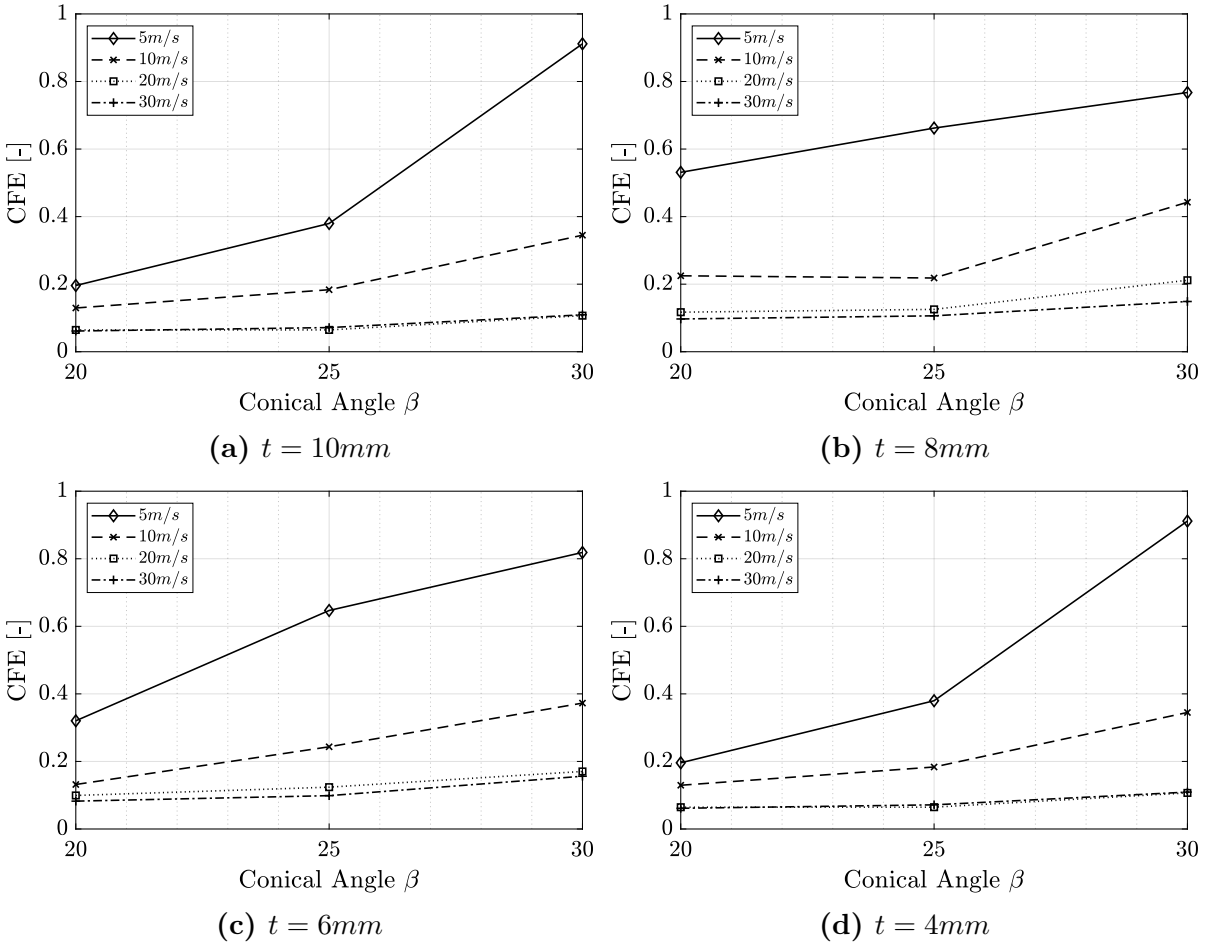

(a) $t = 10mm$ **(b)** $t = 8mm$

(c) $t = 6mm$ **(d)** $t = 4mm$

Figure 6.33: Effect of base conical angle on CFE values for different models.

As mentioned before, the maximum deformable length of the structures increase as the conical angle increases. The increase in the deformable length also means a longer and so bigger and heavier structures. The weight of the structures have a direct influence on the specific energy absorption (SEA). The SEA values increase as the base conical angle increases even if these two parameters (mass and SEA) are inversely proportional to each other. This is caused by the increase in the absorbed energy has a greater effect on the SEA than the increase in the weight of the structures. The effect of the base conical angle on the SEA values are shown on Figure 6.34.

This behavior is also the same for the effect of the angle on the absorbed energy per unit deformation values. Absorbed energy per unit deformation values also increase as the base conical angle increases and so the maximum deformable length. Figure 6.35 shows the trends of the absorbed energy values for the models with impact velocities in range of $5m/s$ to $30m/s$ and absorber thicknesses $4mm$ to $10mm$ as a function of β.

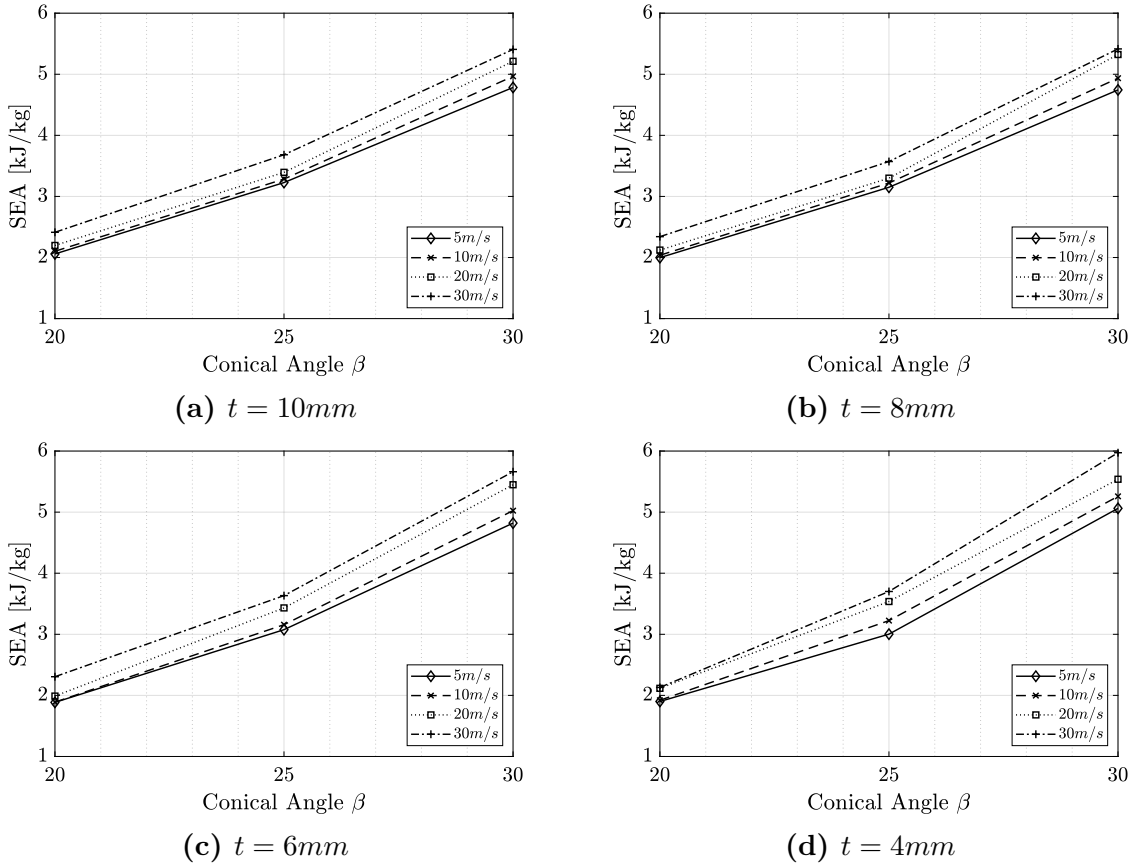

(a) $t = 10mm$ **(b)** $t = 8mm$

(c) $t = 6mm$ **(d)** $t = 4mm$

Figure 6.34: Effect of base conical angle on the SEA values for different models.

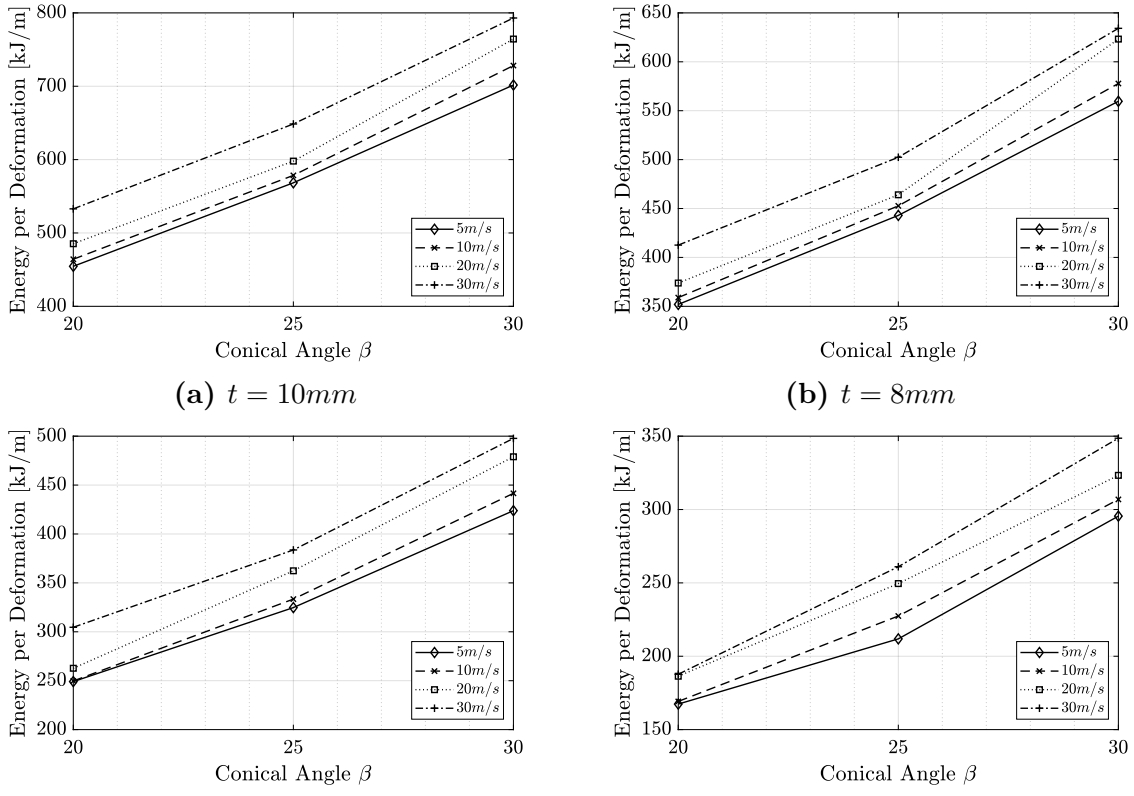

(a) $t = 10mm$ **(b)** $t = 8mm$

(c) $t = 6mm$ **(d)** $t = 4mm$

Figure 6.35: Effect of base conical angle on the absorbed energy values per unit deformation for different models.

6.3.5 Effect of Absorber Thickness

The last parameter to investigate the energy absorption behavior of the conical absorber is the thickness of the absorber. In order to compare the effect, results of the models within the range of base conical angle β between 20° and 30° and impact energy of $100kJ$ are used in this section.

Figure 6.36 shows the effect of the absorber thickness on the absorbed energy values of the models. It is found that, the absorbed energy values increase with the increasing absorber thickness.The effect of the thickness on absorbed energy values is caused by the amount of material available to plastic deformation and so the energy absorption. This situation also limits the compression of each fold during the deformation as the thickness increases. Models with higher thickness, absorbs the initial kinetic energy in significantly less deformation due to the amount of material available for plastic deformation.

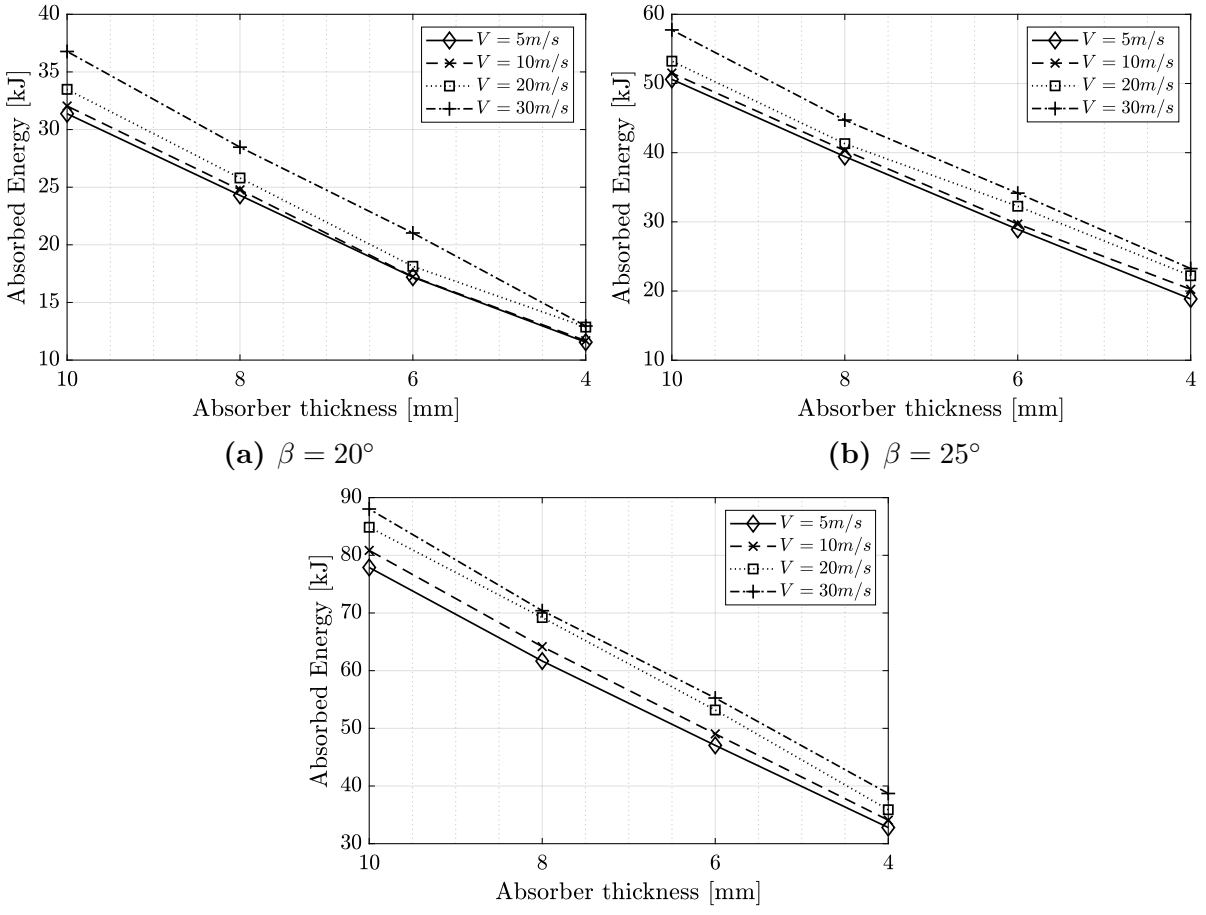

(a) $\beta = 20°$ **(b)** $\beta = 25°$

(c) $\beta = 30°$

Figure 6.36: Effect of the absorber thickness on absorbed energy values of different models.

The dynamic reaction force response of the structures are shown in figure 6.37 as a function of displacement. It is clearly seen that, the initial peak reaction force values increase as the thickness of the absorber increases. The rest of the force response of the structures are also identical.

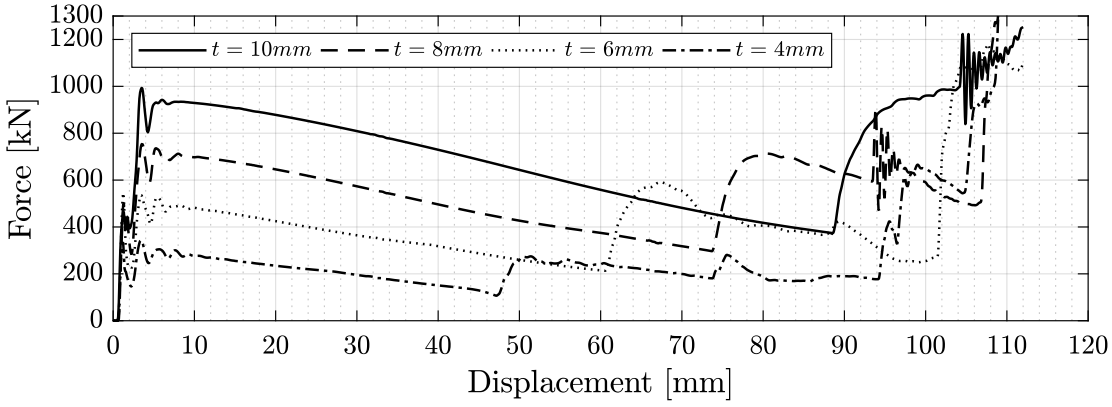

(a) $V = 5m/s$

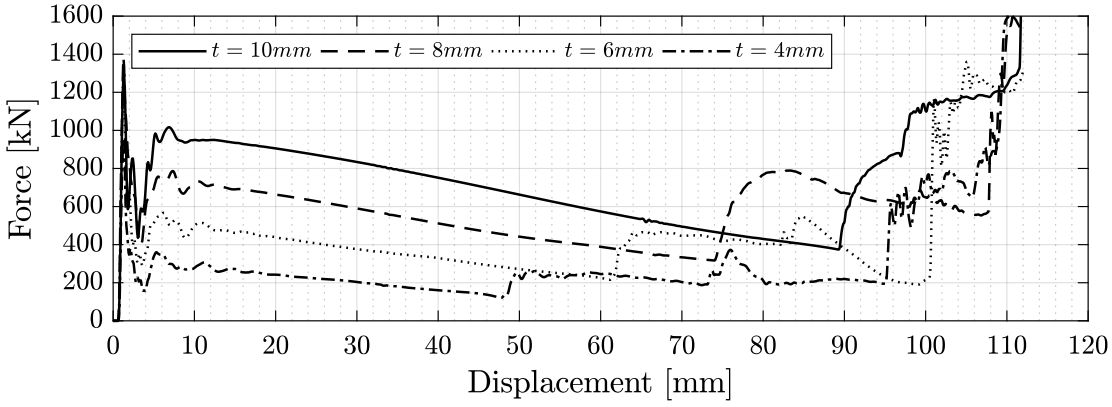

(b) $V = 10m/s$

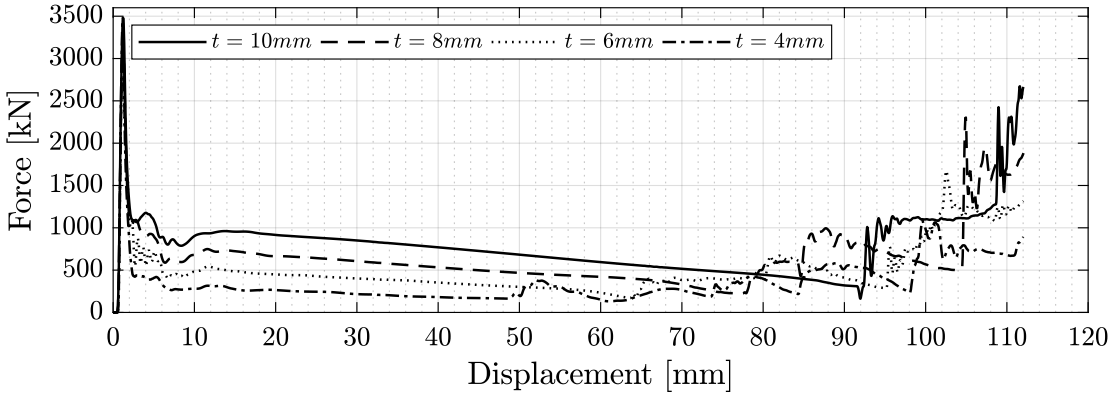

(c) $V = 20m/s$

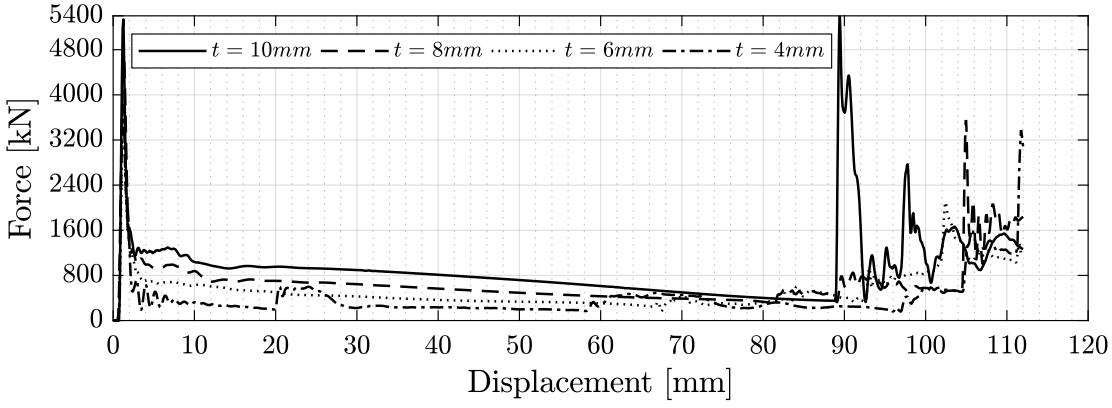

(d) $V = 30m/s$

Figure 6.37: Effect of the absorber thickness on Force-Displacement plots of different models.

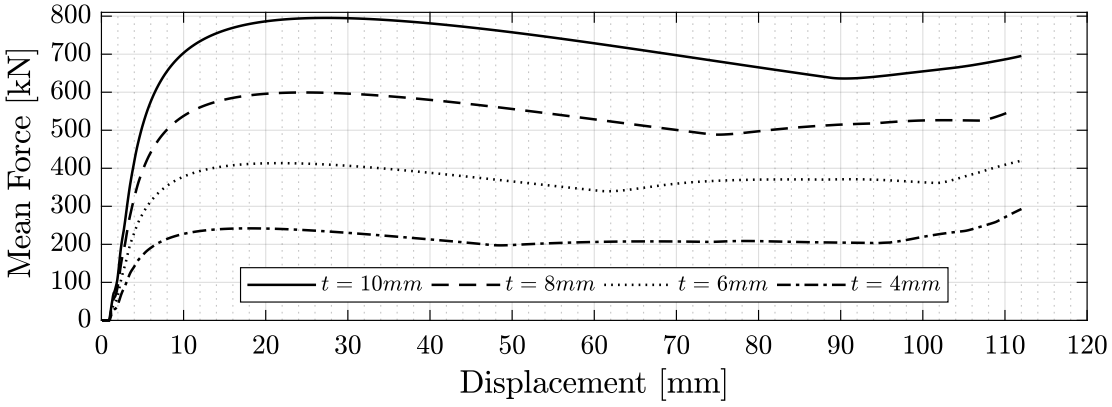

(a) $V = 5m/s$

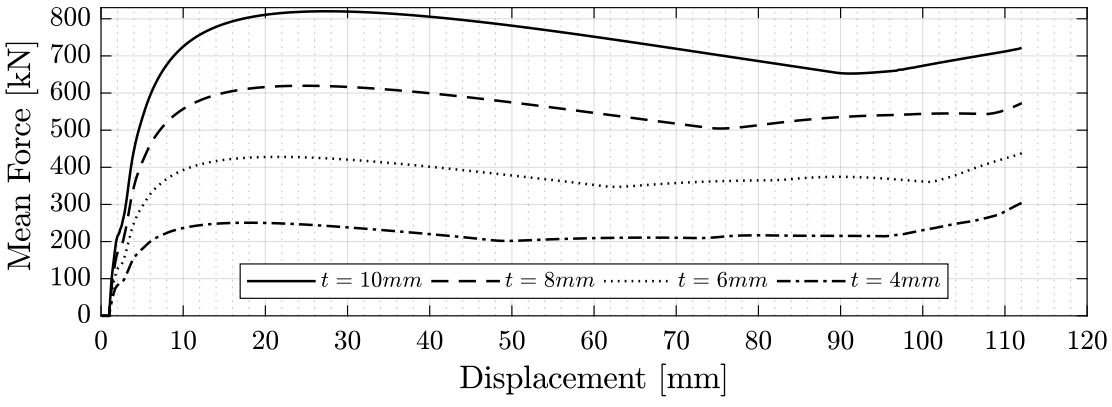

(b) $V = 10m/s$

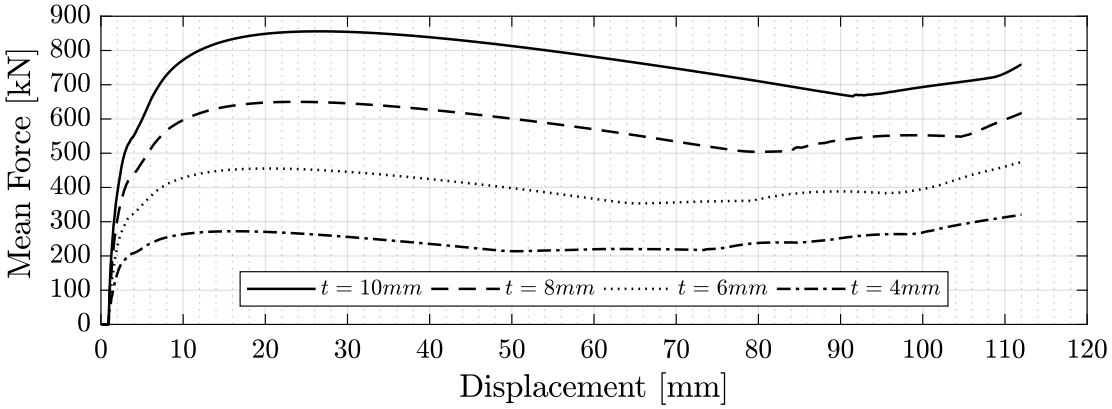

(c) $V = 20m/s$

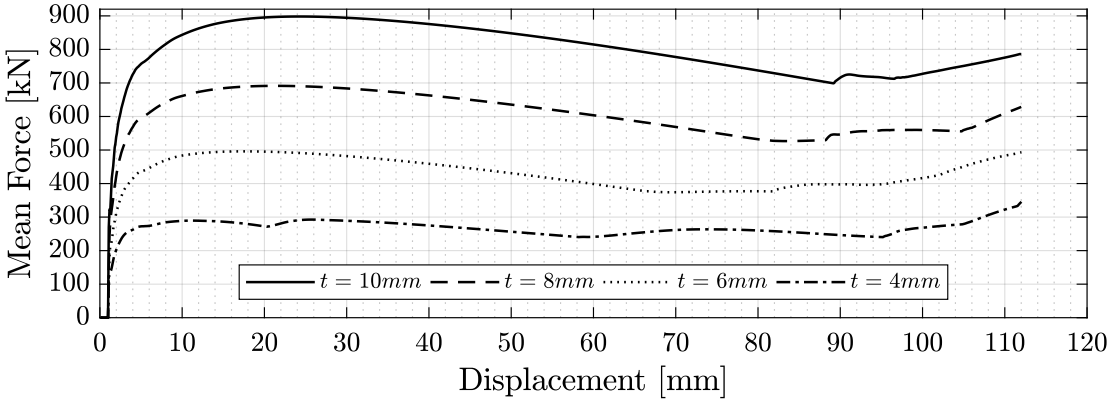

(d) $V = 30m/s$

Figure 6.38: Effect of the absorber thickness on mean dynamic force response of different models.

The main difference of the dynamic responses of the structures are between the second peak points, which are directly related to the absorber thickness. As the thickness decreases, structures become more vulnerable to bending. Structures with lower thickness have more number of folding on the structures. This effect can be seen on the force-displacement curves as an increasing behavior in a ladder pattern. Each fold causes a peak on the force response and the load starts to drop again gradually. The absorber thickness has also a significant effect on the mean dynamic force during the simulations as seen in Figure 6.38. The mean dynamic force plots have a similar but escalated trend as the absorber thickness values increase.

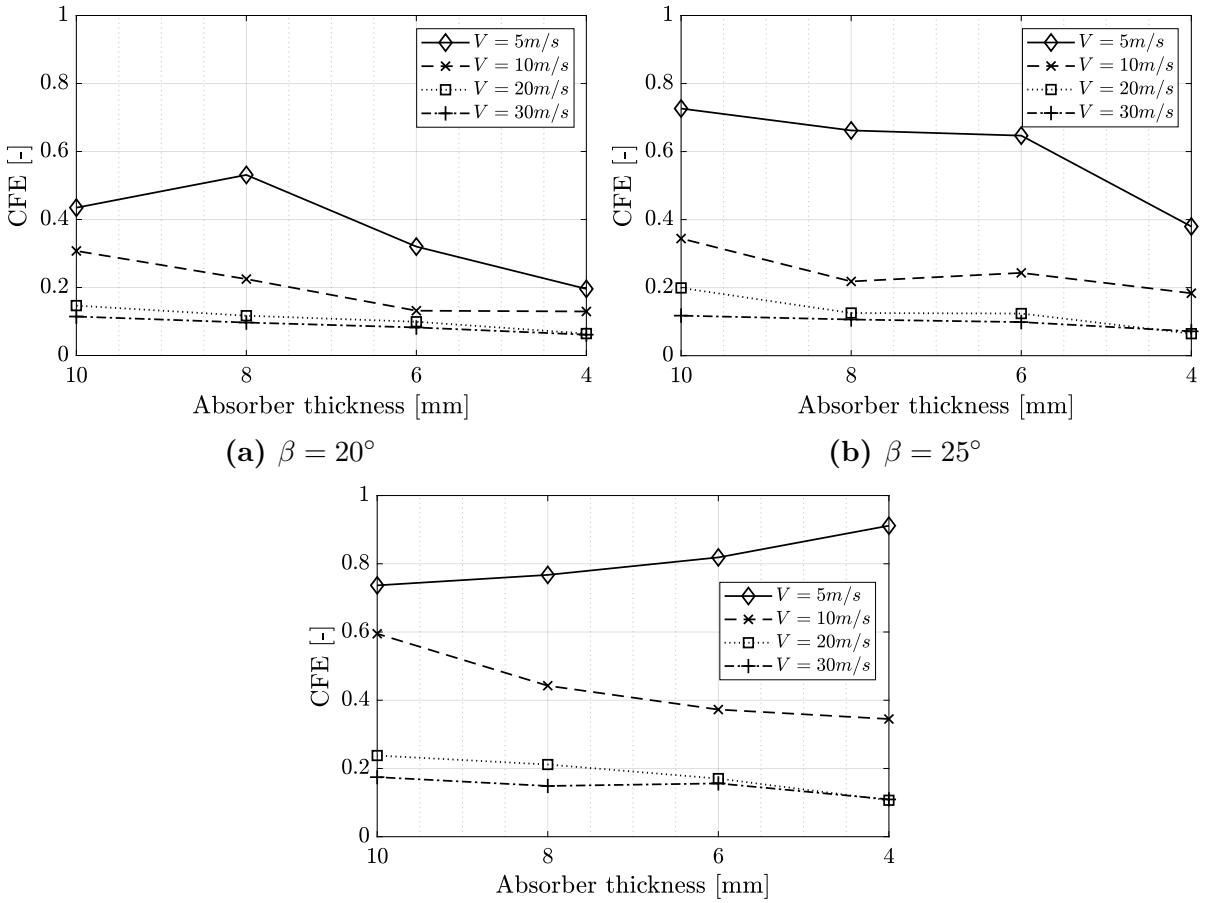

(a) $\beta = 20°$ **(b)** $\beta = 25°$

(c) $\beta = 30°$

Figure 6.39: Effect of the absorber thickness on CFE values of different models.

The crash force efficiency (CFE) values mostly have an increasing behavior as the absorber thickness increases. The effect of the absorber thickness is more significant on the models with lower impact velocity. This situation may be caused by the inertia effects and the strain rate dependency of the material model. Also the models with lower absorber thickness have more contact between surfaces during the crushing when compared to models with higher thickness values. So the ratio of the mean reaction force to the first peak reaction force values may also be affected. The comparison of the CFE values for all models are plotted in Figure 6.39 as a function of thickness for all models.

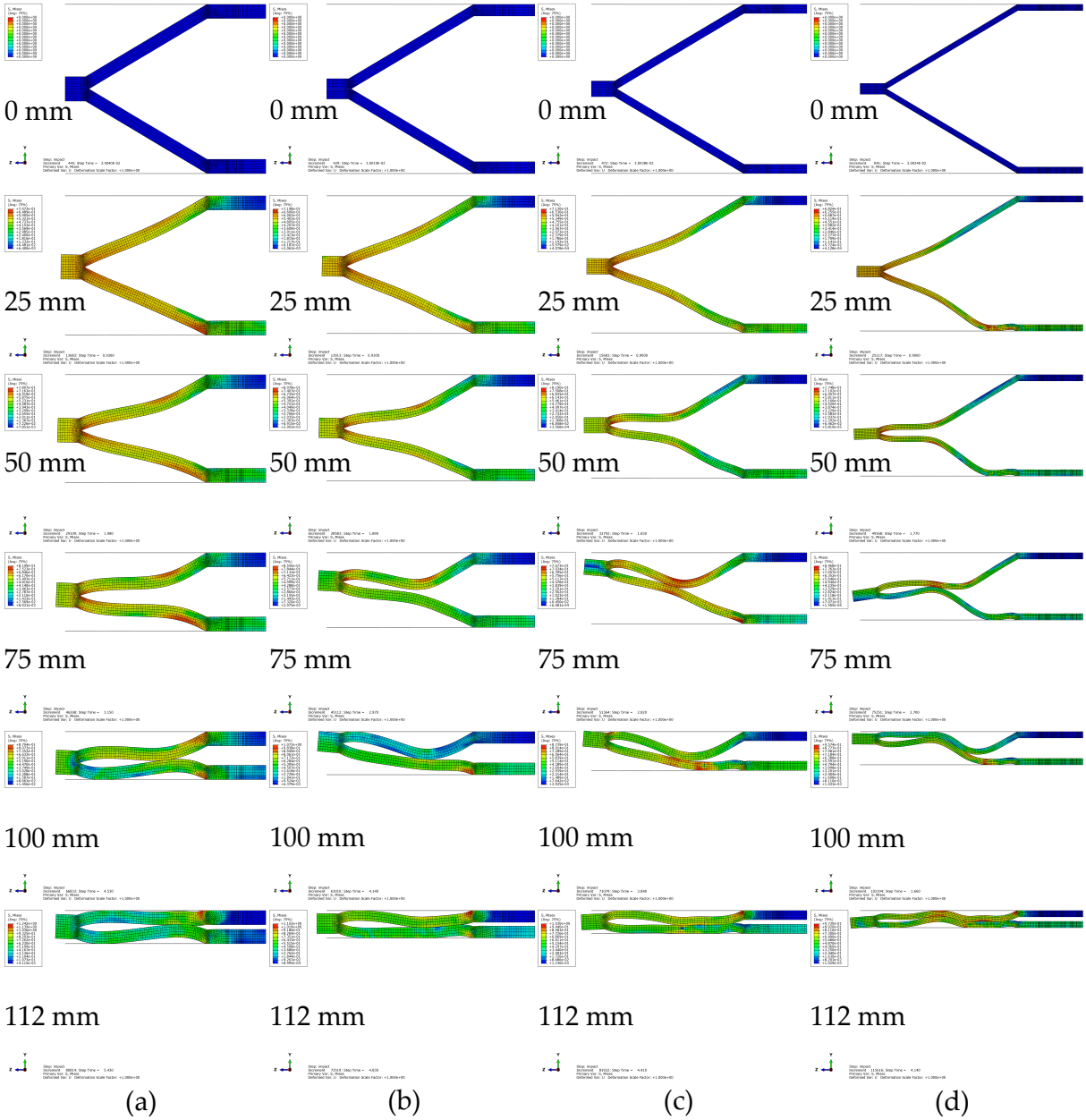

Figure 6.40: Effect of absorber thickness on the deformation history of the model with parameters of $V = 30m/s$, $\beta = 30°$ and $E_{KE} = 100kJ$ for different thickness values; a) $t = 10mm$, b) $t = 8mm$, c) $t = 6mm$ and d) $t = 4mm$

Figure 6.40 shows the deformation modes of the structures for the model with base conical angle β of 30° and impact velocity of $30m/s$ for different deformation values of the numerical simulations. Aforementioned bending and folding effects with decreasing absorber thickness can be seen in Figure 6.40. It can be seen that for lower thickness values, first bending of the structure starts at the impacted end of the conical surface, while for higher thickness values, the conical surface starts bending uniformly. Both models have similar deformation shapes at a certain crush distance but the number of bendings increase significantly as the absorber thickness decreases.

The effect of the absorber thickness on the specific energy absorption (SEA) values of the of the compared models are shown in Figure 6.41. Different from the other parameters, absorber thickness does not have a significant effect on SEA values, although SEA is strictly dependent to the weight of the absorber, which also changed by the thickness of the absorber. However, the ratio of the absorbed energy and the absorber weight stays almost equal as the thickness changes and SEA values do not change significantly. The most notable difference on the SEA values were observed on the models with higher impact velocity values, due to their relatively higher increase on the energy absorption. The maximum difference of SEA values was calculated to be %12 on the model with absorber thickness β of 20° and impact velocity of $30m/s$.

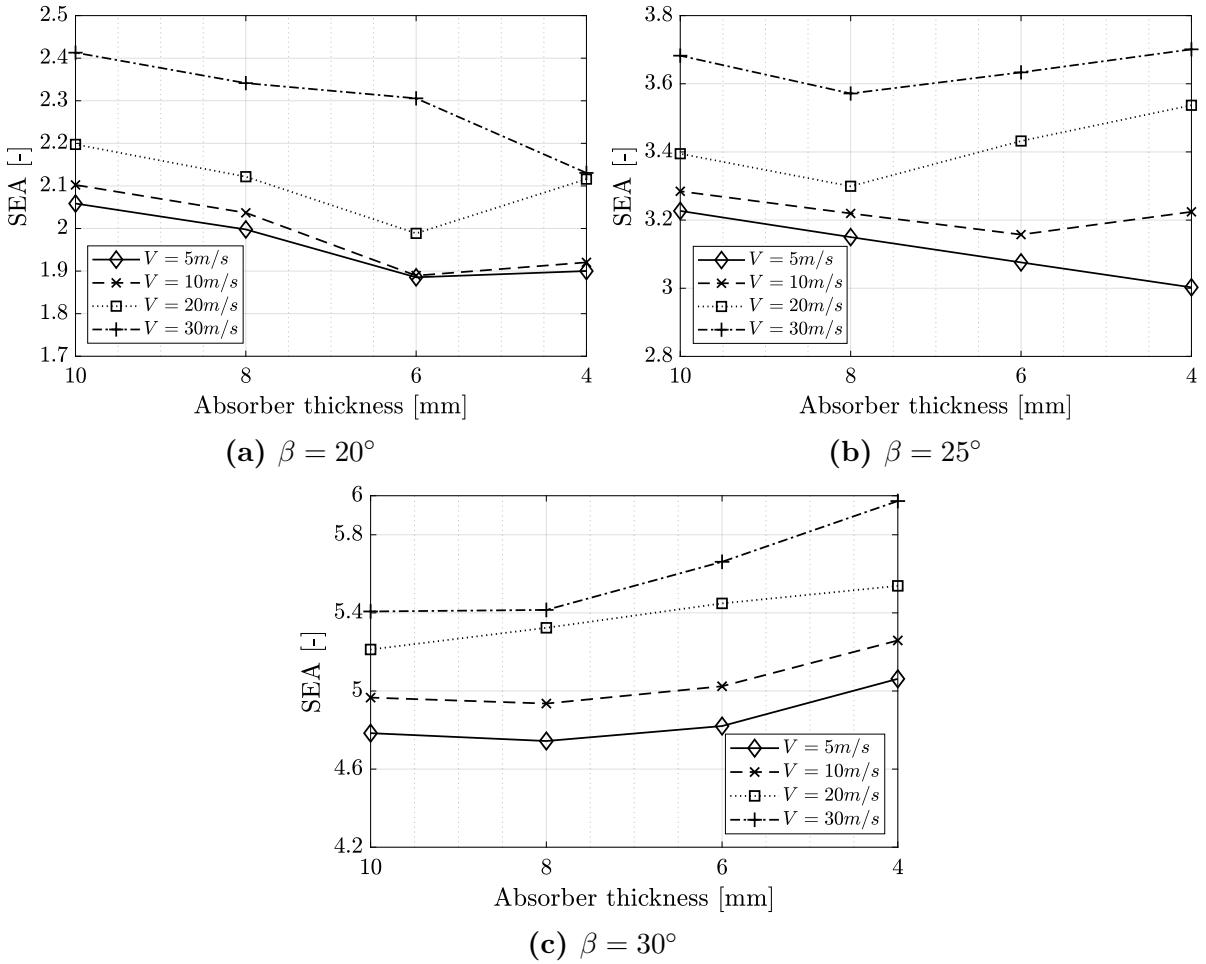

(a) $\beta = 20°$ **(b)** $\beta = 25°$

(c) $\beta = 30°$

Figure 6.41: Effect of the absorber thickness on SEA values of different models.

6.4 Comparison between Quasi-Static and Dynamic Response

In this section, the general response of the structures between quasi-static and dynamic models are compared. The difference between the responses of the structures may be caused by material properties, geometry properties and the inertia effects during loading. The most important performance parameters and the presence of the inertia effects are compared and investigated separately.

6.4.1 Reaction Force

One of the most important performance parameter of an energy absorber is the reaction force. Reaction force response of an energy absorber may change under different conditions such as loading, boundary conditions and material properties. In this case, the effect of loading on the energy absorbing performance of the conical structure is investigated. The force-displacement response of the simulations are plotted in Figure 6.42 for impact velocity values in a range of $0.01m/s$ (quasi-static) and $30m/s$ for the model with $t = 10mm$ and $\beta = 30°$.

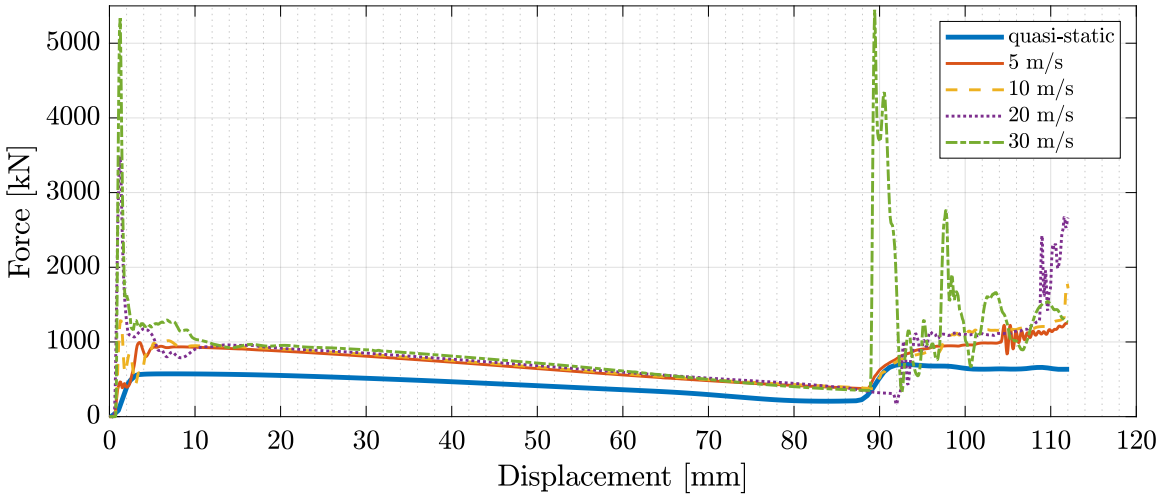

Figure 6.42: Comparison of quasi-static and dynamic Force-Displacement response of the model $\beta = 30°$ and $t = 10mm$.

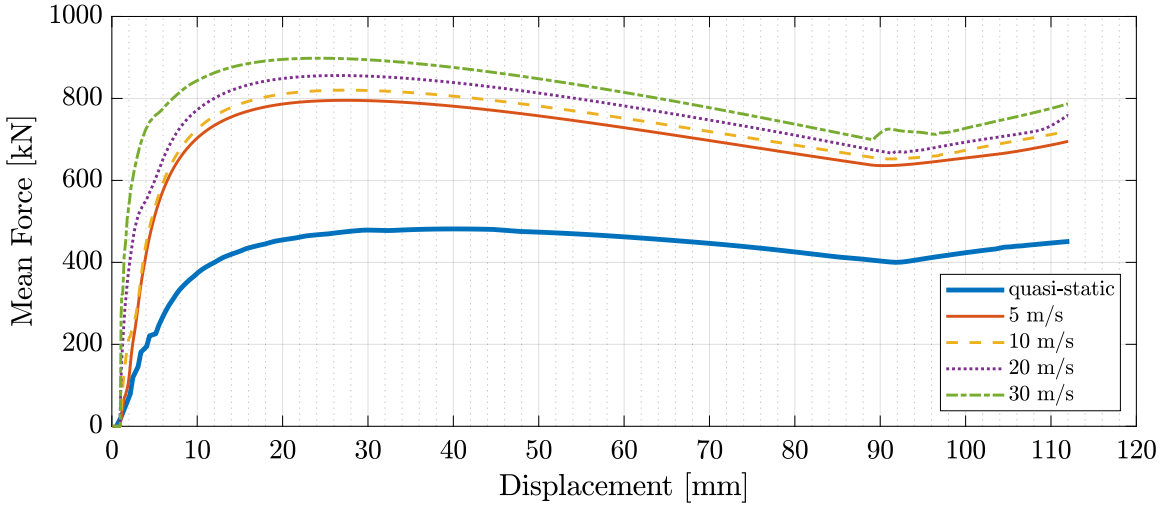

Figure 6.43: Comparison of mean Force-Displacement response of the quasi-static and dynamic models $\beta = 30°$ and $t = 10mm$.

Figure 6.43 shows the comparison of mean dynamic force response of the model with parameters $t = 10mm$ and $\beta = 30°$. It is observed that there is a significant difference between the quasi-static and dynamic cases in terms of mean reaction force response. This is caused by the strain-rate dependent material model used in this study which changes the structures response under different initial impact velocity conditions.

The force-displacement responses of the structure indicate that up to a certain value of impact velocity, the response of the structure has a similar behavior with the quasi-static case. In other words, the inertia effects on the impact response of the structure become apparent for the impact velocity values more than $10m/s$. For the higher impact velocity values, the changes on the deformation modes of the structures begin.

6.4.2 Energy Absorption

As the energy absorbing capacity of the structures are strictly related to the reaction force response, the absorbed energy curves conform with the force-displacement curves. Absorbed energy response of the model with $\beta = 30°$ and $t = 10mm$ is given in Figure 6.44 as a function of displacement. The energy absorption capacity of the structures increase with increasing impact velocity. For the impact velocity values of $20m/s$ and $30m/s$, both reaction force and the absorbed energy plots have a slightly different behavior.

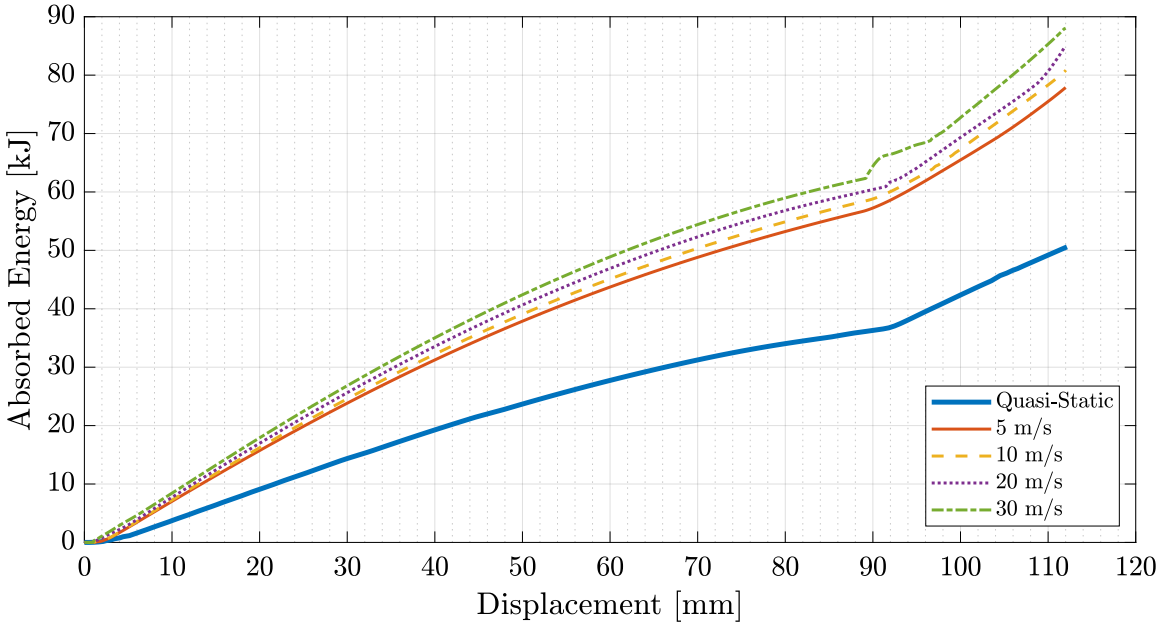

Figure 6.44: Comparison of energy absorption of the model $\beta = 30°$ and $t = 10mm$.

This situation can also be observed in the dynamic amplification factor values. DAF values of the same model are plotted in Figure 6.45 as function of displacement. As seen in the Figure 6.45, DAF values have decreasing trend with increasing deformation which may be caused by the decremental effect of strain-rate and inertia effects as the crushing of the absorber continues.

However, DAF values have a notable difference as the impact velocity increases. In Figure 6.45, DAF values at the displacement values of $10mm$ and $90mm$, at which contact between surfaces of the structure occur, are of great importance. It is seen that the increase on the DAF values of the models with impact velocities of $20m/s$ and $30m/s$ are greater than the models with lower initial velocity.

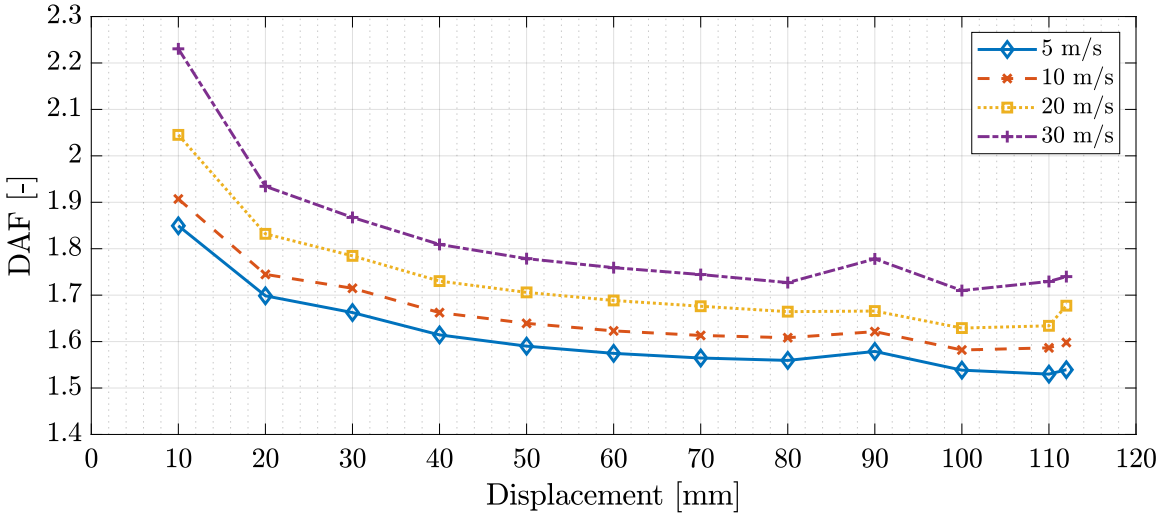

Figure 6.45: Comparison of dynamic amplification factor of the model $\beta = 30°$ and $t = 10mm$.

This situation indicates that some inertia effects may be present at the impact velocity values higher than $10m/s$. The complete comparison of the DAF values under the influence of the variables used in this study is presented in further relevant chapters.

6.4.3 Presence of Inertia Effects

In structural dynamic problems, dynamic loading is modeled using the impact mass and initial impact velocity which constitute the initial kinetic energy of the system. The increased kinetic energy by changing the impact mass has no influence on the reaction force and absorbed energy values of the models. However, the increase in the impact velocity affects the force-displacement response and the energy absorption of the structure even if the kinetic energy is kept constant. The increase of the absorbed energy with increasing impact velocity may be associated with the inertia effects including plastic stress wave propagation and nonlinear response. [48] A similar effect has been observed for axial impact loading of square tubes with a strain rate insensitive material model. [30, 49] The increasing effect of the impact velocity on the structural behavior was associated with inertia effects due to the lateral movement of the sidewalls. The increase of the energy absorption values due to increasing impact velocity values caused by the inertia effects were also observed by Gupta et. al. [37] for axially impacted aluminum conical tubes. Another study by Ahmad [22] presented that both empty and foam-filled conical tubes seem to be less sensitive to the impact velocity beyond $10m/s$.

In the present study, the strain-rate dependency of the used material is taken into consideration. In Figure 6.42, it can be seen that the force-displacement response becomes affected for impact velocities higher than $10m/s$. Also the dynamic amplification factor values are affected by the increasing impact velocity, especially for impact velocity values higher than $10m/s$.

Thus, the increase of the absorbed energy with increasing impact velocity may be associated with the velocity sensitive material model. For this reason, the strain-rate sensitivity properties of the current material model are removed and the simulations were repeated without the effect of the strain-rate.

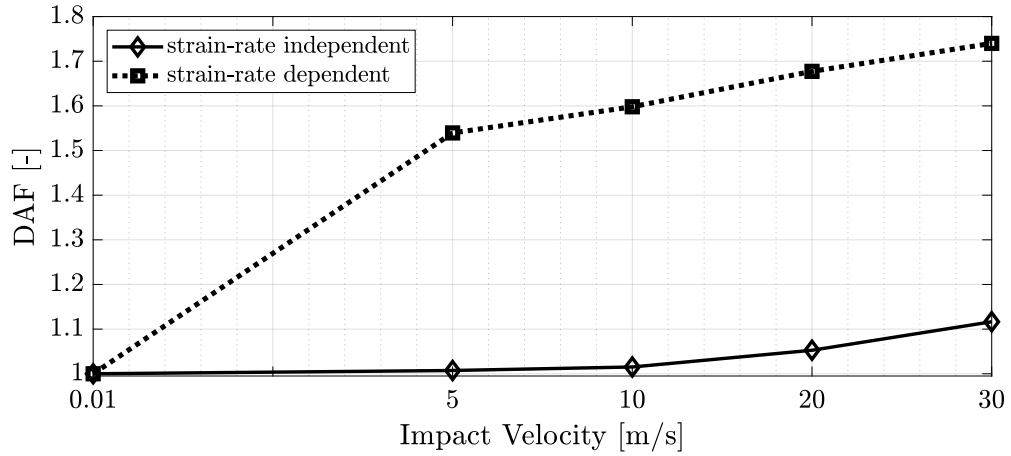

Figure 6.46: Effect of strain rate dependency of the material on the dynamic amplification factor for the model with $\beta = 30°$ and $t = 10mm$.

Figure 6.46 shows the dynamic amplification factor values of the models with and without strain-rate dependency of the current material model as a function of initial impact velocity. It is clearly seen that the dynamic absorbed energy values increase with increasing velocity even if the strain-rate dependency of the material is neglected. Thus, the increase of the absorbed energy with increasing impact velocity may also be associated with the inertia effects including plastic stress wave propagation and nonlinear response.

The influence of inertia forces on the dynamic response of the current geometry has been investigated. The presence of the axial inertia effects can be identified by comparing the force response of at the impacted end and the fixed end of the structure. This approach has been used by several authors to investigate the inertia effects on various structures under dynamic loading. [50, 21] For this purpose, reaction forces on both impacted end and the fixed ends of the model with $t = 10mm$ and $\beta = 30°$ were compared for different impact velocity values. The initial kinetic energy of the simulations were kept constant at $100kJ$ by changing the impact mass.

As seen in Figure 6.47, the load response, at both ends of the structures have similar values for the models with impact velocity values up to $10m/s$. For the models with higher impact velocity values, the force-displacement responses significantly change. Apart from the initial contact and the further contacts between the surfaces of the model, the force-displacement curves have almost the same behavior. Moreover, the initial peak load seem to be much higher at the impacted end of the structures. Also at higher initial velocity values, negative reaction forces were observed during the first impact due to the oscillations of the top surface of the absorber.

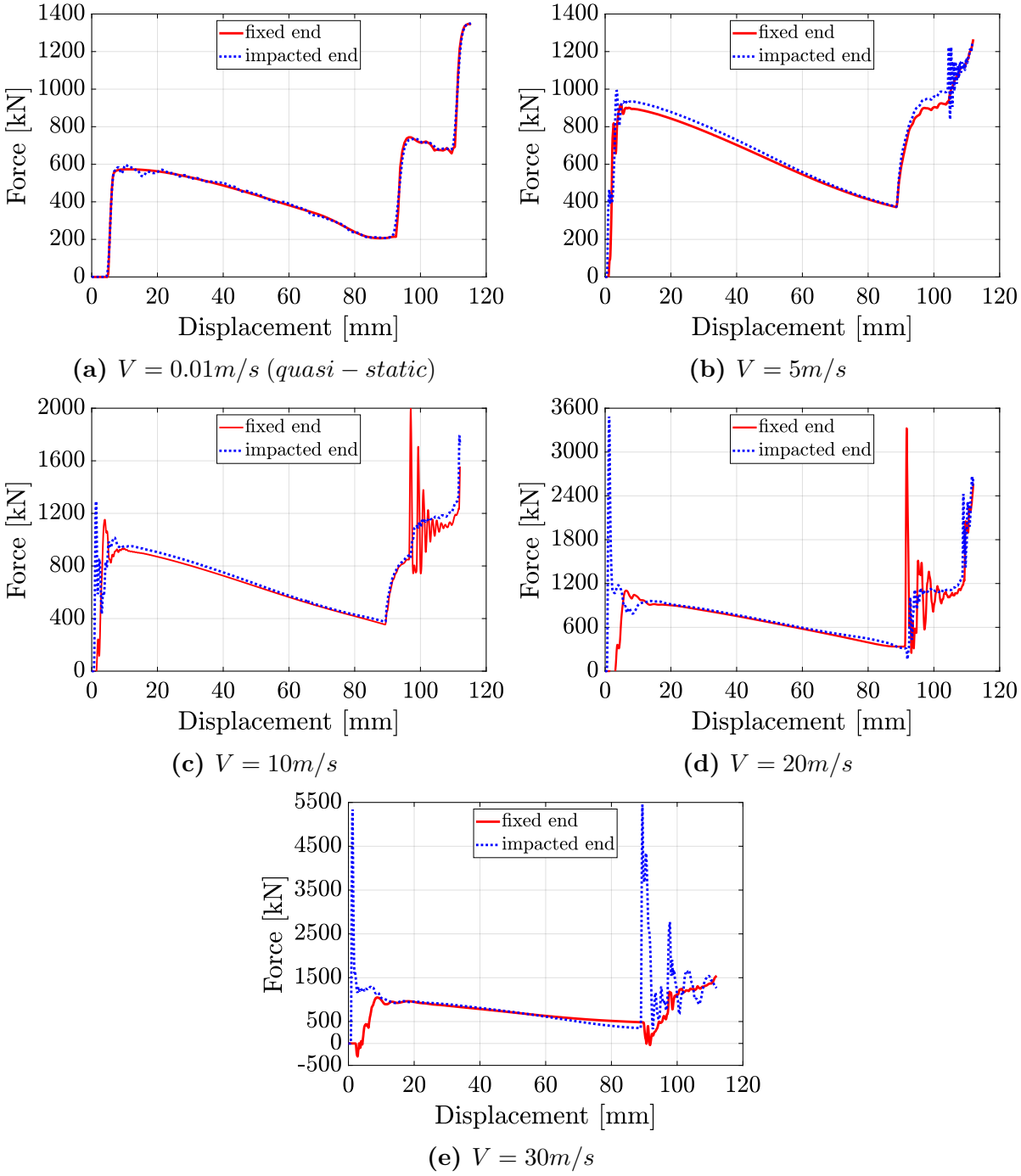

(a) $V = 0.01m/s\ (quasi-static)$ **(b)** $V = 5m/s$

(c) $V = 10m/s$ **(d)** $V = 20m/s$

(e) $V = 30m/s$

Figure 6.47: Force-displacement response of the models for different impact velocities.

The deformation shape of the models are also affected by the impact velocity. The deformed shapes of the model with $\beta = 30°$ and $t = 10mm$ are shown in Figure 6.48 for the deformation amounts of $50mm$ and $75mm$. It is clearly seen that, structures have slightly different deformation shapes and stress distribution on the edge rings in the middle of the absorber. For the model with $\beta = 30°$, the presence of inertia forces may supported the unbuckled portion of the structure for a longer time. As the geometric stiffness of the structure is directly related to the shape of the structure, the increased absorbed energy values for higher impact velocities may be caused by increasing geometrical stiffness of the structure due to inertia effects.

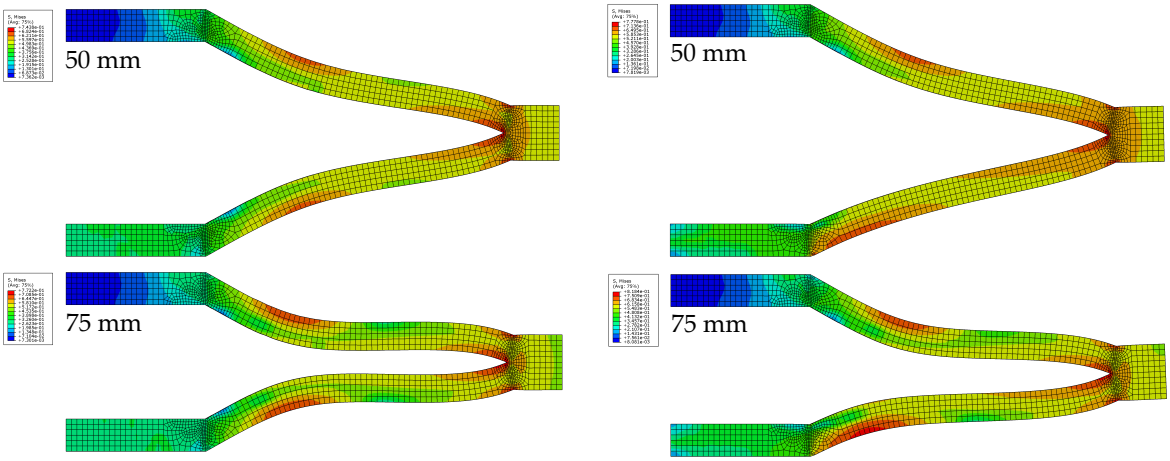

(a) $V = 5m/s$ **(b)** $V = 30m/s$

Figure 6.48: Deformation modes of the model for different impact velocities at selected amount of deformation.

The result of the present section shows that, the dynamic response of the conical structure under axial loading is affected by the impact velocity at relatively higher velocities ($\geq 10m/s$). Thus, the effect of the inertia forces emerge with increasing impact velocity, even if the strain-rate dependency of the material is neglected.

6.5 Combined Effects on Performance Parameters

In this section, the performance parameters of an energy absorber are investigated individually for all variable parameters. The number of simulations and the combinations of the variables created a need for this particular section. Comparison of the influence of all variables for each performance parameter would be the most effective method to gain insight on the impact response of the selected geometry as an energy absorber. The effect of three different variables (velocity, thickness and base conical angle) are compared for each simulation result output, except for the impact mass variable.

Figure 6.49 shows the effect of the impact mass, absorber thickness and impact velocity on the absorbed energy response of the structures. As seen in Figure 6.49 and also in Figure 6.19, impact mass does not have significant effect on absorbed energy, while the effect of the absorber thickness and the base conical angle are non-negligible when the impact velocity is kept constant. However, the maximum deformation length is associated with the initial kinetic energy of the system and increases with increasing impact mass. It can be said that the dynamic or non-linear stiffness of the absorber structure is not dependent on the mass of the impactor in the selected mass range. In other words, impact mass has no influence on the internal forces of the structure to resist the dynamic loading by the striking plate under constant impact velocity. The same result were also observed in the previous studies, which investigated the energy absorbing structures under axial dynamic loading conditions, in the current literature.

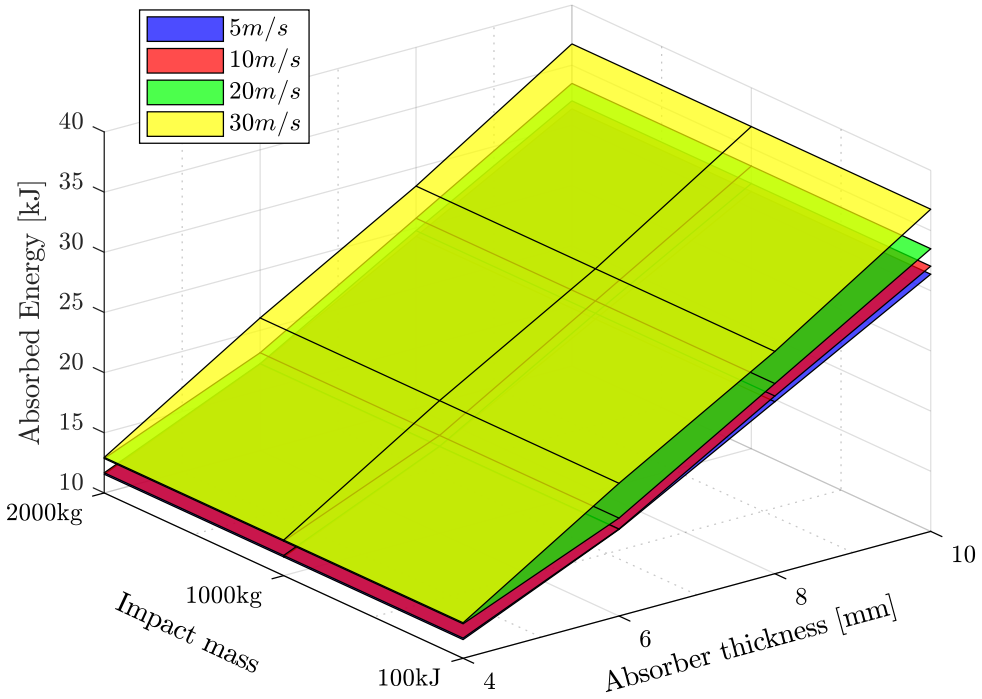

Figure 6.49: Effect of Impact mass, absorber thickness and impact velocity on the amount of absorbed energy.

Based on the current literature, Kathiresan and Manisekar [51] studied on the low velocity axial impact behavior of GFRP conical frusta and stated that the impact mass has no significant effect on the load response of the structure. Ahmad and Thambiratnam [52] observed the same behavior that there is no significant change on the load-deflection curves and the crush and energy absorption of the empty and foam-filled conical tubes are independent on the impact mass. Also Wang et.al. [53] and Nagel [54, 21] found no significant effect of impact mass on dynamic crush behavior of GFRP cylindrical and tapered tubes respectively.

For this reason, the impact mass parameter is not included to any of the following 3-D plots. The effect of the variables on the performance parameters of the selected geometry are plotted as functions of impact velocity, absorber thickness and the base conical angle.

6.5.1 Absorbed Energy

Figure 6.50 shows that the amount of absorbed energy increases in all models as the base cone angle β ,absorber thickness and impact velocity increases. With increasing β angle, structures exhibit more stiff behavior to the axial loading and also gain more deformation length with constant bottom radius and increasing β angle. This situation allows the structures with higher β angles to dissipate more kinetic energy at same impact velocity and absorber thickness. Absorbed energy values also increase with the increasing absorber thickness.

The effect of the thickness on the absorbed energy values is caused by the amount of material available to plastic deformation and so energy absorption. This situation also limits the compression of each fold during the deformation as the thickness increases. The impact velocity has also a non-negligible effect on the energy absorption of the structures due to the inertia effects with increasing impact velocity. When compared together, impact velocity has a less significant effect on the energy absorption capacities of structures.

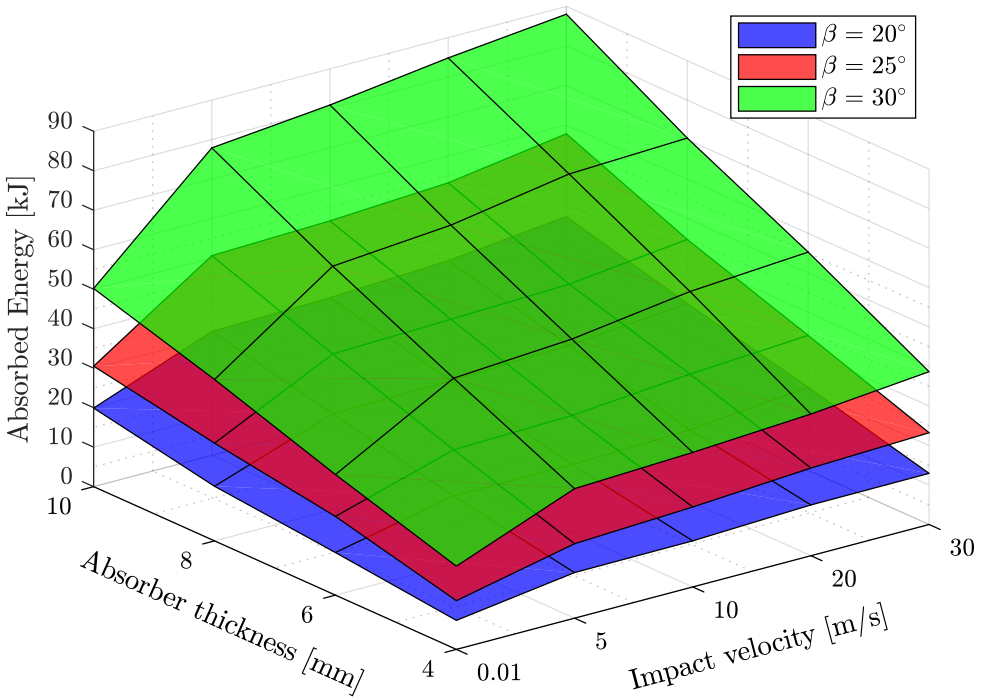

Figure 6.50: Effect of base conical angle, absorber thickness and impact velocity on absorbed energy.

Kathiresan and Manisekar [51] have observed that dynamic energy absorption characteristics of GFRP conical frusta during impact loading increases as the impact velocity increases due to the inertia effect, strain rate effect and the friction effect. Authors also stated that the absorbed energy within a given crush distance for foam-filled conical tubes can be maximized by increasing the wall thickness and/or base conical angle. The results from the study of Azimi and Asgari [38] showed that with thicker walls of absorber causes in increase on the energy absorption characteristics of bi-tubular conical-circular structures under axial and oblique impact loading.

6.5.2 Reaction Force

The peak reaction forces increase significantly with increasing base cone angle β, especially at higher impact velocity values of $20m/s$ and $30m/s$. Increasing β angle ensures more stiff behavior of the structures under impact loading. Another significant effect on the peak reaction force is observed at different absorber thickness values, due to the change in the bending stiffness of the structures. The same increasing effect is also true for mean reaction force responses.

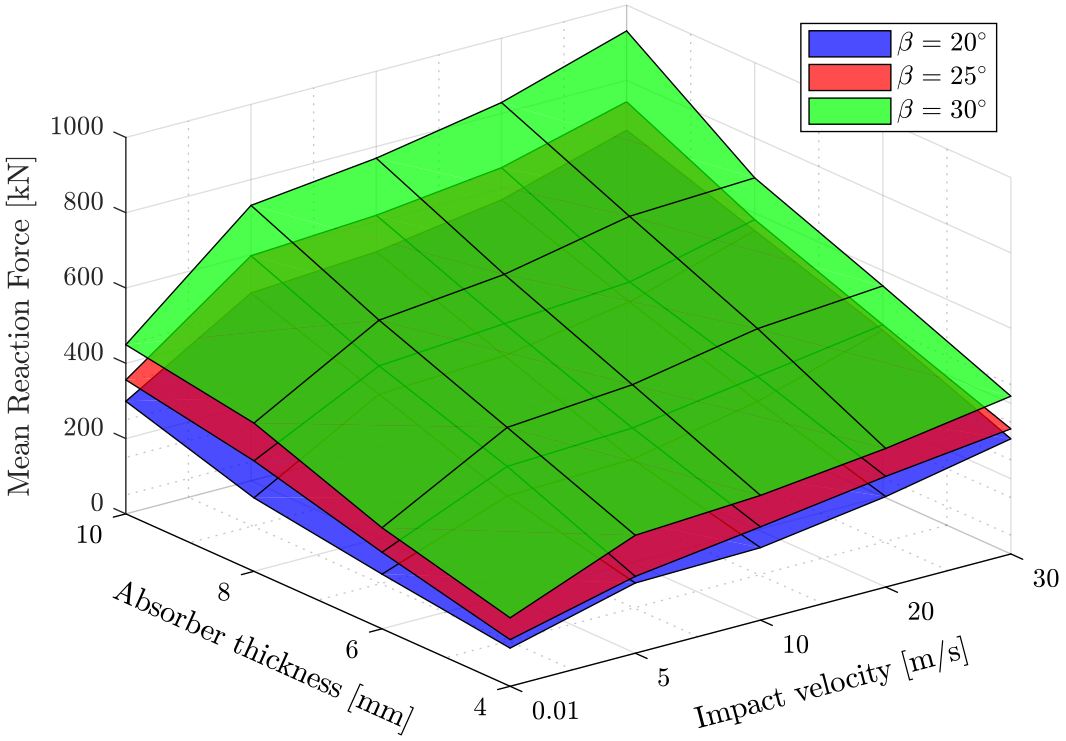

Figure 6.51: Effect of base conical angle, absorber thickness and impact velocity on mean reaction force.

The effect of the impact velocity and the base conical angle on the mean reaction forces are more clearly seen at the higher absorber thickness values. Mean reaction forces have similar behavior with peak reaction forces at different impact velocity, absorber thickness and base conical angle values. The effect of the base conical angle β on the peak reaction forces are more identical at different absorber thicknesses when compared to the mean reaction force. Effects of the variable parameters on mean reaction force values are shown in Figure 6.51. Congruently to the current investigations, Akisanya and Fleck [55] stated that frusta with high base conical angle have shown the ability to support higher loads.

6.5.3 Crash Force Efficiency

Crash force efficiency (CFE) values of the structures exhibit a significantly decreasing behavior as the impact velocity increases. The complete dataset of the CFE values are plotted in Figure 6.52. As the peak reaction force response of the structures increase significantly as the impact velocity increses, the CFE values for higher impact velocities are very low when compared to the quasi-static loading case. Also the the conical angle becomes more effective on the CFE values at relatively lower impact velocity values. It is found that the absorber thickness has a similar effect on both mean and peak reaction force values. Thus, the CFE values does not change significantly within the range of the absorber thickness values of the present study. Overall, the obtained CFE values of the present study are seem to be compatible with the current literature.

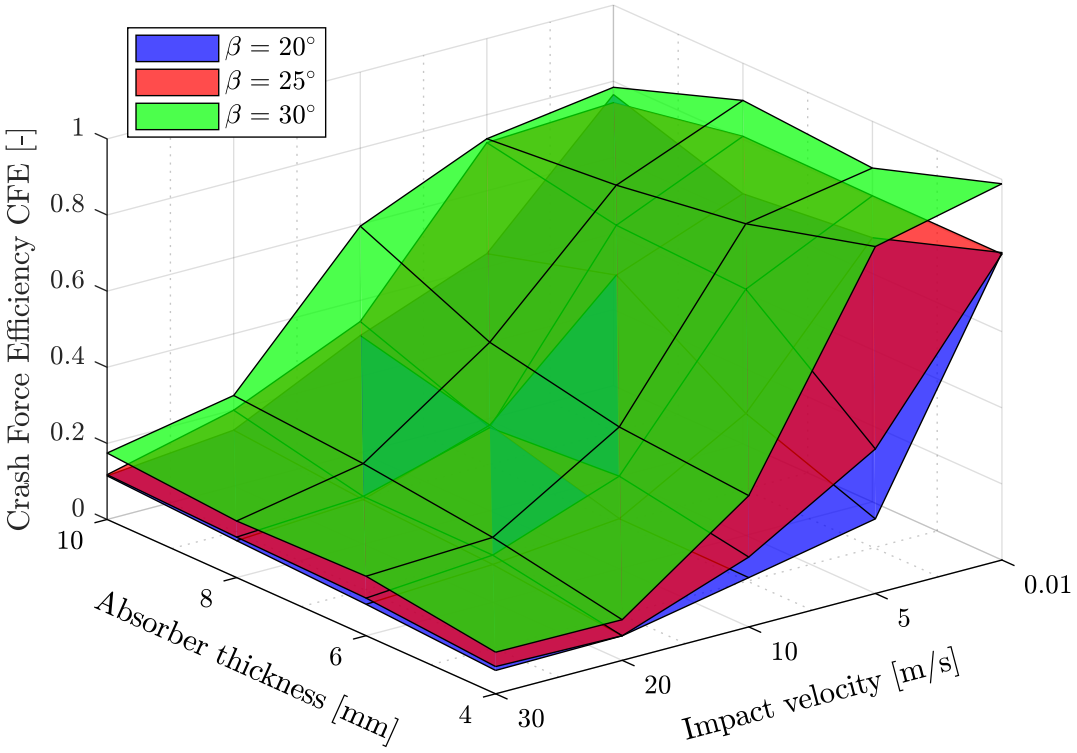

Figure 6.52: Effect of base conical angle, absorber thickness and impact velocity on cfe.

In the study of Kathiresan and Manisekar [56], CFE values between 0.70 and 0.93 were obtained for a conical specimen with thickness of $0.81mm$ and height of $95.6mm$ under impact loading with an initial impact velocity in a range of 4.4 to $6.3m/s$. Also Mirfendereski et. al. [46] studied the empty rectangular frusta under quasi-static and dynamic ($15m/s$) loading cases. The obtained CFE values were 0.72 and 0.25 for quasi-static and dynamic loading cases respectively.

6.5.4 Stroke Efficiency

The stroke efficiency is another performance parameter of energy absorbers. It is desired to be as high as possible in order to have a higher maximum deformable length and so the absorbed energy. Stroke efficiency values of the absorber geometry used in the current study are calculated by dividing the deformation length obtained from simulations to the length of the structure as in equation 8. Calculated values for all models are given in Figure 6.53 by means of base conical angle, impact velocity and the absorber thickness. The impact mass has no effect on the stroke efficiencies as it does not affect the deformation modes during the crush and so the deformation length. Thus, effect of the impact mass is neglected in Figure 6.53 where the effect of all variable parameters are compared together.

Stroke efficiency is directly related to the conical angle β. Besides, the deformation mode has an indirect effect due to the changes in bending shapes of the models. Normally, the maximum deformation length is kept equal for all absorber thickness values.

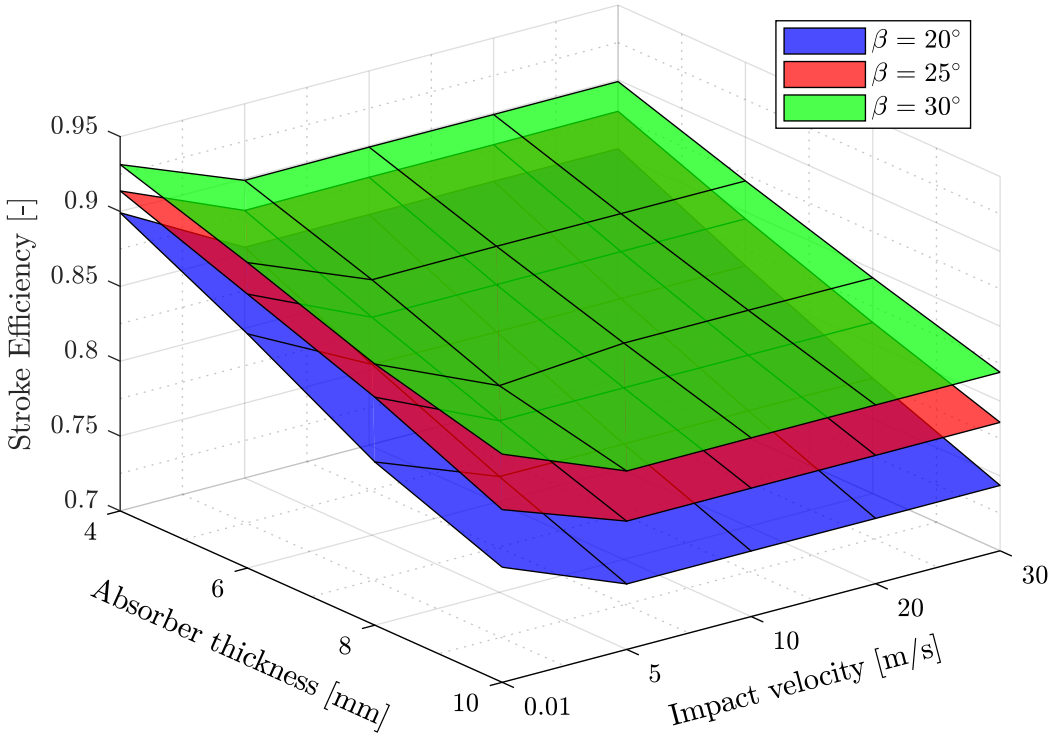

Figure 6.53: Effect of base conical angle, absorber thickness and impact velocity on stroke efficiency.

Based on the deformation modes, the deformed length of the models have a slightly decreasing behavior as the absorber thickness increases. The change in the stroke efficiency caused by the absorber thickness is calculated to be maximum 14%. The conical angle also changes the stroke efficiency in a constant ratio as it increases the maximum length and the total length of the absorber. The effect of the base conical angle does not change with variation of other parameters.

Under quasi-static loading conditions, stroke efficiency values are calculated to be slightly higher than the dynamic loading case, which is caused by the stable deformation of the structures. The impact velocity has no influence on the stroke efficiency values of the models under dynamic loading.

6.5.5 Specific Energy Absorption

Specific energy absorption (SEA) is another important parameter to gain insight about the performance of an energy absorber. The SEA values changes significantly under dynamic loading conditions when compared to the quasi-static case. This is caused by the strain-rate dependency of the material model. The SEA have also a slightly increasing behavior for increasing impact velocity under dynamic loading conditions.

The SEA is not seem to be significantly affected from the increasing absorber thickness values. This is caused by the increasing effect of the absorber thickness on both the absorbed energy values and the mass of the structure.

On the other hand, the specific energy absorption values are significantly affected from the base conical angle as seen in Figure 6.54. Although the base conical angle increases the mass of the body, the increase in energy absorption capacity is relatively higher.

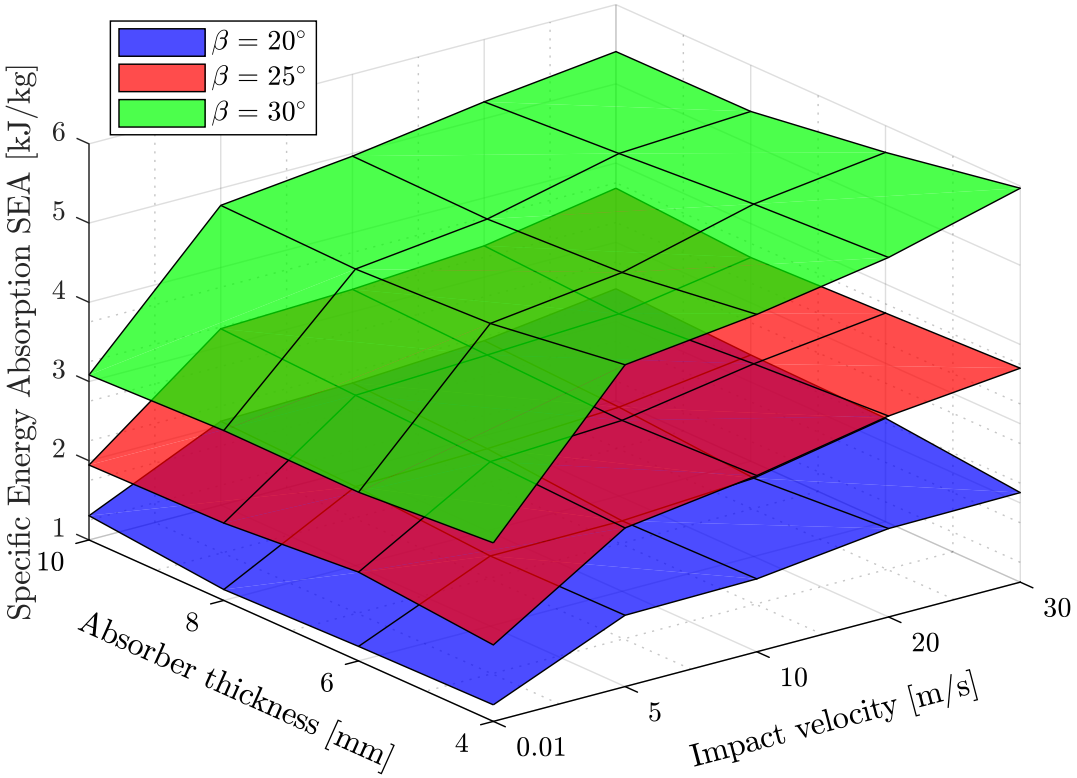

Figure 6.54: Effect of base conical angle, absorber thickness and impact velocity on specific energy absorption SEA.

Obtained SEA values varies from $1.91kJ/kg$ to $5.97kJ/kg$. Guler et al. [9] obtained SEA values in a range of 8.29 to $21.54kJ/kg$ in their study for various conical absorber geometries. Azimi and Asgari [38] have also obtained SEA values between 8.56 to $25.94kJ/kg$ at different impact angles on their newly developed bi-tubular conical-circular structure. Values taken from the current study are significantly low when compared to the current literature. The main reason for this situation is the relatively high mass due to the high thickness and lower deformation length of the geometry investigated in the current study.

6.5.6 Absorbed Energy per unit Deformation

As seen in Figure 6.55, the absorbed energy per unit deformation is affected from both three parameters. The most effective parameter is the absorber thickness because of the increase in the absorbed energy as the thickness increase. The less effective parameter is the impact velocity because it has the less effect on the energy absorption characteristics at a chosen β angle of structure when compared to others under dynamic loading conditions.

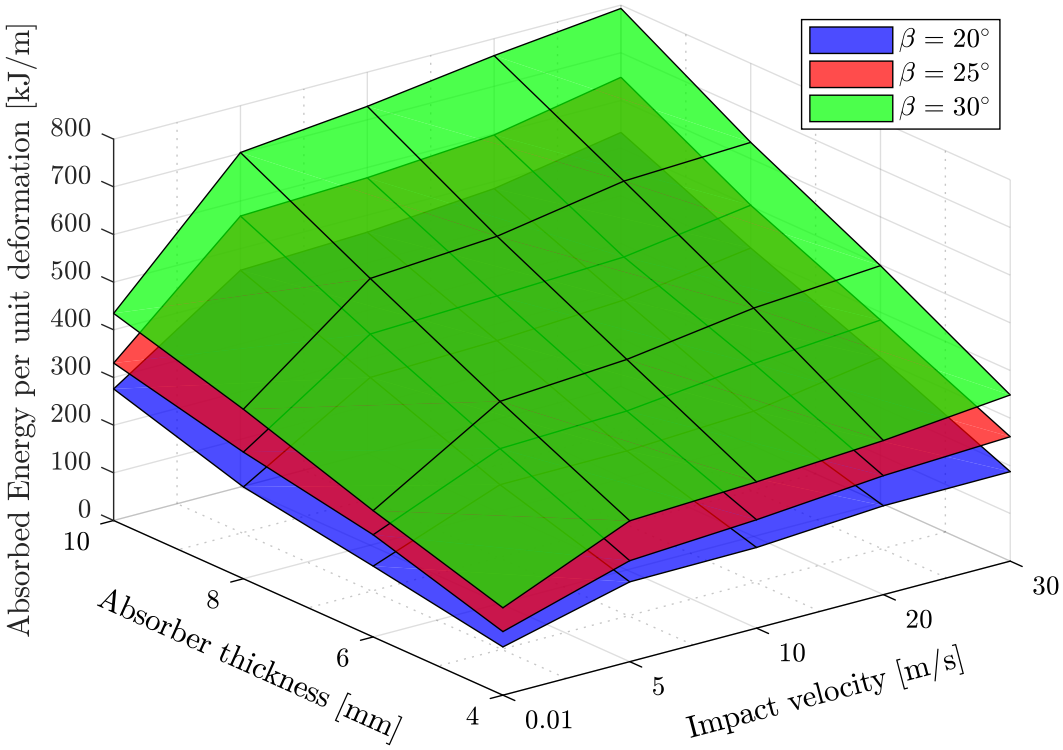

Figure 6.55: Effect of base conical angle, absorber thickness and impact velocity on absorbed energy per unit deformation.

The effect of the base conical angle is slightly changed by the absorber thickness and impact velocity values. The comparison surfaces of Figure 6.55 are almost identical although the conical angle changes the maximum deformable length of the structures significantly.

6.5.7 Dynamic Amplification Factor

The dynamic amplification factor (DAF) is another useful parameter for comparing the dynamic effects on the absorbed energy od the structure. The calculated DAF values are plotted in Figure 6.56 for the models of selected parameters.

DAF values slightly increase as the impact velocity increases due to the inertia effects that explained in previous sections. Also the the conical angle becomes more effective on the DAF values with decreasing absorber thickness.

The effect of the absorber thickness on the DAF values are more stable at models with higher base conical angle values. The maximum change on the DAF is seen in the models with base conical angle of 20° and with lower absorber thickness values. Due to the lower angle and thickness, the models are more prone to bending and have several contact points during the simulations. The geometric stiffness of the models are relatively low and the effect of the inertia forces are observed higher in these models.

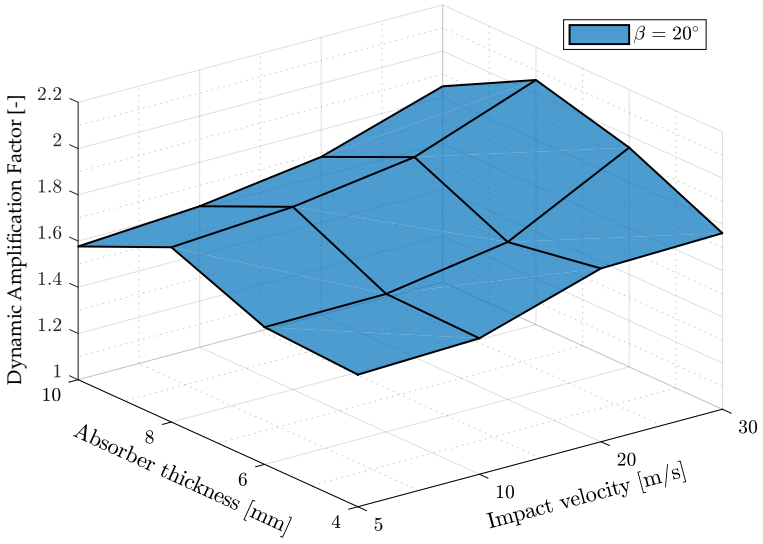

(a) $\beta = 20°$

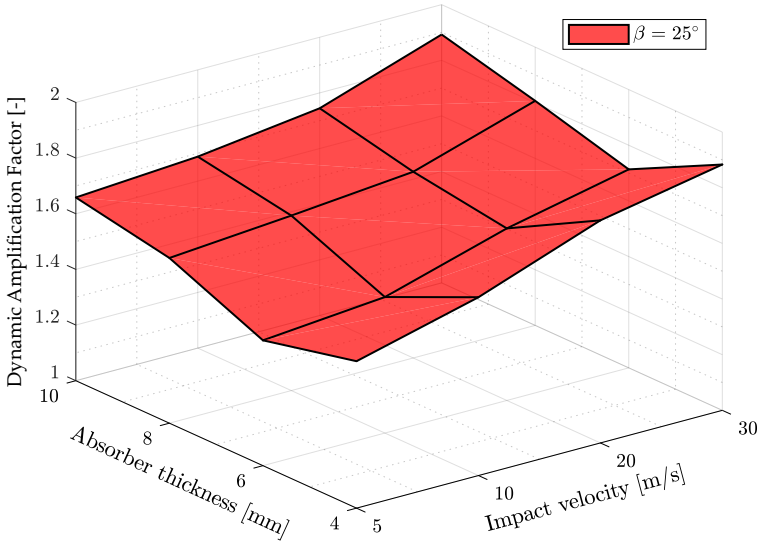

(b) $\beta = 20°$

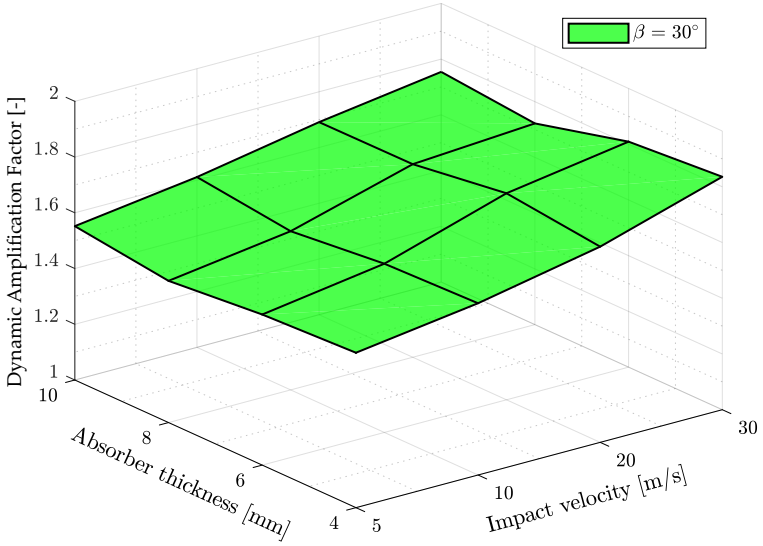

(c) $\beta = 30°$

Figure 6.56: Effect of the absorber thickness and the impact velocity on the DAF values for models with different base conical angle.

7 Conclusion

7.1 Summary and Conclusions

A numerical investigation of the conical energy absorbing structure was examined in this study. In order to obtain detailed information about the dynamic behavior of the structures, the axial impact was simulated by using an explicit package of FEM software Abaqus. In the view of obtained information from the current study, some of the significant conclusions and some guidelines on the design of a low base conical angle structure are summarized below.

1. The dynamic force-displacement response of the conical structure is affected by the absorber thickness, base conical angle and the impact velocity. However, it is observed that the impact mass of the striker has no effect on the dynamic force response of the structures. The impact mass only influences the amount of deformation as it increases the initial kinetic energy. The effect of the conical angle on the force responses become higher as the absorber thickness increases.

2. The energy absorption response of a low angle conical structure under axial dynamic loading is influenced by the absorber thickness, conical angle and impact velocity. Thus, these geometry parameters should be used to control the dynamic response of the structures. However, the conical angle and the absorber thickness are the most effective on the energy absorption of the selected geometry. In other words, structures with higher absorber thickness and conical angle absorb more energy within a selected crush distance.

3. The crash force efficiency values of the current study do not have an explicit and stable behavior. CFE values have a decreasing trend as the impact velocity increases due to the increasing initial peak reaction force response of the structures. On the other hand, CFE values do not seem to be affected from the absorber thickness. However, base conical angle has an increasing effect on CFE values which is caused by the increasing mean reaction force values due to the bending resistance of the structures with higher β values.

4. The specific energy absorption values are strictly affected from the base conical angle β. Increasing conical angle causes the system to be more resistant to any bending action. However, the absorber thickness does not affect the SEA values significantly. Because, higher absorber thickness values increase both the amount of absorbed energy and the mass of the structures.

5. In order to increase the absorbed energy within a given deformation length;

   (a) the conical angle of the structure can be increased for the same absorber thickness values and/or impact velocity,

   (b) absorber thickness of the structure can be increased for the same conical angle and/or impact velocity,

   (c) changing the impact mass has no significant effect.

   (d) increasing the impact velocity also increase the amount of the absorbed energy. This is caused by the inertia effects and the strain-rate dependency of the used material model. However, the effect of the impact velocity is quite low when compared to the effect of the absorber thickness and the conical angle.

7.2 Contributions of the Thesis

The primary aim of this thesis is to gain a better understanding on the impact and energy absorption behavior of truncated conical structures with relatively higher thickness values and to investigate their application as energy absorbing systems.

With respect to the objectives outlined in Chapters 1 and 3, this study has investigated the impact response and energy absorption capabilities of truncated shallow cones under axial impact loading. The effect of the geometry parameters investigated in this study were the base cone angle, impact mass, impact velocity and the thickness of the structure. Several finite element models were developed for the selected parameters to simulate the response of individual conical absorbers. Studies until current stage has provided a good opportunity to investigate and compare dynamic response of truncated cones by means of some important performance parameters.

The energy absorbing capabilities of the current geometry, seems to be promising due to it's relatively high thickness and high energy absorption. However, high thickness leads to a more heavy structure which is not preferable as an energy absorber. Also the conical angle has a great influence on the energy absorbing performance of the structure. Structures with higher angle and lower thickness absorbs slightly more energy than the structures with lower angle and higher thickness. However, current stage of the study is still not sufficient to determine the usability of undertaken geometry as an impact absorber. In consideration of parameters compared above and future work explained below, further studies will be more appropriate to resolve the situation of current geometry to be a possible alternative to the current energy absorber geometry.

7.3 Recommendations for Future Work

In order to obtain sufficient investigation of the geometry undertaken in the current study, suggestions for further works indicated below.

Longer Deformation Zone

As mentioned in previous chapters of the current study, amount of the stroke length of an energy absorber is a significant design requirement. It is necessary to have a longer stroke of energy absorbers both to improve the energy dissipation performance of the structure and to gain a comparable length of geometry with the energy absorbers studied in the literature and used in the industry. In this manner, instead of changing the base cone angle of the structure, it should be investigated to use more than one structure coupled together to obtain sufficient deformation stroke. In Figure 7.1, one of the possible structure that four of the current absorber structure coupled together is visualized.

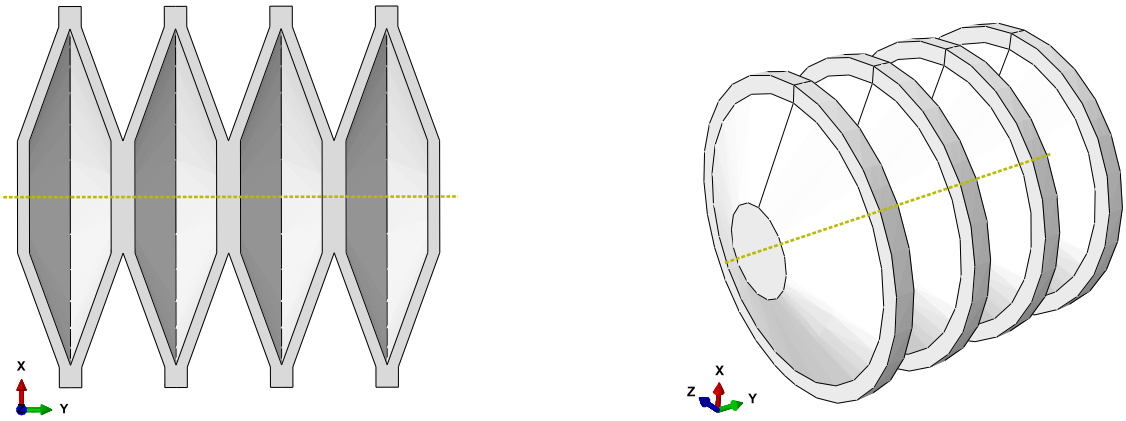

(a) **(b)**

Figure 7.1: Four structures coupled together a) cross-sectional view b) isometric view

Bibliography

[1] Heinz-Peter Bader. Dozens hurt in head-on vienna commuter train crash. Retrieved from : `http://www.reuters.com`, January 2013 (Online; Accessed Jan. 2016).

[2] J Marsolek and H-G Reimerdes. Energy absorption of metallic cylindrical shells with induced non-axisymmetric folding patterns. *International Journal of Impact Engineering*, 30(8):1209–1223, 2004.

[3] MF Horstemeyer, H Li, J Siervogel, L Kwasniewski, J Wekezer, B Christiana, and G Roufa. Material and structural crashworthiness characterization of paratransit buses. *International journal of crashworthiness*, 12(5):509–520, 2007.

[4] Xiaochuan Liu, Jun Guo, Chunyu Bai, Xiasheng Sun, and Rangke Mou. Drop test and crash simulation of a civil airplane fuselage section. *Chinese Journal of Aeronautics*, 28(2):447–456, 2015.

[5] Dellner. Company website. Retrieved from : `http://www.dellner.com/assets/img/slider_1_m.jpg`, 2016 (Online; Accessed Jan. 2016).

[6] VOITH. Connect and protect:coupler and front end systems. Retrieved from : `http://resource.voith.com/vt/publications/downloads/1994_e_g1712en_internet.pdf`, 2014 (Online; Accessed Nov. 2015).

[7] M Abbasi, S Reddy, A Ghafari-Nazari, and M Fard. Multiobjective crashworthiness optimization of multi-cornered thin-walled sheet metal members. *Thin-walled structures*, 89:31–41, 2015.

[8] AAN Aljawi and AAA Alghamdi. Investigation of axially compressed frusta as impact energy absorbers. *Computational methods in contact mechanics IV*, page 431–443, 1999.

[9] M.A. Guler, M.E. Cerit, B. Bayram, B. Gerceker, and Karakaya E. The effect of geometrical parameters on the energy absorption characteristics of thin-walled structures under axial impact loading. *International Journal of Crashworthiness*, 15(4):377–390, 2010.

[10] ABAQUS. 6.13, analysis user's manual. *Dassault Systemes Simulia Corp., Providence, RI*, 2013.

[11] ABAQUS. 6.13, getting started with abaqus interactive edition. *Dassault Systemes Simulia Corp., Providence, RI*, 2013.

[12] EN ISO. 6892-1. metallic materials-tensile testing-part 1: Method of test at room temperature. *International Organization for Standardization*, 2009.

[13] P. Verleysen, J. Peirs, J. Van Slycken, K. Faes, and L. Duchene. Effect of strain rate on the forming behaviour of sheet metals. *Journal of Materials Processing Technology*, 211(8):1457–1464, 2011.

[14] European Railway Agency. Railway safety performance in the european union. Retrieved from : `http://www.era.europa.eu/Document-Register/Documents/SPR2014.pdf`, January 2014. [Accessed on Nov. 2015].

[15] A. A A Alghamdi. Collapsible impact energy absorbers: An overview. *Thin-Walled Structures*, 39(2):189–213, 2001.

[16] VOITH. Voith lightweight components: New energy absorbers made of fibre composite plastics. Retrieved from : `http://www.voith.com/en/press/press-releases-99_58828.html`, 2014 (Online; Accessed Nov. 2015).

[17] Dellner. Dellner company brochure. Retrieved from : `http://www.dellner.com/assets/Archive/Dellner_Brochure.pdf`, 2014 (Online; Accessed Nov. 2015).

[18] Axtone. Crash components for emu/dmu multiple units. Retrieved from : `http://www.axtone.eu/en/multiple-units--dmu-and-emu-.html`, 2015 (Online; Accessed Nov. 2015).

[19] Guoxing Lu and TX Yu. *Energy Absorption of Structures and Materials*. Woodhead Publishing, 2003.

[20] CEN. Railway applications - crashworthiness requirements for railway vehicle bodies. Technical Report EN 15227:2008, European Commitee for Standardization, 2008.

[21] Gregory Nagel. *Impact and energy absorption of straight and tapered rectangular tubes.* Phd thesis, Queensland University of Technology, 2005.

[22] Zaini Ahmad. *Impact and energy absorption of empty and foam-filled conical tubes.* Phd thesis, Queensland University of Technology, 2009.

[23] A.G. Hanssen, M. Langseth, and O.S. Hopperstad. Static and dynamic crushing of circular aluminium extrusions with aluminium foam filler. *International Journal of Impact Engineering*, 24(5):475–507, 2000.

[24] A.G. Hanssen, M. Langseth, and O.S. Hopperstad. Static and dynamic crushing of square aluminium extrusions with aluminium foam filler. *International Journal of Impact Engineering*, 24(4):347–383, 2000.

[25] JM Alexander. An approximate analysis of the collapse of thin cylindrical shells under axial loading. *The Quarterly Journal of Mechanics and Applied Mathematics*, 13(1):10–15, 1960.

[26] AG Mamalis and W Johnson. The quasi-static crumpling of thin-walled circular cylinders and frusta under axial compression. *International Journal of Mechanical Sciences*, 25(9-10):713–732, 1983.

[27] N. Jones W. Abramowicz. Dynamic axial crushing of square tubes. *International Journal of Impact Engineering*, 2(2):179–208, 1984.

[28] N. Jones W. Abramowicz. Dynamic progressive buckling of circular and square tubes. *International Journal of Impact Engineering*, 4(4):243–270, 1986.

[29] AG Mamalis, W Johnson, and GL Viegelahn. The crumpling of steel thin-walled tubes and frusta under axial compression at elevated strain-rates: some experimental results. *International Journal of Mechanical Sciences*, 26(11):537–547, 1984.

[30] M Langseth and OS Hopperstad. Static and dynamic axial crushing of square thin-walled aluminium extrusions. *International Journal of Impact Engineering*, 18(7-8):949–968, 1996.

[31] AG Mamalis, DE Manolakos, MB Ioannidis, PK Kostazos, and C Dimitriou. Finite element simulation of the axial collapse of metallic thin-walled tubes with octagonal cross-section. *Thin-Walled Structures*, 41(10):891–900, 2003.

[32] YS Tai, MY Huang, and HT Hu. Axial compression and energy absorption characteristics of high-strength thin-walled cylinders under impact load. *Theoretical and applied fracture mechanics*, 53(1):1–8, 2010.

[33] F Tarlochan, F Samer, AMS Hamouda, S Ramesh, and Karam Khalid. Design of thin wall structures for energy absorption applications: Enhancement of crashworthiness due to axial and oblique impact forces. *Thin-Walled Structures*, 71:7–17, 2013.

[34] NK Gupta, GL Easwara Prasad, and SK Gupta. Plastic collapse of metallic conical frusta of large semi-apical angles. *International Journal of Crashworthiness*, 2(4):349–366, 1997.

[35] AAA Alghamdi, AAN Aljawi, and TM-N Abu-Mansour. Modes of axial collapse of unconstrained capped frusta. *International Journal of Mechanical Sciences*, 44(6):1145–1161, 2002.

[36] GL Easwara Prasad and NK Gupta. An experimental study of deformation modes of domes and large-angled frusta at different rates of compression. *International journal of impact engineering*, 32(1):400–415, 2005.

[37] NK Gupta et al. Experimental and numerical studies of impact axial compression of thin-walled conical shells. *International journal of impact engineering*, 34(4):708–720, 2007.

[38] M. Asgari M.B. Azimi. A new bi-tubular conical–circular structure for improving crushing behavior under axial and oblique impacts. *International Journal of Mechanical Sciences*, 105:253–265, 2016.

[39] Cook W.H. Johnson, G.R. A constitutive model and data for metals subjected to large strains, high strain rates and high temperatures. In *Proceedings of the 7th International Symposium on Ballistics, The Hague, Netherlands, 1983*, 1983.

[40] Ali Ghamarian and Hamidreza Zarei. Crashworthiness investigation of conical and cylindrical end-capped tubes under quasi-static crash loading. *International Journal of Crashworthiness*, 17(1):19–28, 2012.

[41] J. S. Lin, X. Wang, and G. Lu. Crushing characteristics of fiber reinforced conical tubes with foam-filler. *Composite Structures*, 116(1):18–28, 2014.

[42] Alper Tasdemirci, Ali Kara, Kivanc Turan, and Selim Sahin. Dynamic crushing and energy absorption of sandwich structures with combined geometry shell cores. *Thin-Walled Structures*, 91:116–128, 2015.

[43] William S Cleveland. Robust locally weighted regression and smoothing scatterplots. *Journal of the American statistical association*, 74(368):829–836, 1979.

[44] MathWorks. *Curve fitting toolbox: for use with MATLAB® user's guide*. MathWorks, 2002.

[45] R. Seifried, H. Minamoto, and P. Eberhard. Viscoplastic effects occurring in impacts of aluminum and steel bodies and their influence on the coefficient of restitution. *Journal of Applied Mechanics*, 77(4):041008, 2010.

[46] L. Mirfendereski, M. Salimi, and S. Ziaei-Rad. Parametric study and numerical analysis of empty and foam-filled thin-walled tubes under static and dynamic loadings. *International Journal of Mechanical Sciences*, 50(6):1042–1057, 2008.

[47] M. Kathiresan, K. Manisekar, and V. Manikandan. Performance analysis of fibre metal laminated thin conical frusta under axial compression. *Composite Structures*, 94(12):3510–3519, 2012.

[48] Norman Jones. *Structural impact*. Cambridge university press, 2011.

[49] M Langseth, OS Hopperstad, and T Berstad. Crashworthiness of aluminium extrusions: validation of numerical simulation, effect of mass ratio and impact velocity. *International Journal of Impact Engineering*, 22(9-10):829–854, 1999.

[50] D Karagiozova and Norman Jones. Dynamic buckling of elastic–plastic square tubes under axial impact—ii: structural response. *International Journal of Impact Engineering*, 30(2):167–192, 2004.

[51] M Kathiresan and K Manisekar. Low velocity axial collapse behavior of e-glass fiber/epoxy composite conical frusta. *Composite Structures*, 166:1–11, 2017.

[52] D.P. Thambiratnam Z. Ahmad. Dynamic computer simulation and energy absorption of foam-filled conical tubes under axial impact loading. *Computers & Structures*, 87(3-4):186–197, 2009.

[53] Lu Wang, Xueming Fan, Hao Chen, and Weiqing Liu. Axial crush behavior and energy absorption capability of foam-filled gfrp tubes under elevated and high temperatures. *Composite Structures*, 149:339–350, 2016.

[54] GM Nagel and DP Thambiratnam. A numerical study on the impact response and energy absorption of tapered thin-walled tubes. *International journal of mechanical sciences*, 46(2):201–216, 2004.

[55] N.A. Fleck A.R. Akisanya. Plastic collapse of thin-walled frusta and egg-box material under shear and normal loading. *International journal of mechanical sciences*, 48(7):799–808, 2006.

[56] M Kathiresan and K Manisekar. Axial crush behaviours and energy absorption characteristics of aluminium and e-glass/epoxy over-wrapped aluminium conical frusta under low velocity impact loading. *Composite Structures*, 136:86–100, 2016.

[57] Klaus-Jürgen Bathe. *Finite element procedures*. Klaus-Jurgen Bathe, 2006.

[58] Robert D. Cook, David S. Malkus, Michael E. Plesha, and Robert J. Witt. *Concepts and Applications of Finite Element Analysis, 4th Edition*. Wiley, 2001.

[59] James M. Gere and Barry J. Goodno. *Mechanics of Materials, 7th Edition*. Cengage Learning, 2008.

[60] Crisbon Delfina Joseph. Experimental measurement and finite element simulation of springback in stamping aluminum alloy sheets for auto-body panel application. Master's thesis, Mississippi State University, 2003.

[61] European Commission. Eu transport in figures. *Statistical pocketbook*, 2016.

Publications of the PhD Student

- E. Özyurt, H. Yılmaz, P. Pascenko, (2015) An investigation on dynamic response of truncated thick walled cones with edge ring under axial compressive impact load, *International Journal of Scientific and Technological Research*, Vol 1, No.9, 21-30
- H. Yılmaz, E. Özyurt, P. Pascenko, (2015) Elastic buckling of thin conical caps with edge ring constraint under uni-axial compression, *International Journal of Scientific and Technological Research*, Vol 1, No.9, 1-9
- H. Yılmaz, E. Özyurt. P. Tomek, (2017) A Comparative study between numerical and analytical approaches to load carrying capacity of conical shells under axial loading, *International Journal of Engineering Trends and Technology (IJETT)*, Vol 52, No.1
- H. Yılmaz, I. Kocabas, E. Özyurt, (2017) Empirical equations to estimate non-linear collapse of medium-length cylindrical shells with circular cutouts, *Thin-Walled Structures*, Vol 119, 868-878.
- E. Özyurt, H. Yılmaz, P. Tomek, (2018) Prediction of the influence of geometrical imperfection to load carrying capacity of conical shells under axial loading. *Sigma Journal of Engineering and Natural Sciences* Vol 36, No.1, 11-20